SATELLITE AND GROUND BASED OBSERVATIONS OF LIGHTNING FLASHES IN THE STRATIFORM AND ANVIL REGIONS OF CONVECTIVE SYSTEMS

by

Michael Jay Peterson

A thesis submitted to the faculty of
The University of Utah
in partial fulfillment of the requirements for the degree of

Master of Science

Department of Atmospheric Sciences

The University of Utah

December 2011

The University of Utah Graduate School

STATEMENT OF THESIS APPROVAL

The thesis of **Michael Jay Peterson**

has been approved by the following supervisory committee members:

Chuntao Liu	, Chair	**09/21/2011** Date Approved
Edward J. Zipser	, Member	**09/20/2011** Date Approved
Timothy J. Garrett	, Member	**10/06/2011** Date Approved

and by **Kevin D. Perry** , Chair of

the Department of **Atmospheric Sciences**

and by Charles A. Wight, Dean of The Graduate School.

ABSTRACT

Flashes in the anvil and stratiform regions of storms are identified and their statistics are analyzed from Tropical Rainfall Measuring Mission (TRMM) observations between 1998 and 2009. In total, ~5% of all lightning flashes are observed in either the anvil or stratiform region. Global distributions and seasonal and diurnal variations of these flashes are discussed. Electric Charging Regions (ECRs) are identified by grouping areas with 30 dBZ radar echo at 6 km from TRMM Precipitation Radar (PR) observations. Then, flashes in the anvil and stratiform regions are associated to their nearest ECRs. About ~15% of all ECRs near lightning have been found to be associated with at least one stratiform or anvil lightning flash. The relationships between these flashes and their nearest ECRs are discussed.

To validate the results from TRMM observations, ground-based observations from the Tropical Warm Pool International Cloud Experiment (TWP-ICE) are analyzed. Based on the results of both data sets, flashes in the anvil region are found to often occur near the edges of convective cells within single cell systems, and many of them occur in relatively early stages of convection. Stratiform flashes, on the other hand, are more common as convective systems weaken, and many of them occur within multicellular systems.

For Mieko

TABLE OF CONTENTS

ABSTRACT…… iii

LIST OF TABLES …… vii

ACKNOWLEDGEMENTS…… viii

Chapters

1 INTRODUCTION …… 1

1.1 History of Lightning Detection …… 1
1.2 Past Studies on the Relationships between Lightning and the Properties of Thunderstorms …… 5
1.3 Past Studies of Lightning Outside Convective Regions of Thunderstorms … 9
1.4 Motivation and Objectives of this Study …… 13

2 TRMM DATA AND METHODOLOGY …… 16

2.1 Definitions of Stratiform and Anvil Lightning Flashes…… 19
2.2 Electric Charge Region (ECR) Definition…… 21
2.3 Flash-to-ECR Association…… 29

3 TRMM STATISTICS …… 32

3.1 Global Statistics of Stratiform and Anvil Flashes…… 32
3.2 Statistics of Storm Properties near Lightning Flashes …… 43
3.3 Statistics of ECRs Associated with Lightning …… 50
3.4 Relationships between ECR Convective Intensity and Flash Counts …… 57
3.5 Relationships between Convective Intensity of ECRs and Flash Distances …… 63

4 TWP-ICE DATA AND METHODOLOGY …… 67

4.1 Definitions of Stratiform Lightning, Anvil Lightning, and ECRs using TWP-ICE Data …… 67
4.2 Comparison of TRMM and TWP-ICE Statistics… …… 78
4.3 Tracking Convective Systems during TWP-ICE …… 86

5 TWP-ICE CASE STUDY 90

5.1 Case 1: January 22nd, 2006 90
5.2 Case 8: February 7th, 2006 96
5.3 Case 9: February 9th, 2006 104
5.4 Case Study Summary..... 112

6 SUMMARY 118

7 REFERENCES 124

LIST OF TABLES

Table		Page
2.1	List of available properties near the location of LIS-observed lightning flashes obtained from TRMM level 1 data ……	22
2.2	List of available convective and physical properties of ECRs obtained from TRMM level 1 data ……	25
2.3	Stratiform fractions in ECRs with at least 4 PR pixels over land and over the ocean. ECR samples in the subtropics during the winter are excluded …	26
3.1	Global statistics of all lightning within the PR swath between 36° N and 36° S characterized by type from observations between 1998-2009. These statistics have been normalized by total sampled pixels at different latitudes to counteract sampling bias. Anvil flashes over the region with interference of the South Atlantic Anomaly (shown in Figure 3.2.b and d) are not counted……	33
3.2	Global statistics of all ECR lightning flashes and population of ECRs associated with stratiform and anvil flashes between 36°N and 36°S normalized by latitude. Flashes farther than 200 km from the ECR center and anvil flashes over Argentina are not included in this sample ……	51
4.1	Stratiform fractions of lightning-producing ECRs larger than 4 PR pixels observed during Jan and Feb in the TWP-ICE region (10.8°-13.6°S, 129.8°-132.2°E) ……	75
4.2	Sample size of flashes observed during January and February in the TWP-ICE region by the TRMM LIS, TWP-ICE LINET, and TWP-ICE LINET with a modified stratiform/convective algorithm forcing all flashes in areas with >30 dBZ at 6 km to be convective ……	77
4.3	Overview of the properties of 15 convective systems examined during TWP-ICE. Bold columns represent selected cases to be discussed in Chapter 5 ……	88

ACKNOWLEDGEMENTS

This research was supported by NASA Grant NNX08AK28G under the direction of Dr. Erich Stocker. Thanks also go to John Kwiatkowski and the rest of the Precipitation Processing System (PPS) at NASA Goddard Space Flight Center, Greenbelt, MD, for data processing assistance.

CHAPTER 1

INTRODUCTION

Lightning is both a beautiful and destructive force of nature. Electrical discharges from lightning flashes not only are harmful to humans on the ground, but also have the potential to damage structures and electrical systems. Lightning can be particularly dangerous in regards to aviation. For this reason, it is important to examine the various types of storms that produce distant lightning flashes, as well as lightning flashes in the stratiform and anvil regions of thunderstorms, since often these regions are considered safe for air traffic.

1.1 History of Lightning Detection

Lightning observation techniques have come a long way over the past century. As early as the 1920s, meteorologists were using direction-finding radios to detect lightning flashes. This is possible because lightning flashes cause not just flashes in the visible, but radio impulses (sferics) as well. Thunderstorms, then, could be tracked by triangulating their positions at a particular time using readings from multiple sites. The first direction finders generally operated in the VLF band (3-30 kHz), which has the advantage of good propagation through the Earth's atmosphere. Because of this, thunderstorms can be detected at incredible distances. Early VLF direction finders were often the Watson-Watt

type, which consisted of perpendicular loop antennas connected to a cathode-ray-tube screen. These direction finders used the measured magnetic components of source sferics to determine direction in real time. However, these stations also were subject to certain limitations. Direction accuracies were quite low for these devices, and polarization errors (radiation refracted by the ionosphere having undergone a rotation in polarization causing false readings) were common.

As technology improved, so did techniques for detecting lightning strokes. In 1960, Lewis et al. described a hyperbolic sferics direction finding array, using sferic time-of-arrival calculations in place of the outdated magnetic component measurement method. This technique, which is still used today, though with much better equipment and accuracy, in theory eliminates polarization errors completely. However, these improvements did not address the biggest drawback to using LF and VLF sources for detecting lightning: the fact that cloud-to-ground (CG) returns strokes completely dominate the signals in these bands. For this reason, VLF/LF networks are great for observing CG flashes, but underdetect intracloud (IC) flashes.

Another approach for remotely detecting lightning is through the use of sensors that operate in the VHF band. Using a time-of-arrival technique developed by Oetzel and Pierce (1969) and time interval meters (TIM) with 10 ns accuracies, Murty and MacClement developed a VHF direction finder in 1973. The key benefit of using the VHF band is the fact that the amplitudes of sources from IC flashes are comparable with those produced by CG flashes. For this reason, VHF direction finders are useful in measuring total lightning activity within a storm, though the range of observations is limited compared to VLF sensors (just 100 km in the case of Murty and MacClement's

prototype in 1973). By 1978, Murty and MacClement had improved on their design, adding a third antenna in order to not only remove the ambiguity in the measured azimuth angle, but also to allow for the measurement of the elevation angle as well, allowing lightning sources (which can be considered points in the VHF band) to be mapped in three dimensions (MacClement and Murty 1978).

Around the same time, new passive remote sensing techniques were being developed to observe lightning from above, taking advantage of visible and near-infrared emission from lightning strokes. A number of satellites were launched under the Defense Meteorological Satellite Program (DMSP) throughout the mid-to-late 1970s with scanners onboard that would take pictures of lightning from space. Many of these devices were classified by the Air Force at the time. The sensors onboard two satellites used in Orville and Spencer (1979) had a spatial resolution of 3.8 km across. As the satellites orbited, pictures corresponding to each individual scan were compiled into a composite image of lightning activity below the satellites. Since this technique only worked at night, the two satellites had to be sun-synchronous, and they were positioned such that one observed lightning at dusk local time and the other observed lightning at midnight local time at the point of observation.

Throughout the 1980s, emphasis was placed on developing a sensor that could observe lightning from space during the day and at night from a geostationary satellite. The ambitious project was called the Lightning Mapper Sensor (LMS) system (Davis et al. 1983), and the hope was that it could be launched in the late 1980s. Numerous studies were conducted using the U2 and other high-altitude aircraft/spacecraft, including open shutter photography of lightning flashes (Vonnegut et al. 1989), motion pictures

(Vonnegut et al. 1985; Vaughan 1990), and near-infrared observations (Christian and Goodman 1987). Based on these results, space borne observations of lightning were shown to be not only feasible, but also doable given the state of technology at the time. High-altitude U2 observations of near-infrared illumination by lightning were even shown to be similar to ground-based measurements (Christian and Goodman 1987).

While the LMS has yet to be launched at the time of this writing, two new satellites went on to benefit from this work: the Optical Transient Detector (OTD) (1995-2000), and the Lightning Imaging Sensor (LIS) (1997-present) onboard the Tropical Rainfall Measuring Mission (TRMM) Satellite. The OTD is widely considered a prototype for the LIS. Both use the same design to detect lightning from space, which, unlike previous satellites, is capable of detecting lightning from space both during the day and at night with detection efficiencies as high as 90% (Boccippio et al. 2002). Since the LIS is used in the present study, technical details and restrictions will be discussed in Chapter 2.

Meanwhile, back on Earth, a number of advanced ground-based lightning detection networks were being deployed, benefiting from improvements in computer technology and the introduction of GPS for extremely accurate time-of-arrival calculations. Many of these networks are local Lightning Mapping Array (LMA) networks (and the Lightning Detection and Ranging (LDAR) II network in Houston) that operate in the VHF band, which are able to determine 3-D lightning source locations to a very high accuracy compared to their predecessors (Thomas et al. 2004). Such networks can be found in such places as New Mexico, Oklahoma, Northern Alabama, Washington DC, Houston, and the Kennedy Space Center.

Other networks, including the National Lightning Detection Network (NLDN) domestically, make use of a modern version of the magnetic direction finders that have been used since the early days of measuring sferics pulses. Unlike the previous generation, these systems consist of a large number of sites linked digitally for real-time observations of CG return strokes (Orville 2008).

Improved VLF/LF networks have also recently come online. Lightning Location Network (LINET), for instance, has the added benefit of being able to back out the altitude at which lightning flash sources occur based on deviations of arrival times from sensors close to lightning events compared to the expected result from 2-D propagation. This is particularly useful for differentiating between IC and CG lightning flashes (Betz et al. 2004). Since, along with the LIS, LINET will be used extensively in this study, more information on LINET will be presented in Chapter 4. Another VLF network that has been getting a lot of attention recently is the World Wide Lightning Location Network (WWLLN). By siting more than one hundred sensors around the globe, the goal of WWLLN is to be able to provide real-time global lightning location observations to within 10 km accuracy with detection efficiencies above 50%, even for data-sparse regions, including the oceans (Lay et al. 2004).

1.2 Past Studies on the Relationships between Lightning and the Properties of Thunderstorms

Along with improvements in technology came advancements in theory behind lightning initiation. Particularly helpful was the availability of radar data alongside data from ground-based observations of lightning. Using these two data sources, it became

possible to examine lightning in the context of the structure of the larger storm system. In 1960, for instance, Shackford observed that lightning flash rates were related to both the reflectivity maximum above the freezing level and reflectivity profile for a particular storm (Shackford 1960). Later, in 1964, Battan added that the atmospheric properties that control the updraft also control lightning and precipitation (Battan 1964).

Early attempts to explain lightning activity with storm structure resulted in a number of empirical studies that managed to link lightning initiation with radar echoes just above the freezing level (e.g., Larsen and Stansbury 1974; Marshall and Radhakant 1978). Such relationships using reflectivity in the mixed-phase region indicate that the presence of graupel plays an important role in lightning initiation, which is now known to be a key ingredient in the noninductive charging mechanism (Takahashi 1978; Jayaratne et al. 1983; Williams et al. 1989; Saunders et al. 1991).

Studies on the relationship between lightning and storm structure continued throughout the late 1980s, 1990s and 2000s. Rutledge and MacGorman (1988) studied CG lightning activity throughout the life of a MCS observed on June 10th/11th, 1985 during the Preliminary Regional Experiment for STORM (PRE-STORM) project. Emphasis was not only on relating lightning to storm structure, but electrical structure as well in the context of CG polarity. They observed that highest flash rates of negative CG flashes occurred in the convective line when the system was experiencing a peak in rainfall intensity. Keighton et al. (1991) also used radar data and CG lightning location data to correlate CG lightning locations with radar-observed storm structure throughout the life of a severe MCS in Oklahoma on May 23rd, 1981. This particular storm developed into a tornadic supercell and later merged with ordinary cells, forming a squall

line with a trailing stratiform region. Using these data, CG flash rates were shown to be related to the apparent strength of the updraft.

Relationships between ice mass and lightning activity were also examined using ground-based observations. Carey and Rutledge (2000) used observations over the Tiwi Islands on November 28th, 1995 during the Maritime Continent Thunderstorm Experiment to study the electrification process in tropical island convection. After this storm reached maturity, lightning and surface electric fields were observed to be highly dependent on mixed-phase ice mass and rainfall. Deierling et al. (2008) later found high correlation coefficients of 0.8 and 0.9 between ice mass estimates above the melting level and total lightning activity for 11 storms of a variety of types in two different climate regimes. Correlations between total lightning activity and updraft characteristics (mean speed, maximum speed, volume) were also examined for these storms (Deierling and Petersen 2008), and updraft volume was found to correlate better with lightning activity than other characteristics. Lund et al. (2009) also used composite lightning-detection network and radar data (in this case the Oklahoma LMA and a combination of the KOUN S-band polarimetric radar and 2 mobile C-band Doppler radars) to observe lightning locations relative to storm structure for a small MCS observed on Jun 19th, 2004 during the Thunderstorm Electrification and Lightning Experiment. They found that lightning initiated in or near regions containing graupel, suggestive of the noninductive charging mechanism.

Each of these aforementioned studies used ground-based observations to examine lightning and electrification in individual storm systems. However, ground-based lightning networks have one key drawback: they are regional and tend to be concentrated

in certain parts of the globe. Satellite observations are one way to examine lightning globally and provide a new perspective. Using satellites to examine lightning globally is not a new idea, however. Orville and Spencer (1979) used two satellites capable of taking pictures of lightning flashes from space to improve on Brooks' (1925) estimate of the frequency of lightning flashes around the globe. Land-ocean flash ratios were estimated (~8-20 at dusk), and seasonal and latitudinal variations were also observed. Global distributions of midnight lightning were examined in a later study (Orville and Henderson 1986) and found to agree with known patterns in global circulation.

More recently, the OTD and LIS have observed lightning in all types of storms systems around the globe. The LIS is particularly well suited for lightning research because, unlike the OTD, it works in conjunction with an array of sensors aboard the TRMM satellite. TRMM was conceived as a joint venture between the National Aeronautics and Space Administration (NASA) and National Space Development Agency (NASDA) of Japan with the goal of measuring the rainfall and energy exchange of the tropics and subtropics (Kummerow et al. 1998). It was launched in late 1997 and has been observing the tropics ever since. In addition to the LIS, the TRMM sensor package includes the TRMM Microwave Imager (TMI), the Precipitation Radar (PR), and the Visible and Infrared Scanner (VIRS). Using TRMM observations, a number of studies have examined lightning production and the properties of storms, including ice water path estimated from PR reflectivity (Petersen et al. 2005), maximum PR reflectivity and minimum TMI brightness temperatures (Toracinta et al. 2002; Cecil et al. 2005), rain yields for storms over the tropics (Takayabu et al. 2006), and volume of intense convection in storms over Southeast Asia (Xu et al. 2010).

1.3 Past Studies of Lightning Outside Convective Regions of Thunderstorms

Observations of the electrical structure of storm systems were not just limited to convective regions. Rutledge and MacGorman (1988) observed lightning flashes in a large, 80 km across, stratiform region associated with the large MCS observed during the PRE-STORM project. These flashes were primarily positive CG flashes, and their results led them to propose a relationship between the areally integrated stratiform precipitation and positive CG flash frequency.

There has been much speculation as far as the roles of the different charging mechanisms in developing charged regions outside the convective core. Regions outside of the convective core are often referred as the "anvil" region. However, there are differences between the raining (stratiform) and nonraining areas within the broad anvil in regards to both precipitation structure, and electrification processes. A large MCS is shown in Figure 1.1. This MCS consists of a number of convective cells (Figure 1.1c) with a large region of stratiform rain behind them (Figure 1.1d). There is also an extensive region with no precipitation that still lies within the cloud shield (Figure 1.1b and d). Figure 1.2 shows a cross section starting in this region, crossing a convective cell and ending in the stratiform region (indicated as a solid line in Figure 1.1). The non-raining anvil region has little reflectivity within the sensible range of the PR in this case, despite cold infrared cloud-top temperatures. The raining anvil, or stratiform region, on the other hand, lies behind the convective line, and contains modest-to-moderate radar echoes well above the freezing level, including a radar bright band in regions of melting

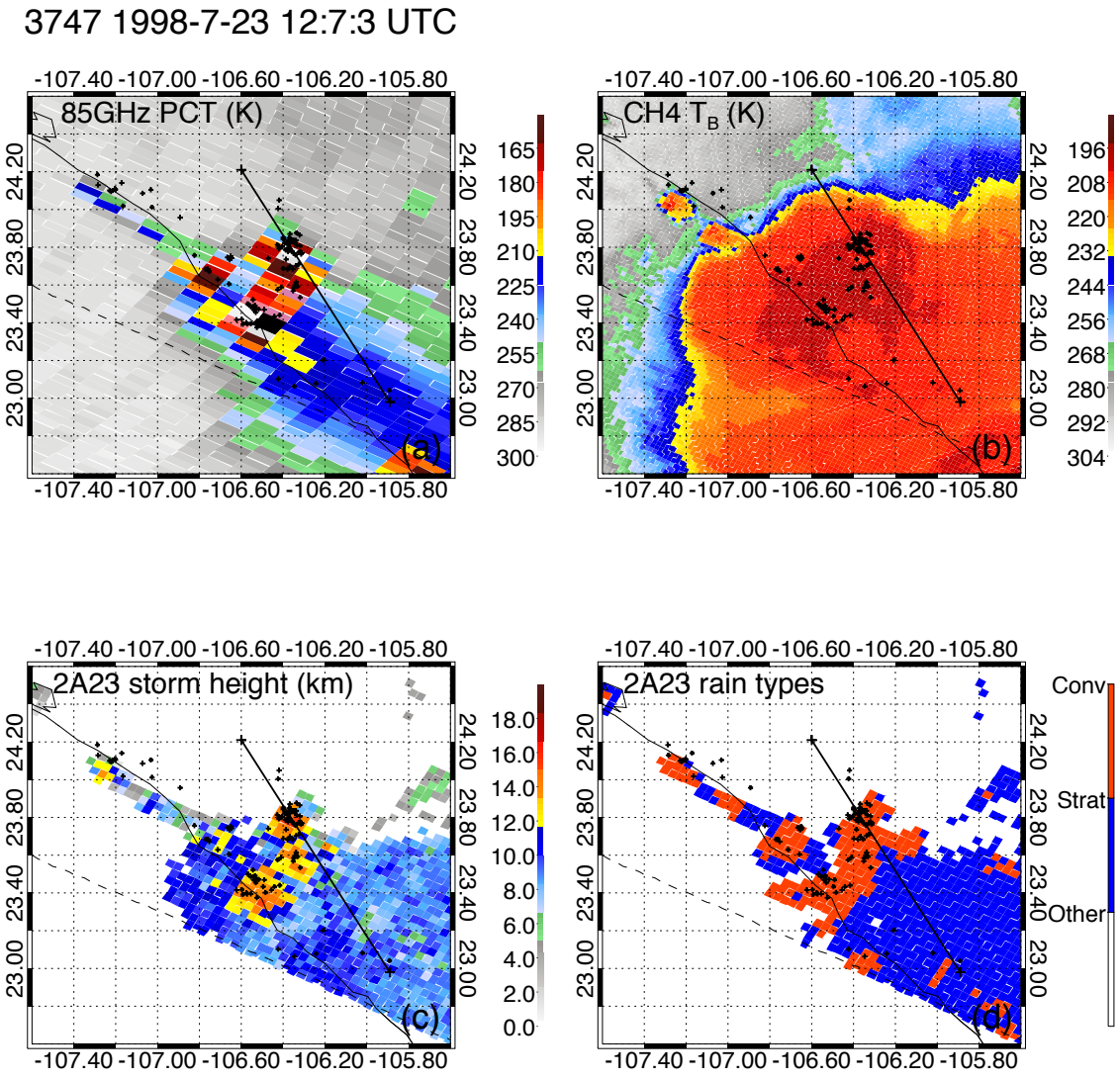

Figure 1.1 The structure of a mature MCS with a sizable stratiform region. a) TRMM TMI 85 GHz Polarization Corrected Temperature (PCT) (Spencer et al. 1989); b) VIRS infrared brightness temperature; c) PR echo top height; d) PR 2A23 convective/stratiform classification. Small plus signs indicate the locations of individual lightning flashes, and the black line indicates a cross section through the convective region of the storm.

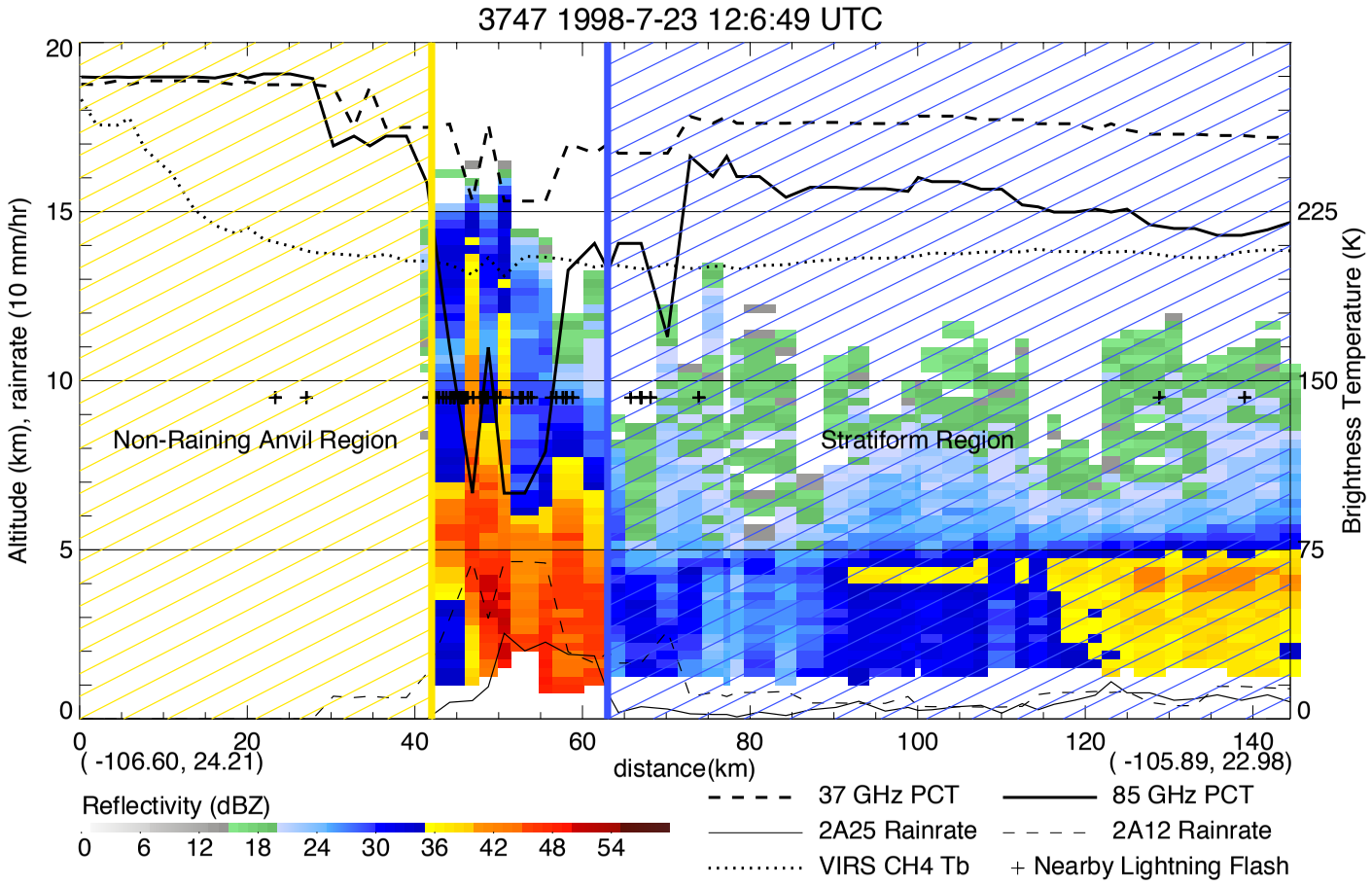

Figure 1.2 Cross sections of PR reflectivity (colored pixels), TMI 85 GHz PCT (thick solid line), TMI 37 GHz PCT (thick dashed line), TMI 2A12 rain rate (thin solid line), PR 2A25 rain rate (thin dashed line), and VIRS infrared brightness temperature (dotted line). Lightning flashes close to the cross section line indicated as the solid line in Figure 1.1 are shown as black plus signs. Thatched regions correspond to the nonraining anvil region (yellow) and stratiform region (blue) along this cross section.

hydrometeors. Since bright bands such as this contain mixed-phase precipitation, they are thought to be significant sources of charge by in situ charge generation (Rutledge and MacGorman 1988), which may be enhanced by mesoscale updrafts within the stratiform region (Ely et al. 2008; Lang and Rutledge 2008).

Observations of the charge structure within the stratiform region reveal that charge in this region is often concentrated in several vertically stacked, horizontally broad layers of opposing polarity that are thought to serve as conduits for lightning propagation. In one case, Carey et al. (2005) used radar reflectivity and Dallas-Ft Worth LDAR composites to examine lightning flash locations relative to storm structure for an MCS on June 16th, 2002. A positive charge zone was detected that penetrated through the transition zone and into the stratiform region. A number of positive CG lightning flashes were observed that initiated in the convective region and progressed into the stratiform region following this sloping pathway, which matches hypothetical trajectories taken by snow particles.

As many as six of these stacked layers have been observed in nature, often more than 100 km across (Marshall and Rust 1993; Stolzenburg 1994; Lang et al. 2004; Marshall et al. 2009). This layered structure has been successfully reproduced in computer simulations of charging mechanisms (Schuur and Rutledge 2000), which indicate that the uppermost three are the result of charge advection from the convective core, while the lowest two are primarily the result of mixed-phase processes within the stratiform region itself.

Unlike the stratiform region, the nonraining anvil region (referred to as just the anvil region from here on out) typically does not have moderate reflectivity in the mixed-

phase region, and therefore, is thought to accumulate charge primarily as the result of advection from the convective core. Anvil regions can include both overhanging anvil clouds out in front of a convective system or behind the stratiform region. The charge structure of anvil clouds can also be quite complex, with the advected charge being concentrated in a narrow layer in the middle of the anvil and the formation of screening layers of opposite polarity along its lower and upper boundaries. Negative screening layers were proposed by Marshall et al. (1989), but were not always observed in subsequent studies. Charge advection in anvil clouds was also found to not be continuous in time and to not occur throughout the entire anvil (Dye et al. 2007). Neighboring charged anvil clouds have also been found to interact with one another, and in one case, two anvil clouds of opposite polarity were able to produce lightning flashes up to 60 km from the storm core (Kuhlman et al. 2009).

1.4 Motivation and Objectives of this Study

Each of the past studies on lightning outside the convective core is based on the results of analyzing ground-based observations. Moreover, most of these studies rely on a mere handful of lightning flashes in a small number of convective systems over a few key regions of the world. Satellite observations have the potential to address these limitations, yet so far there has been no global study on the lightning in the stratiform or anvil regions. The goal of this study is to fill this gap by using 12 years of observations from the TRMM satellite.

Specifically, the present study seeks to address the following questions:

- How common are stratiform and anvil flashes globally?

- Where do stratiform and anvil flashes tend to occur? Are there significant land-sea or regional differences?
- When are stratiform and anvil flashes likely to occur? Are there significant seasonal or diurnal cycles in stratiform or anvil lightning production?
- What types of thunderstorms have stratiform and anvil lightning? Can we identify them based on their convective intensity?
- Where do stratiform and anvil flashes occur with regards to storm structure? How far away from convection do they occur?

The last two questions are particularly important with regards to aviation safety, which is an area of interest of this study. The weather radar onboard aircraft usually can detect and give threat warning of convective cores with high radar reflectivity at flight level. However, relatively lower radar reflectivities at altitudes in the stratiform and anvil regions are usually treated as a safe zone. Given that lightning flashes have been observed to propagate over large distances through the stratiform region and between charged anvils, there may still be the potential for lightning to strike an aircraft in these regions. Identifying storms where this situation might arise is therefore very useful from a practical standpoint.

To address these questions, 12 years of TRMM PR, TMI, VIRS and LIS observations are used to identify stratiform and anvil flashes. The regions where charge generation is likely are identified. The relationship between the properties of these regions and the nearby flashes are examined. The procedure by which this is carried out and specifics on the definitions used to identify stratiform and anvil flashes is described in detail in Chapter 2. Results including the statistics of stratiform and anvil flashes

around the globe and their relationship to the properties of nearby convection is discussed in Chapter 3.

TRMM can only observe snapshots of individual convective systems. However, it is important to understand the lightning in the stratiform and anvil regions at different stages of the life cycle of the thunderstorms. Therefore, in addition to TRMM statistics, case studies are performed by using C-band polarimetric radar and LINET observations during the Tropical Warm Pool International Cloud Experiment (TWP-ICE) field campaign (May et al. 2008). Since ground-based observations are not directly comparable with TRMM, a slightly different methodology is used, which is described in Chapter 4. Then, in Chapter 5, stratiform and anvil flashes are examined in the context of the life cycles of convection through case studies of individual convective systems that occurred during the TWP-ICE field campaign. Finally, the major conclusions are summarized in Chapter 6.

CHAPTER 2

TRMM DATA AND METHODOLOGY

TRMM satellite observations are suitable for the examination of lightning with respect to storm structure due to the various sensors onboard. As mentioned in Chapter 1, the TRMM sensor package includes the Lightning Imaging Sensor (LIS), the TRMM Microwave Imager (TMI), the Precipitation Radar (PR), and the Visible and Infrared Scanner (VIRS). Using observations from these sensors, it is possible to discriminate lightning flashes from LIS relative to the three-dimensional structure of storms over the tropics using PR reflectivity, VIRS infrared brightness temperatures, and TMI microwave polarization-corrected brightness temperatures (PCTs, Spencer et al. 1989). A number of past studies have used TRMM observations to examine relationships between flash counts and storm properties (Toracinta et al. 2002; Petersen et al. 2005; Cecil et al. 2005; Takayabu et al. 2006; Xu et al. 2010), but these studies did not take advantage of PR observations to examine the locations of lightning flashes with respect to storm structure, particularly the differentiation of lightning flashes in convective versus stratiform areas.

In this study, 12 years (1998-2010) of TRMM PR, TMI, VIRS, and LIS observations are used. The process used in this study for obtaining the statistics of stratiform and anvil flashes and statistics of the properties of nearby storms with flashes in these regions from TRMM observations is presented in Figure 2.1. First, data from the

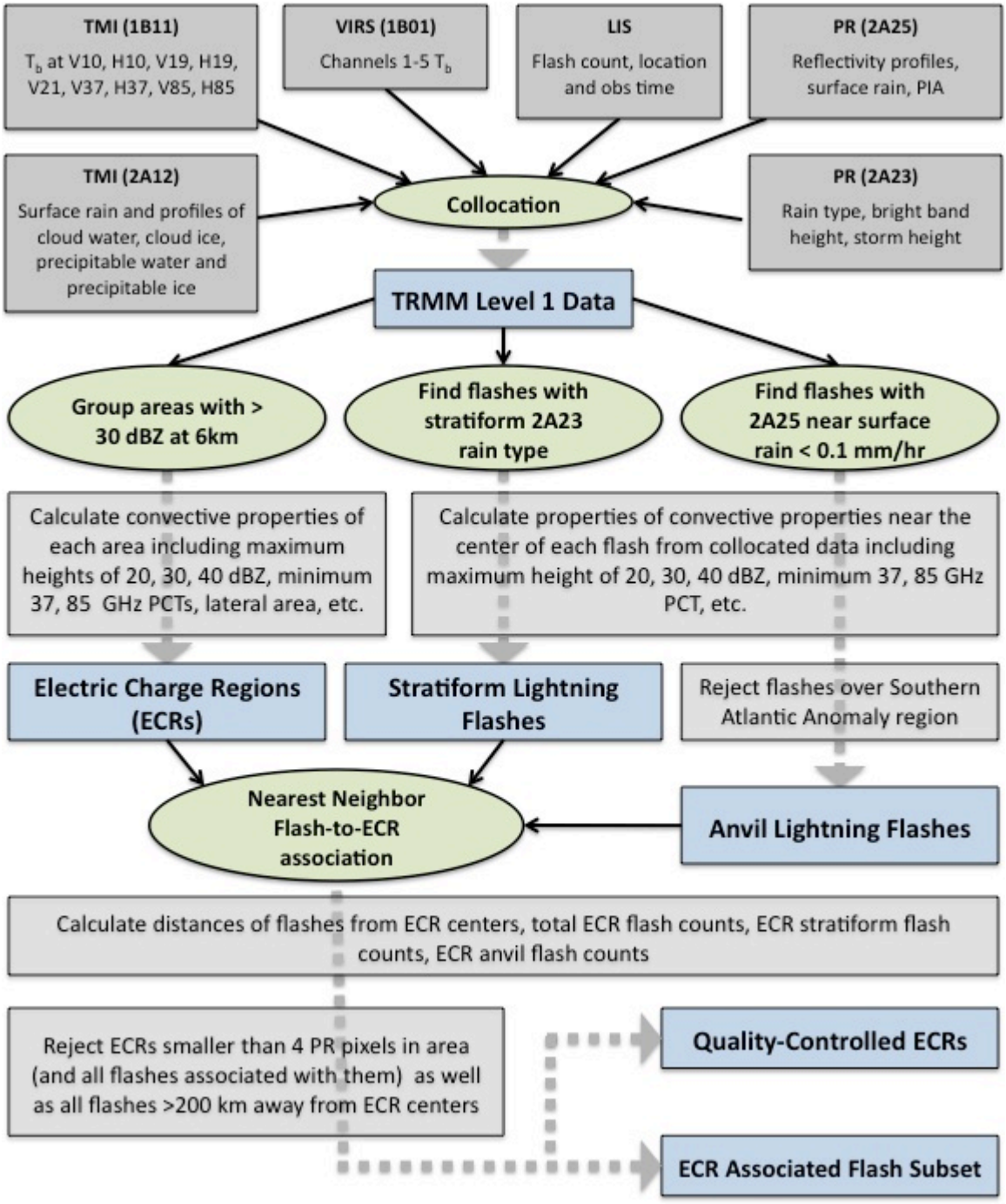

Figure 2.1 Flowchart depicting the processes by which TRMM data are manipulated in this study.

PR, TMI, VIRS, and LIS sensors need to be collocated spatially since each of these sensors has a different horizontal resolution and scan orientation (Kummerow et al. 1998). This collocation is accomplished by defining a common sample volume and a unified coordinate system, which is PR pixel in this case. LIS lightning flashes and VIRS infrared brightness temperatures are assigned to a PR pixel by the nearest neighbor method (Nesbitt et al. 2000; Liu et al. 2008). Collocation between the TMI and PR, however, is more complicated. In addition to the different incidence angles, the spatial resolution of the TMI varies greatly with wavelength. While the instrument field of view is smaller than the distance between scans at 85 GHz, the field of view is much larger at lower frequencies (Kummerow et al. 1998), resulting in oversampling, especially in the 10 GHz channel. The nearest neighbor method is also employed in the collocation of PR and TMI pixels; however, multiple PR pixels are assigned to a single TMI pixel due to the differing spatial resolutions (Liu et al. 2008).

An additional correction must be made in TMI-PR collocation due to the conical scan of the TMI. The 52^{o} inclination can cause problems in the case of microwave scattering by elevated hydrometeors. In order to compensate for this effect, a simple parallax correction is used which moves the TMI coordinates backwards or forwards one scan, depending on the orientation of the scan. This improves the agreement between the TMI, PR, and VIRS for strong convective systems, but induces errors when observing small, shallow precipitation systems (Liu et al. 2008). The collection of collocated data is called TRMM Level 1 data, which is used in the next step of defining stratiform and anvil flashes, and identifying regions likely containing significant amounts of charge aloft.

2.1 Definitions of Stratiform and Anvil Lightning Flashes

In order to define lightning flashes that occur in the stratiform and anvil regions of storms, as well as address the limitations of these definitions, it is necessary to understand how the LIS observes lightning flashes from space. The TRMM LIS is a staring optical transient detector that determines lightning flashes by looking for rapid changes in cloud illumination at the 777.4 nm atomic oxygen emission wavelength, characteristic of lightning. The use of this band allows flashes to be detected day or night. The LIS is made up of a 128x128 charge-coupled device (CCD) imaging array with a 2 ms update rapid scan (Boccippio et al. 2000). The preboost spatial resolution of the LIS is approximately 5 km, compared to the 4 km PR footprint. Since the LIS can only see a particular point for roughly 80 seconds, the minimum detectible flash rate is about 0.7 flashes/minute (Cecil et al. 2005). The LIS is thought to have an 85% detection efficiency (Boccippio et al. 2002), can miss isolated lightning flashes, and has difficulty distinguishing individual flashes in storms with very high flash rates (Cecil et al. 2005).

The locations of LIS-detected flashes are defined as the centers of illuminated area, not by the point of initiation or termination. Because of this, if a flash spans a large area, the properties near its center may be very different than those at its initiation and ending locations. Also, despite quality control algorithms to remove noise and false flashes, the South Atlantic Anomaly – or, the region of the earth over which the Van Allen radiation belt reaches below 200 km from the Earth's surface, affecting satellites in near earth orbit – produces some interference (Boccippio et al. 2000; Boccippio et al. 2002), though for most purposes, these artifacts have a negligible effect on the total statistics.

Flashes in the stratiform and anvil regions are distinguished from those in the convective core by examining the PR reflectivity profiles near the center location of each flash reported by the LIS. The 2A23 rain type algorithm (Awaka et al. 1998) uses three-dimensional PR data to classify PR pixels as stratiform, convective, or other. Flashes centered in regions where the 2A23 output ranges from 100 (certainly stratiform) to 159 (the scale goes to a maximum of 199 meaning possibly stratiform, but rain not expected at the surface) with rain detected near the surface are deemed stratiform. However, due to the sensitivity of the TRMM PR, light rain corresponding to rain rates of less than ~0.1 mm/hr is not detected (Iguchi et al. 2000). In this study, no distinction is made between the leading convective anvil and the trailing anvil behind the stratiform region. Unlike stratiform flashes, no 2A23 rain type criteria are imposed on the determination of flashes in the anvil region. Anvil flashes are defined as lightning flashes centered over regions with no detectible near surface rain rate (e.g., rain rates less than this minimum threshold of 0.1 mm/hr).

A number of quality control steps must then be performed due to the limitations of the data set and the above definitions. First, since the LIS has a much wider swath than the PR, and the discrimination of lightning depends on PR observations, all flashes that occur outside the PR swath are omitted from the sample. Also, since the anvil flash definition requires no detectible PR near surface rain rate, the erroneous flashes caused by interference from the South Atlantic Anomaly is amplified to the point that these flashes make up a sizable percentage of the sample. For this reason, all anvil flashes in the affected region are eliminated when discussing the global statistics. Lastly, normalization has been applied in order to correct for the known latitude-dependent

sampling bias of TRMM.

After these flashes are identified, the properties of PR and TMI at the centers of each flash are summarized. A summary of the calculated flash center properties is presented in Table 2.1.

2.2 Electric Charge Region (ECR) Definition

Previous studies examining lightning production using TRMM observations either accumulate individual pixels to grids without considering the convective system as a whole (e.g., Petersen et al. 2005; Takayabu et al. 2006), or using the properties of precipitation features without considering the detailed structure of the various convective regions in the precipitating area (Toracinta et al. 2002; Cecil et al. 2005; and Xu et al. 2010 among others). However, many thunderstorms are quite large, often encompassing multiple individual cells, and while this approach may be sufficient when only total flash counts are considered, it may be important to resolve convective features on a smaller scale when taking into account the locations of individual lightning flashes.

For instance, a large MCS that was observed in 2004 over central Africa is shown in Figure 2.2. While the entire MCS constitutes a single precipitation feature, individual convective regions within this system can be observed, and are outlined in white on Figure 2.2d. Since this MCS is a multicell system dominated by one large, intense convective cell containing most of the lightning flashes, many of the proxies of convective intensity (minimum TMI brightness temperatures, maximum heights of PR echoes) would relate all of the flashes within the feature to the strength of this large cell. Flashes outside this cell, however, are more likely to be related to the convective

Table 2.1 List of available properties near the location of LIS-observed lightning flashes obtained from TRMM level 1 data.

Parameter	Description
PR-Based	
Echo Top (maxht15)	Maximum height of PR echo
20 dBZ Echo Top (maxht20)	Maximum height of 20 dBZ echo
30 dBZ Echo Top (maxht30)	Maximum height of 30 dBZ echo
40 dBZ Echo Top (maxht40)	Maximum height of 40 dBZ echo
Near Surface Rain (nearsurfrain)	2A25-derived near surface rain rate
Near Surface Z (nearsurfz)	2A25-derived near surface reflectivity
Rain Type (raintype)	2A23-derived rain type
Storm Height (stormh)	2A32-derived storm height
TMI-Based	
37 GHz PCT (pct37)	37 GHz polarization corrected temperature
85 GHz PCT (pct85)	85 GHz polarization corrected temperature
VIRS-Based	
Channel 4 T_b (virsch4)	VIRS 10.8 μm wavelength brightness temperature

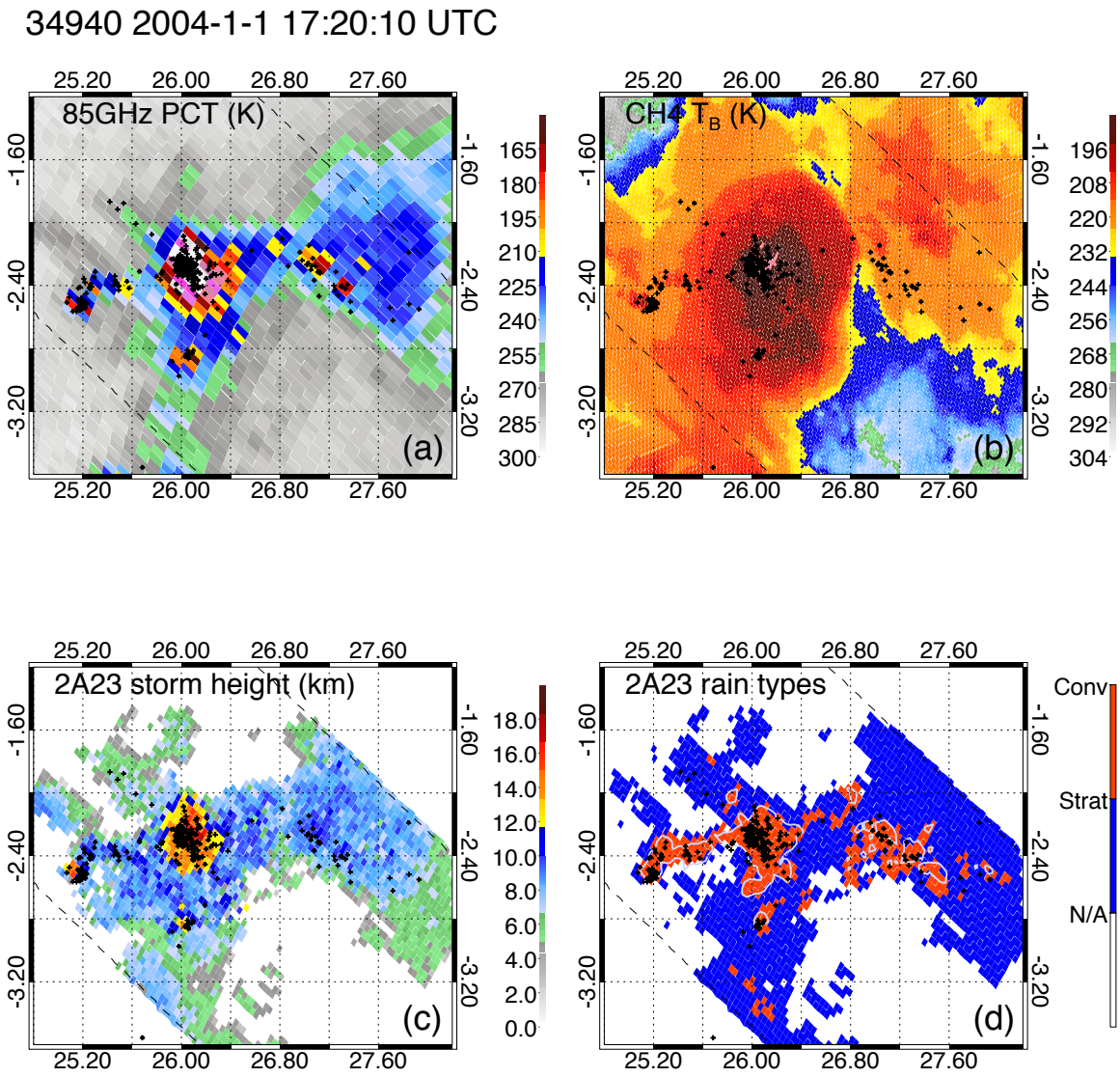

Figure 2.2 An example of locations of lightning flashes (black dots) in an MCS over central Africa in 2004. a) TRMM TMI 85 GHz Polarization Corrected Temperature (PCT) (Spencer et al. 1989); b) VIRS infrared brightness temperature; c) PR echo top height; d) PR 2A23 convective/stratiform classification. White contour is area with PR reflectivity > 30 dBZ at 6 km. Note that most lightning flashes are within convective area, but there are a few flashes over the stratiform region.

properties of other, nearer, convective cells rather than this one area of intense convection.

For this reason, a new approach must be employed to identify charging regions on smaller scales. However, identifying these regions is not merely a matter of convective/stratiform separation. Instead, a better candidate would be able to identify regions where charge separation is taking place. However, since TRMM has no way of observing electric fields from space, we have to settle for identifying regions where there is the *potential* for charge separation. To do this, we employ a similar methodology used by Marshall and Radhakant (1978). The idea here is to look for regions of moderate reflectivity in the mixed-phase region, indicative of the presence of graupel, a key ingredient in the noninductive charging mechanism (Takahashi 1978; Jayaratne et al. 1983; Saunders et al. 1991). Since the presence of graupel in the mixed-phase region potentially correlates with the presence of charge separation, these regions will be referred to as Electric Charge Regions (ECRs).

In this study, ECRs are arbitrarily defined as contiguous regions where 30 dBZ echoes exceed 6 km, which is consistent with Marshall and Radhakant (1978), and the characteristics of each ECR are summarized. The available convective and physical characteristics of these ECRs are listed in Table 2.2. But, what exactly is an ECR, and, more importantly, what are they not? Since no TRMM 2A23 rain type restriction is placed on the ECR definition, an ECR can consist of both convective and stratiform areas defined by TRMM 2A23 rain type algorithm, so long as 30 dBZ echoes exceed 6 km. The stratiform fractions of the ECRs used in this study are summarized in Table 2.3. While ECRs can include regions with stratiform precipitation in nature, a dominant

Table 2.2 List of available convective and physical properties of ECRs obtained from TRMM level 1 data.

Parameter	Description
PR-Based	
Area	ECR size
Flash Count in ECR (flashcount)	Number of lightning flashes within ECR size
Land/Ocean (landocean)	ECR centered over land or over the ocean
Echo Top (maxht)	Maximum height of PR echo in ECR
20 dBZ Echo Top (maxht20)	Maximum height of 20 dBZ echo in ECR
30 dBZ Echo Top (maxht30)	Maximum height of 30 dBZ echo in ECR
40 dBZ Echo Top (maxht40)	Maximum height of 40 dBZ echo in ECR
Number of ECRs (ncell)	Number of ECRs embedded in the continuous rain region, called radar precipitation feature (RPF).
View Time (viewtime)	Length of time during which the ECR was observed by TRMM
TMI-Based	
Minimum 37 GHz PCT (min37pct)	Minimum 37 GHz polarization corrected temperature in ECR
Minimum 85 GHz PCT (min85pct)	Minimum 85 GHz polarization corrected temperature in ECR
Area with 85 GHz PCT less than 150K (nlt150)	Area within the ECR with 85 GHz PCTs less than 150K.
Area with 85 GHz PCT less than 200K (nlt200)	Area within the ECR with 85 GHz PCTs less than 200K.
VIRS-Based	
Minimum IR (minir)	Minimum VIRS Channel 4 brightness temperature

Table 2.3 Stratiform fractions in ECRs with at least 4 PR pixels over land and over the ocean. ECR samples in the subtropics during the winter are excluded.

Stratiform Fraction of ECRs	< 20%	20-50%	50-80%	>80%
All	84.60%	12.90%	1.69%	0.80%
Land Only	87.39%	10.90%	1.16%	0.55%
Ocean Only	81.14%	15.39%	2.35%	1.12%
All with Flashes	92.16%	7.35%	0.41%	0.08%
Land Only with Flashes	91.60%	7.81%	0.48%	0.10%
Ocean Only with Flashes	93.84%	5.93%	0.21%	0.02%

portion of them are convective. In fact, 84.6% of ECRs are almost entirely convective overall, and 92.2% of ECRs with lightning are also primarily convective. On the other hand, less than 1% of ECRs are almost entirely stratiform. Only 0.08% of ECRs with lightning are made up of more than 80% stratiform area. Therefore, it is clear that most ECRs are dominated by convective regions, but since the sample includes some parts of the stratiform region and does not include shallow convection, the term "ECR" is not synonymous with "convective cell".

There are some drawbacks to using a constant-altitude definition, however, particularly in the case of subtropical wintertime lightning storms. This type of definition is invalid in these circumstances because the height of the freezing level is significantly lower during the winter than it is during the summer. The height of 6 km no longer corresponds to around -10^{o} C and may not be within the mixed-phase region. Since the freezing level is lower in the winter in these regions, many convective regions do not meet the ECR definition employed in this study, resulting in a higher fraction of lightning outside ECRs. This can be seen in Figure 2.3, which examines the seasonal cycles of the 20 and 30 dBZ echo tops at the lightning flash locations over the northern Atlantic (25° N - 36° N, 40° W - 74° W; Figure 2.3a,c) and the northern Pacific (25° N - 36° N, 144° E - 170° E; Figure 2.3b,d).

As shown in Figure 2.3a, and especially 2.3b, there is a significant oscillation in the 20 dBZ echo tops at the center locations of lightning flashes throughout the year in these two regions. Echo tops in regions where lightning occurs over the northern Atlantic are up to 2 km lower in the winter than the summer, while the summer-winter difference over the northern Pacific exceeds 4 km. This means that winter storms are substantially

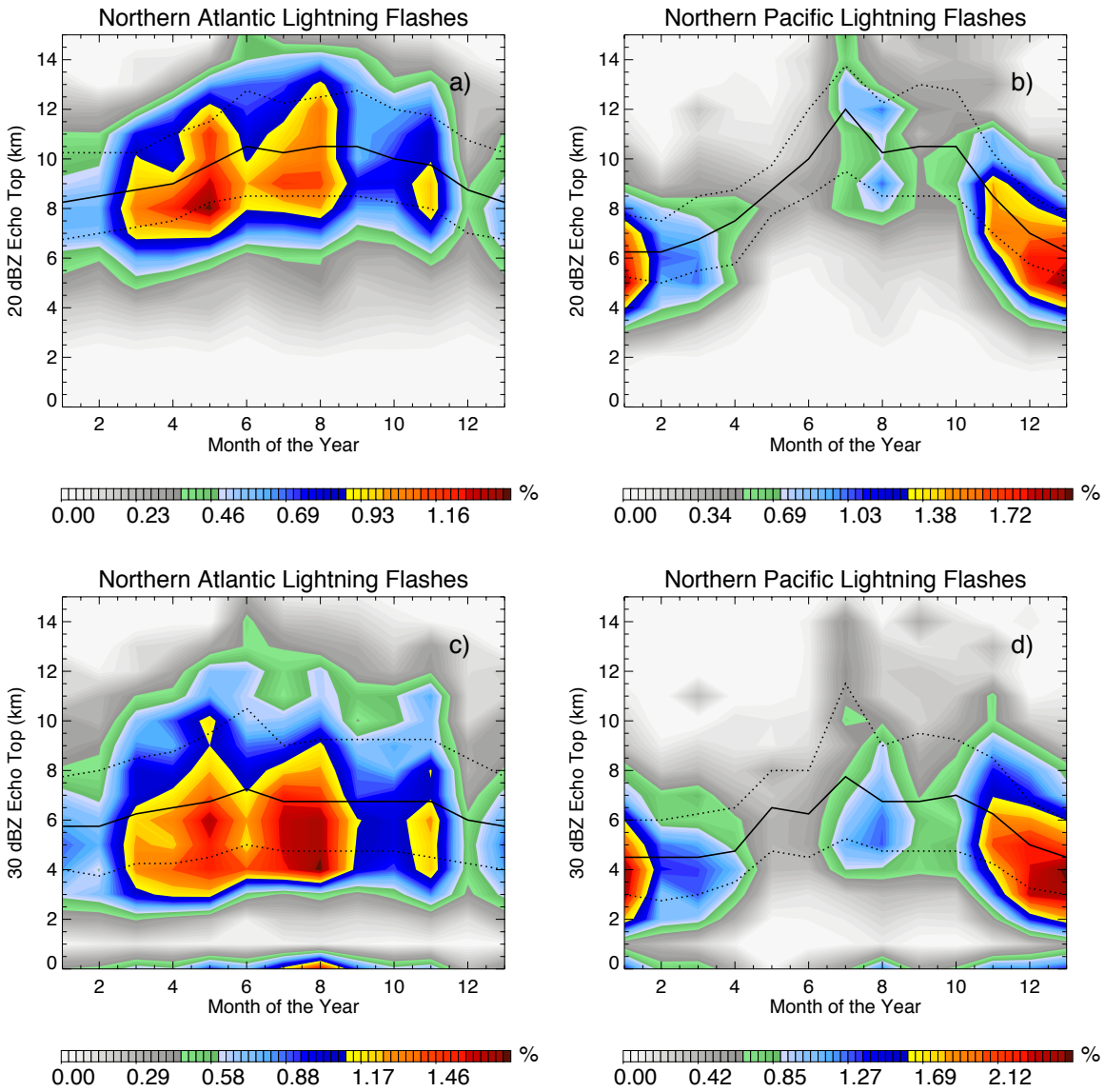

Figure 2.3 The seasonal cycles of 20 dBZ echo tops at the locations of lightning flashes a) over the northern Atlantic and b) northern Pacific regions outlined in Figure 3.1c, as well as the seasonal cycles of 30 dBZ echo tops at the locations of lightning flashes c) over the northern Atlantic and d) northern Pacific. Two-dimensional histograms are shaded, and the weekly median, 25th percentile, and 75th percentile are overlain.

more compact than summer storms in these regions, resulting in a winter bias to lightning flashes in regions that do not meet the ECR definition. This is clear from looking at the seasonal cycle of 30 dBZ echo tops over the northern Atlantic (Figure 2.3c) and northern Pacific (2.3d). These two regions correspond to maxima in lightning flashes outside ECRs, which are shown in these seasonal cycles. In both regions, the majority of lightning flashes occur outside ECRs, particularly over the northern Pacific, where more than 75% of its winter lightning occurs outside ECRs. The seasonal cycle is not so drastic for lightning flashes over the northern Atlantic, which sees most of its lightning during the warm season; however, the oscillations that are evident still beg the question of whether these storms should remain in the sample. While the inclusion of these regions hardly affects the global statistics of lightning and ECRs, wintertime subtropical ECRs and lightning flashes have been removed as a quality control measure when the statistics of ECRs are discussed in the latter part of Section 3 (3.3-3.5).

2.3 Flash-to-ECR Association

In order to investigate the relationship between the flashes and the convective properties of the nearby convective regions, each lightning flash is then associated with a nearby ECR using the nearest neighbor method. While it is impossible to say with any certainty that these associations represent the true source of charge for the lightning flashes, particularly because TRMM only sees a snapshot of convection and lightning is defined as a point at the center of illumination, it is still useful to examine the properties of nearby convection at the time of lightning occurrence. This is particularly useful for aviation safety applications.

In order to investigate the representative convective regions and the flashes they might have generated, small ECRs with less than 4 PR pixels (~80 km^2) and all lightning flashes associated with them are omitted when discussing relationships between ECRs and lightning flashes. This is based on the assumption that tiny areas of convection and artifacts within the stratiform region likely are not major contributors to the charge structure of the overall convective system. However, this may not be true for the dissipating convective region where only a tiny area with convective characteristics remains, yet there is still a significant amount of charge aloft over the region. Since one main purpose of this analysis is to investigate if there is a way to estimate the probability of stratiform and anvil lightning only based on the properties of nearby convection, only ECRs with at least a few pixels are used in the analysis at the moment.

Also, lightning flashes that occur at incredible distances (> 200 km) from the nearest ECR are omitted. This filter also prevents contamination from bad associations resulting from missing PR data and situations arising from flashes being generated from convective systems just outside the PR domain.

After applying these filters, the sample of lightning flashes is reduced to 64% of its original size. However, despite these reductions, the subset includes over 3.9 million flashes, which is still robust. The reduction in sample size is not the same for each type of lightning, however. While the sample is reduced to 64% of its original size for all flashes, only 62% of anvil flashes and 47% of stratiform flashes remain after filtering. The largest cause for the disproportionate removal of stratiform and anvil flashes is the 4 PR pixel minimum ECR size restraint. While it does a good job in removing small ECRs embedded within the stratiform region, stratiform flashes near these small ECRs are also

removed. Despite these reductions, there are still 150,000 to 200,000 flashes of each type in the subset. This subset will be employed when discussing the properties of ECRs near lightning flashes, and will be denoted “associated flashes” to avoid confusion. Note that this subset is only used to discussing the properties of ECRs in the section 3.3, 3.4 and 3.5.

CHAPTER 3

TRMM STATISTICS

3.1 Global Statistics of Stratiform and Anvil Flashes

The global statistics of all lightning flashes, those in the stratiform, and those in the anvil region are summarized in Table 3.1. In the total, about 6 million lightning flashes were observed from 1998 to 2009 and between 36°N and 36°S, yet stratiform and anvil flashes make up only a small percentage (5-7%) of them. Stratiform flashes appear to be slightly more common than anvil flashes. For each type of flash, lightning is more common over land than over the ocean. The land-sea ratios are slightly higher for anvil lightning (4.7:1) and significantly lower for stratiform flashes (3.0:1). This is because stratiform flashes account for a slightly higher fraction of oceanic lightning (7.57%), and a slightly lower fraction of lightning over land (5.64%). The opposite is true for anvil flashes, which account for a higher fraction of flashes over land (5.51%) and over the ocean (5.22%).

The global distribution of lightning is shown in Figure 3.1a. Lightning is common in a number of key regions around the world, including but not limited to the Congo Basin in Africa, Argentina, Colombia, northern India, Bangladesh, the Maritime Continent, and the southeast United States, which is consistent with earlier studies (e.g., Christian et al. 2003; Zipser et al. 2006). However, certain regions are more likely to see

Table 3.1 Global statistics of all lightning within the PR swath between 36^{o} N and 36^{o} S characterized by type from observations between 1998-2009. These statistics have been normalized by total sampled pixels at different latitudes to counteract sampling bias. Anvil flashes over the region with interference of the South Atlantic Anomaly (shown in Figure 3.2.b and d) are not counted.

	Global		Land Only		Ocean Only	
	Count	%	Count	%	Count	%
All	5934492		4840322		1094205	
Anvil	324052	5.46	266894	5.51	57160	5.22
Stratiform	334660	5.64	251818	5.20	82844	7.57

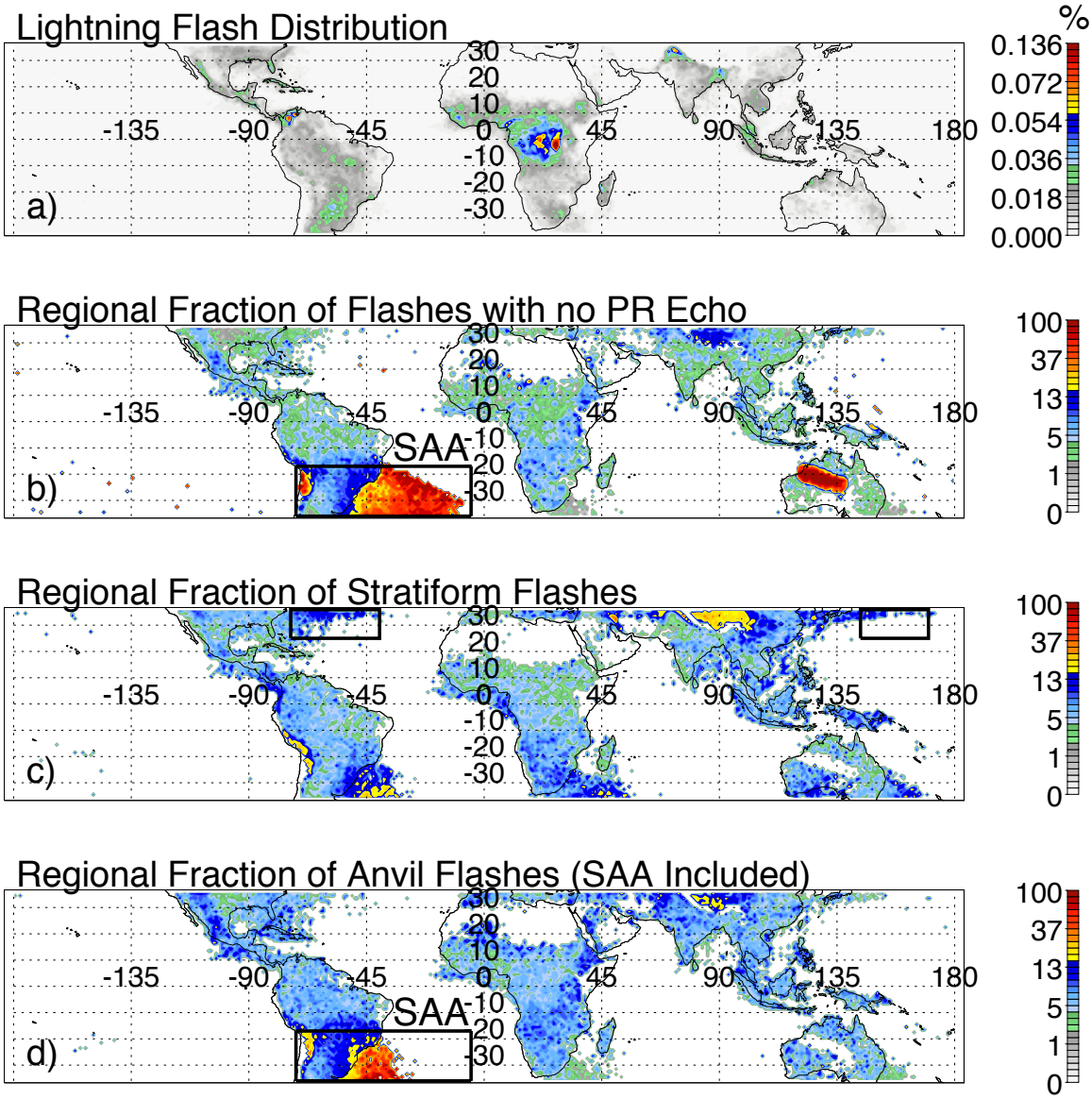

Figure 3.1 Global distribution of a) lightning flashes, and the regional fractions of b) flashes centered over areas with no PR echo, c) flashes in the stratiform region, and d) anvil lightning flashes in 1° by 1° boxes. The region most affected by the South Atlantic Anomaly has been outlined and labeled "SAA," and two regions with large fractions of stratiform flashes offshore are outlined for later discussion. Note that due to no PR observations over central-west Australia, this region has been removed from the sample, except in panel.

stratiform or anvil lightning than others. As seen in Table 3.1, high stratiform lightning fractions can be seen in a number of oceanic regions in Figure 3.1c (this remains the case for many regions in the open ocean, but not enough samples were available in these regions for them to be shown in this figure, and the overall stratiform fraction of all open ocean regions is 10.17%). While the fraction of stratiform lightning over most land-based regions ranges from 4-8%, the stratiform fraction reaches above 13% off the east coasts of major continents in the subtropics, and off the west coasts of Central America and Africa in the tropics, as well as the Bay of Bengal and the Maritime Continent. Many of these storms, particularly those close to shore, are likely the result of convective systems moving offshore along the prevailing winds as they mature. However, this is not the only explanation, as stratiform lightning accounts for a high percentage of lightning far offshore. These stratiform flashes, particularly in the two boxed regions over the northern Atlantic and northern Pacific in Figure 3.1c, are likely the result of different regional weather regimes. Over land, stratiform lightning is about 5% of total lightning flash everywhere, except over the Andes and the Himalayas, where stratiform flashes tend to be quite common (Figure 3.1 c). This is likely due to misclassifications of shallow convection over high-terrain regions as stratiform by the 2A23 rain type algorithm (Fu and Liu 2007).

Before discussing the statistics of anvil lightning, two important sources of artifacts should be discussed. The first is the South Atlantic Anomaly (SAA). As TRMM flies through this region where the innermost planetary radiation belt is abnormally low, high signal-to-noise ratios in LIS observations occur, resulting in random artifact lightning flashes. The effect of this interference is evident in Figure 3.1b, which shows

the regional fractions of lightning flashes within the PR swath where there is no PR reflectivity detected at the flash center. While only a few percent of lightning flashes in most regions of the world are centered in regions with no PR echo, a significant fraction of lightning flashes have no PR echo over Southern South America and the adjacent Atlantic coast. Most of these flashes are likely clear air artifacts caused by interference from the SAA. Fortunately, the total number of these flashes is quite small, so this effect does not have large impact on the total flash count. However, as seen in Figure 3.1d, these artifacts can lead to a large uncertainty in the statistics of a small subset of lightning flashes, such as anvil flashes which require weak radar echoes at flash locations such that the derived near surface rain rate is zero. Because of this, anvil flashes over this region (17°-72° W, 17°-36° S) are removed from the global sample, in order to prevent an overestimation of the anvil flashes and any statistical bias that these artifacts may cause. Unfortunately, Argentina is one of the world's most electrically active regions. However, since this removal has only been done for anvil flashes, there is slightly more uncertainty in the numbers and fractions of anvil flashes in the tropics and subtropics shown in Table 3.1.

Another region with unreasonably high fractions of lightning with PR echoes is west central Australia (Figure 3.1b). Unlike the SAA region, all lightning flashes in this region have no PR echoes associated with them, whatsoever. This is because the PR is turned off as TRMM flies over this region in order to avoid interference to surface facilities, as requested by the Australian Government. Since there is no PR data here, all flashes in this region are treated like flashes outside the PR swath, and removed from the samples of each type of lightning.

Like stratiform flashes, anvil flashes are also quite common over mountainous regions, including those mentioned for stratiform flashes as well as across the Rockies and down the Sierra Madres. Anvil flash fractions are also significantly higher over Mozambique and Ethiopia, and desert regions, including parts of the Sahara and western Saudi Arabia and Yemen. Desert regions are less humid, and consequently may have fewer storms, but when storms do occur, extreme amounts of surface heating can possibly lead to some small and isolated, but intense, convective cells. In these cases, if strong updrafts can be generated, they would lead to strong upper-level outflow, and potentially result in more anvil flashes. The statistics in Figure 3.1 were also examined for lightning associated with ECRs larger than 4 PR pixels (not shown), and the regional fractions of stratiform and anvil flashes over these regions were greatly reduced. This indicates that flashes in high terrain regions often occur in small convective systems.

Figure 3.2 shows the seasonal cycles for lightning over the tropics (3.2a and b) and the subtropics (3.2 c and d). In each latitude range, lightning is more common in the summer than the winter; however, the behavior of the fractions of stratiform and anvil flashes varies by region. In the northern tropics (0°-20° N), for instance, the fraction of stratiform flashes hovers around 5% throughout the year, while the fraction of anvil flashes remains fairly constant around 6%. A similar trend exists for the southern tropics (0°-20° S) in Figure 3.2b, but the seasonal cycles are much more noisy. Despite the noise, the stratiform fraction varies on the order of 1% throughout the year, and is slightly lower in the winter than the summer, and lags a month and a half behind the seasonal cycle for all lightning. However, this is insignificant due to the small amplitude and amount of noise visible in the curve.

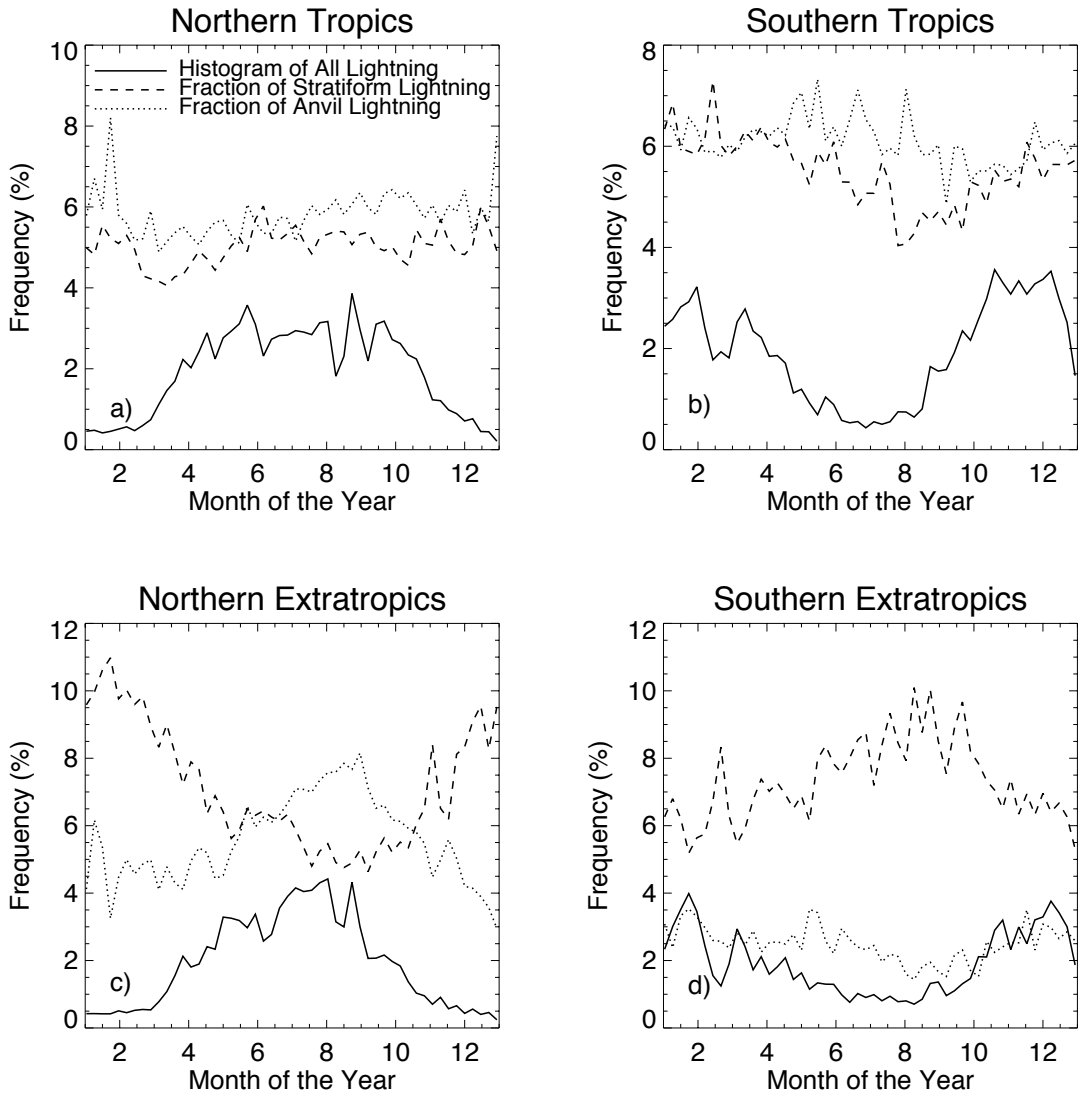

Figure 3.2 Seasonal cycles of all lightning flashes and those over stratiform and anvil regions in a) the northern hemisphere tropics (0°-20°N); b) the southern hemisphere tropics (0°-20°S); c) the northern hemisphere extratropics (20°-36°N); and d) the southern hemisphere extratropics (20°-36°S).

Unlike the tropics, the seasonal variations of the fractions of stratiform and anvil lightning in the subtropics are quite pronounced. As seen in Figure 3.2c, the stratiform fraction of lightning in the northern subtropics (0°-36° N) varies from close to 4% in the summer to a staggering 11% during the winter. At the same time, the anvil flash fraction varies 4% throughout the year, and is both in phase with the seasonal cycle for all lightning, and 6-months out of phase with the stratiform fraction curve. Similar trends can be observed for the southern extratropics (0°-36° S) in Figure 3.2d, though with significantly smaller amplitudes. The stratiform fraction, for instance, only varies 3% throughout the year, though the stratiform fraction is still higher in the winter when there is less lightning and lower in the summer when there is more lightning. The anvil flash fraction, on the other hand, is much lower than in the northern hemisphere, varying between 2 and 3%. This is likely due to the removal of Argentina, one of the key regions for lightning production, and may also be due to the lack of land mass in the southern hemisphere if anvil flashes more commonly occur in deep convection over land.

While Figure 3.2 describes the seasonal cycles for these various latitude belts in general, regional seasonal cycles can be quite different due to the different weather regimes that call each region home. The seasonal cycles of lightning for the two oceanic regions boxed in Figure 3.1c are shown in Figure 3.3. Similar to Figure 3.2c, more lightning is observed over the northern Atlantic region in the summer than in the winter (3.3a). The stratiform flash fraction in this region varies between 7 and 11% throughout the year, and is highest in winter and spring, and lowest in the fall. At the same time, the anvil flash fraction is between 3 and 4% most of the year, but reaches as high as 9% in the late summer.

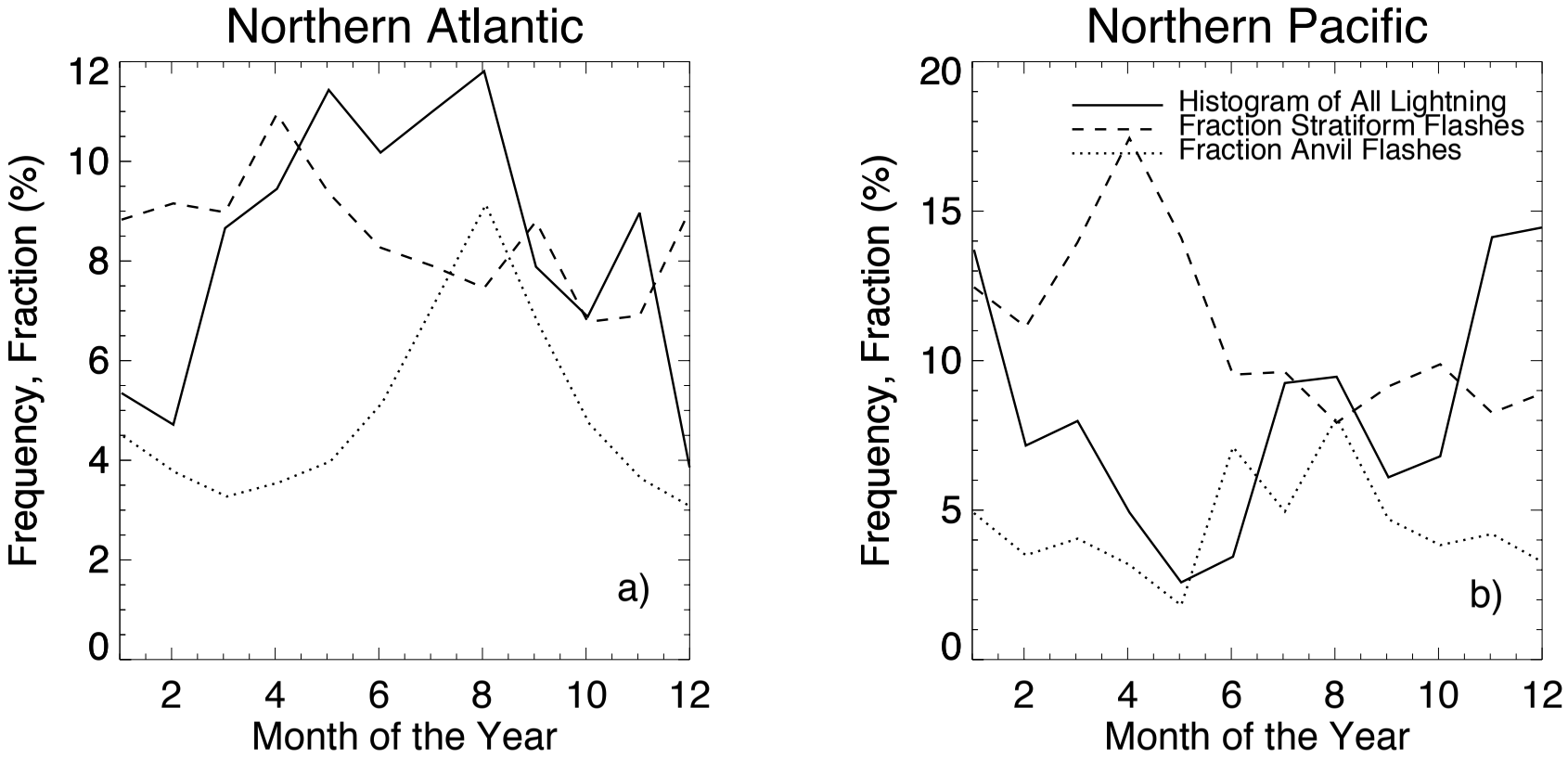

Figure 3.3 Histogram of total lightning flashes and monthly fractions of stratiform flashes and anvil flashes a) the northern Atlantic [25°-36°N, 40°-74°W]; and b) the northern Pacific [25°-36°N, 144°-170°E]. These two regions are boxed in Figure 3.1c.

The seasonal variations of stratiform and anvil flashes over the northern Pacific region (boxed in Figure 3.1c) is very different, however. Here, the seasonal cycle is reversed, and most lightning is observed during the winter rather than during the summer. Stratiform flashes in this region can account for as much as 17% of the total during the spring, while the stratiform flash fraction never falls below 8% over the course of the year. Despite the fact that most flashes occur during the winter, the anvil flash fraction is highest during the summer, and varies between 3% and 7% seasonally.

These regions share many similarities – midlatitude oceanic regions off the east coast of a major continent, over warm ocean currents (Gulf Stream and Kuroshio Current) in lee of a large, cold land mass (Canada and Siberia) – however they exhibit very different seasonal variations. These differences come from the prominence of different weather regimes over these regions. The northern Pacific region is well known for its winter lightning storms, which are the result of two scenarios: cold air outbreaks from Siberia, and typical extra-tropical cyclones. In the case of a Siberian cold air outbreak, freezing levels are quite low, and 20 dBZ echo tops usually occur around just 2 km and hardly any radar echoes can be seen above 4 km (Yamamoto et al. 2006).

Looking to a much shorter time scale, the diurnal cycles of lightning are presented in Figure 3.4 for both lightning over land (3.4a) and over the ocean (3.4b). Most lightning over land occurs in the early afternoon, including stratiform and anvil flashes. However, while the diurnal variation of anvil flashes is in phase with the diurnal cycle of all lightning, stratiform flashes peak nearly 2 hours after the other two. At the same time, anvil flashes over land are more concentrated in the afternoon hours, leading to a diurnal cycle with a larger amplitude than the other two groups. The diurnal cycle for stratiform

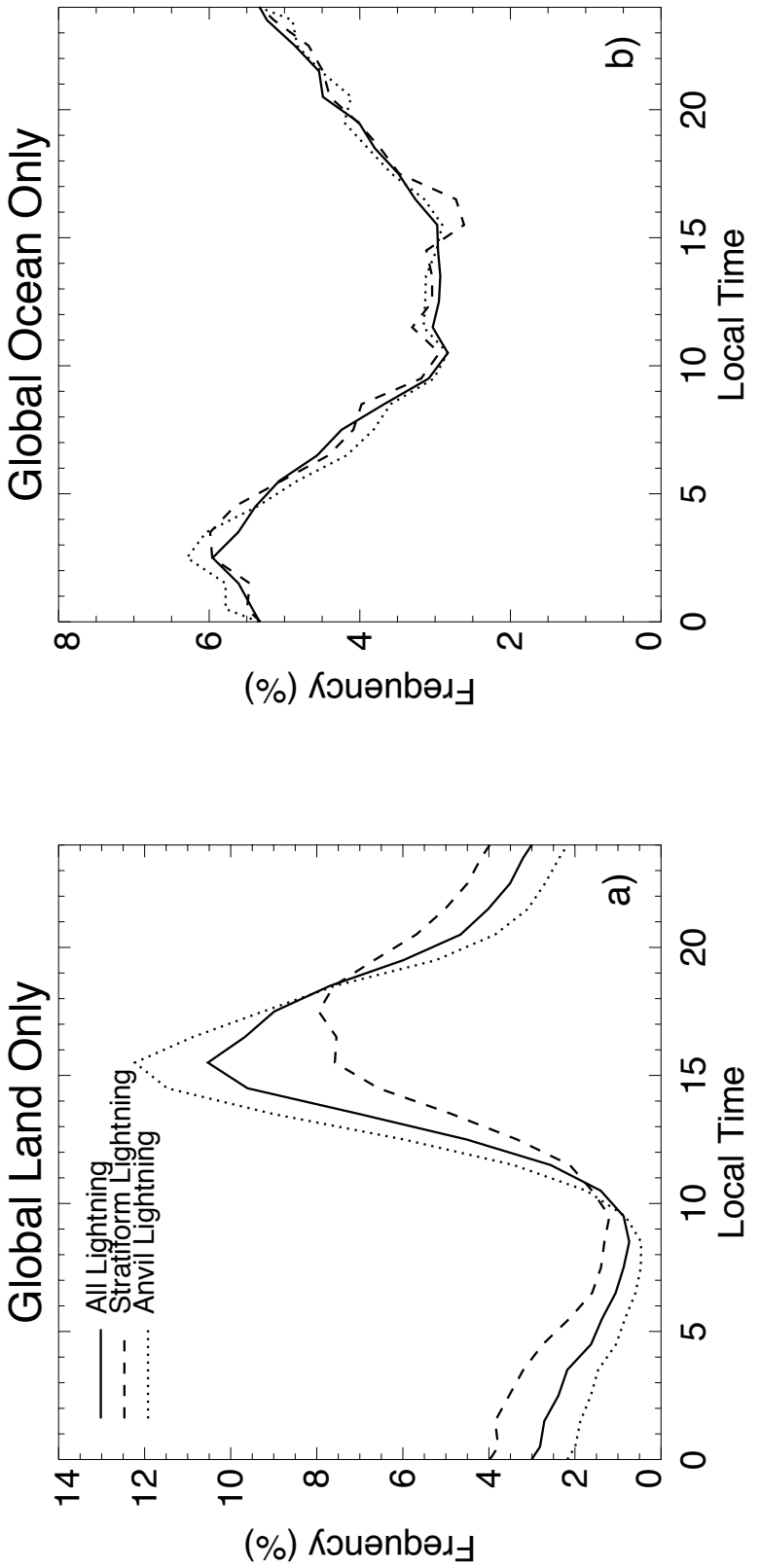

Figure 3.4 The diurnal cycles of all lightning flashes and those over stratiform and anvil regions a) over land; and b) over the oceans.

flashes, on the other hand, seems to have more nighttime lightning flashes, and a smaller percent of stratiform flashes occur during the afternoon than the other two types.

The diurnal cycle for oceanic flashes is completely different. Unlike over land, there is little difference between the three curves for flashes over the ocean. Not only that, but the diurnal cycle is reversed for oceanic flashes, and lightning is most common at night rather than in the afternoon.

The differences in the diurnal cycles of stratiform and anvil flashes over land imply that the life cycle of convection may be relevant in predicting stratiform and anvil flashes. These diurnal cycles are consistent with typical diurnal cycles of convection seen in previous studies (Hendon and Woodberry 1993; Nesbitt and Zipser 2003; Liu and Zipser 2009). Typical land-based thunderstorms form in the early afternoon, and then mature and decay in the evening and overnight. Since anvil flashes occur mostly in the afternoon, it is possible that they often occur in relatively early stages of convection as opposed to mature or dissipating convective storms. In contrast, since stratiform precipitation only prevails after a system matures, stratiform flashes are more common later in the day than the other types.

3.2 Statistics of Storm Properties near Lightning Flashes

Additional differences between stratiform and anvil flashes emerge when examining the statistics of the characteristics at the center location of each flash. While these properties may or may not be similar to those at the endpoints of each flash for large lightning flashes, a number of interesting trends emerge that shed some light on the environment through which these flashes propagate.

Figure 3.5 shows statistics of selected convective properties near the center location of stratiform and anvil flashes. Anvil flashes tend to occur in areas with significantly warmer than average VIRS infrared brightness temperatures and TMI 85 GHz PCTs (Spencer et al. 1989) of all flashes. Stratiform flashes, however, tend to occur in regions with average VIRS infrared brightness temperatures, and slightly warmer than average 85 GHz PCTs. In fact, nearly 80% of stratiform flashes occur in environments with 85 GHz PCTs less than 250K, compared to just 20% for anvil flashes. This trend is reinforced by PR data, where 70% of anvil flashes occur in regions of no detectible PR echo (<17 dBZ). Furthermore, over 90% of anvil flashes have no echoes exceeding 30 dBZ in the entire PR profile. While stratiform flashes are also more likely than average to have lower 30 dBZ echo tops, and even no 30 dBZ echo in the column, storm heights lower than 6 km are extremely rare (Figure 3.5d), and only a quarter of stratiform flashes have no 30 dBZ echoes in the profile.

A possible explanation for these relatively warm brightness temperatures near anvil flashes is that convective anvils are located along the edge of storm systems in regions with large reflectivity gradients. Because of this, there is a large potential for beam filling and edge contamination to occur, leading to higher brightness temperatures. Furthermore, the slant path of the TMI also has the potential to introduce collocation problems between the flash location and TMI pixel locations.

The 4 km spatial resolution and sensitivity of the TRMM PR can also cause problems for anvil flashes along the edge of a convective system. If a flash occurs right on the edge of a convective cell, there can be a fine line between whether the flash occurs in a convective pixel with modest reflectivity or over apparently clear air. This is further

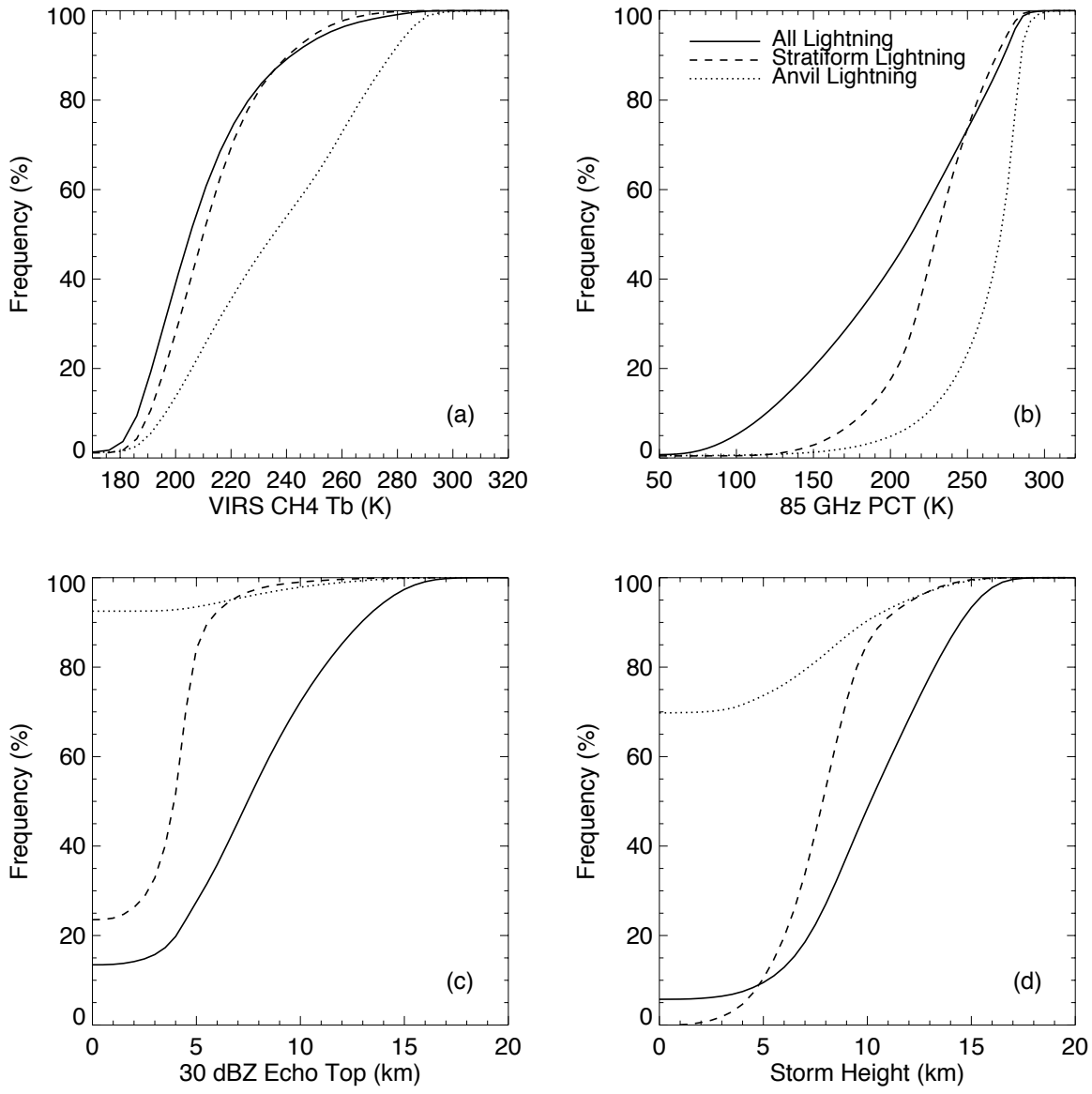

Figure 3.5 The cumulative distribution function of VIRS, PR, and TMI observations at the center of each lightning flash. a) VIRS channel 4 brightness temperature; b) 85 GHz polarization corrected temperature; c) the maximum height of 30 dBZ; and d) echo top height.

exacerbated by the definition of lightning flashes as the center of illumination detected by the LIS. Not only could the flash straddle the edge of a convective core, causing vastly different results depending on which bin the illuminated center falls, but also cases where lightning flashes occur between two different convective anvils that could lead to generally weak convective properties near the flash location.

Figure 3.6 shows an example of a convective system that demonstrates some of these situations. In this case, there are two neighboring ECRs and a number of anvil flashes. Most anvil flashes occur along the northern flank of the system, and many of these flashes occur right at the edge of the 12 km PR echo top height (2A23 storm height) contour in Figure 3.6c. Note that a few flashes have PR echo top value height of 0. These flashes were detected in the anvil cloud with reflectivity values below the sensitivity of the PR. Also, there are two flashes between the two convective regions under the same cirrus cloud shield. Figure 3.7 shows all of the illuminated pixels observed by LIS that are associated with the flash on the right in Figure 3.6. The flash propagated following the arrow drawn on Figure 3.7 from the southern small convective core to the northern convective core through an area with no PR echo. Lightning flashes propagating between separate convective cores, like this example, are likely to result in no PR echoes at their center, which is consistent with the statistics.

However, this is not the only situation that can lead to no PR echo aloft. In Figure 3.6, there are also a number of lightning flashes outside the cirrus shield that would be classified as anvil flashes. The illuminated pixels associated with the westernmost of these flashes are shown in Figure 3.8. The entire area illuminated by this flash lies outside the regions with radar echo and cold microwave brightness temperatures. There

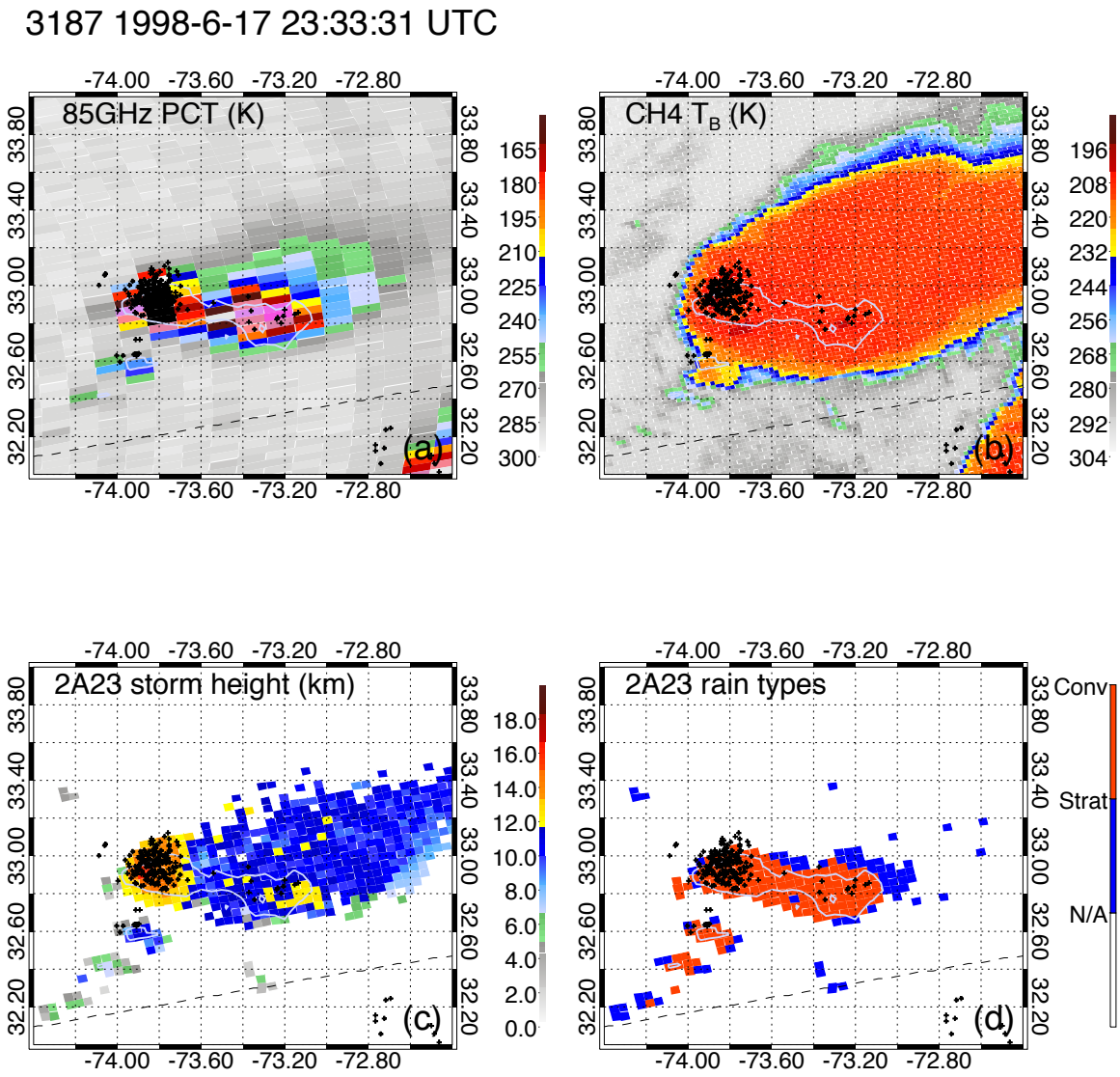

Figure 3.6 An example of a thunderstorm with clear air anvil lightning over north Atlantic in June 1998. a) TRMM TMI 85 GHz polarization corrected temperature; b) VIRS infrared brightness temperature; c) 2A23 storm height represents the PR detected echo top height; and d) PR 2A25 near surface rain rate. Areas >30 dBZ at 6 km are outlined in white, and lightning flashes are indicated by small plus signs.

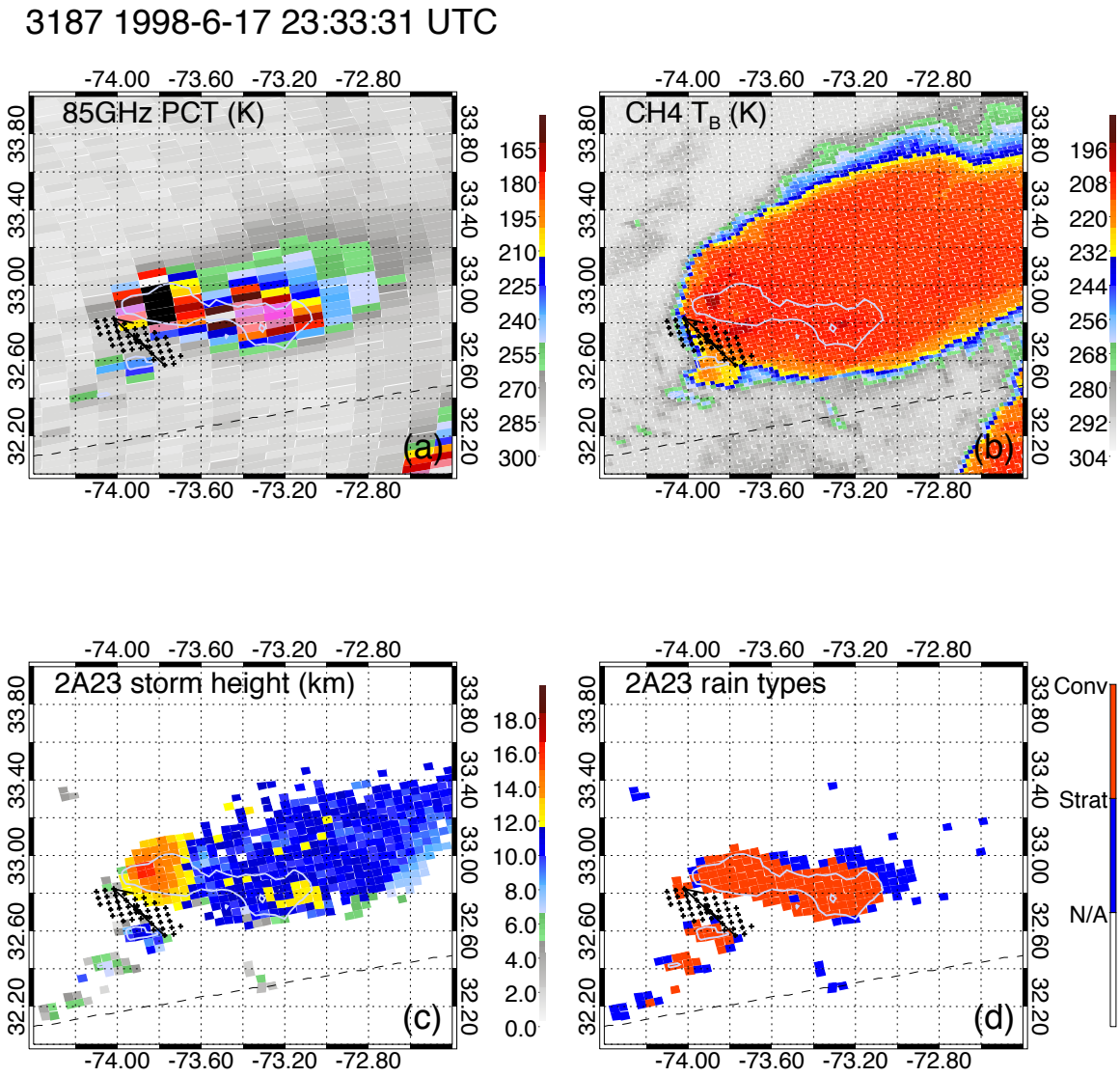

Figure 3.7 Same as 3.6, but with plus signs signifying illuminated pixels for a particular flash instead of individual lightning flashes. The arrow indicated the direction of propagation of the lightning flash.

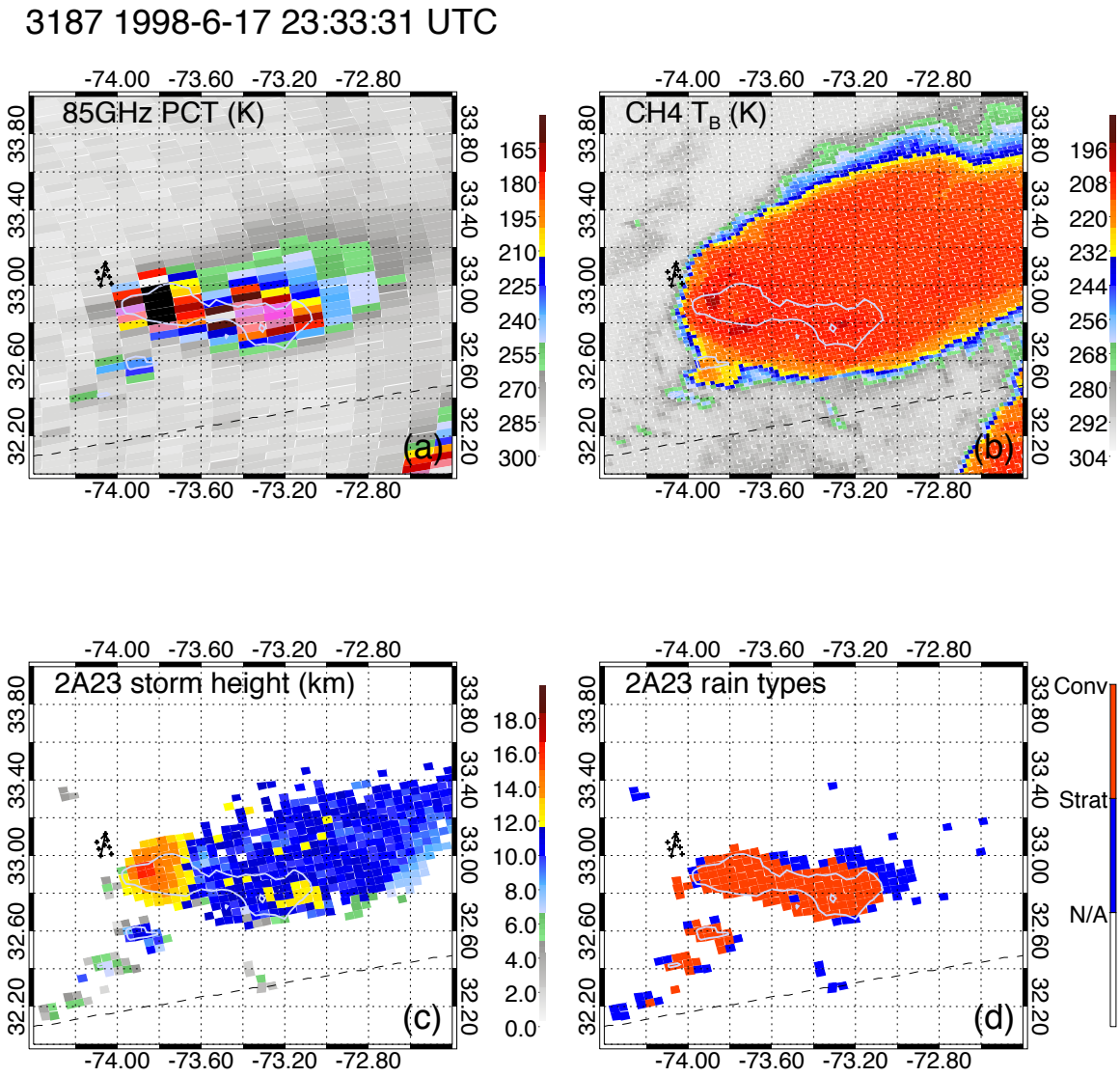

Figure 3.8 Same as 3.6, but with plus signs signifying illuminated pixels for a particular flash instead of individual lightning flashes. The arrow indicated the direction of propagation of the lightning flash.

could be a few different explanations for this case. For one, it is possible that this lightning flash occurred within a thin anvil cloud. However, it is also possible this flash is a LIS artifact. Note that the system shown occurred in the region affected by the SAA.

3.3 Statistics of ECRs Associated with Lightning

The focus of the previous sections of this chapter has been the statistics of individual lightning flashes and the properties of the regions in which they are centered. For the remainder of the chapter, emphasis is placed on the properties of nearby charging regions (ECRs) with the goal of finding specific combinations of storm properties that may signify the likely occurrence of stratiform or anvil lightning flashes. The global statistics of the ECRs and their associated flashes are summarized in Table 3.2. As in Table 3.1, stratiform and anvil flashes only make up a small fraction of the sample, in this case, 3.94% and 4.70%, respectively. However, at the same time, between 15% and 17% of ECRs with lightning have at least one flash of either type associated with them. This means that, while the numbers of stratiform and anvil flashes are small, they are actually relatively common on a storm-by-storm basis, just at lower flash rates.

Statistics of some of the properties of ECRs with lightning are summarized in Figure 3.9. The distributions are weighted by flash counts for each type of lightning in order to further reduce errors and highlight the properties of ECRs capable of producing a large number of flashes, though few ECR have more than 10 anvil or stratiform flashes associated with them.

Figure 3.9a and b describe the physical characteristics of ECRs associated with each type of lightning flash. Both stratiform and anvil flashes tend to occur near ECRs

Table 3.2 Global statistics of all ECR lightning flashes and population of ECRs associated with stratiform and anvil flashes between 36°N and 36°S normalized by latitude. Flashes farther than 200 km from the ECR center and anvil flashes over Argentina are not included in this sample.

	ECR Flashes		ECRs with Lightning	
	Count	%	Count	%
All	4580418		681309	
Anvil	215390	4.70	111673	16.40
Stratiform	180292	3.94	105647	15.51

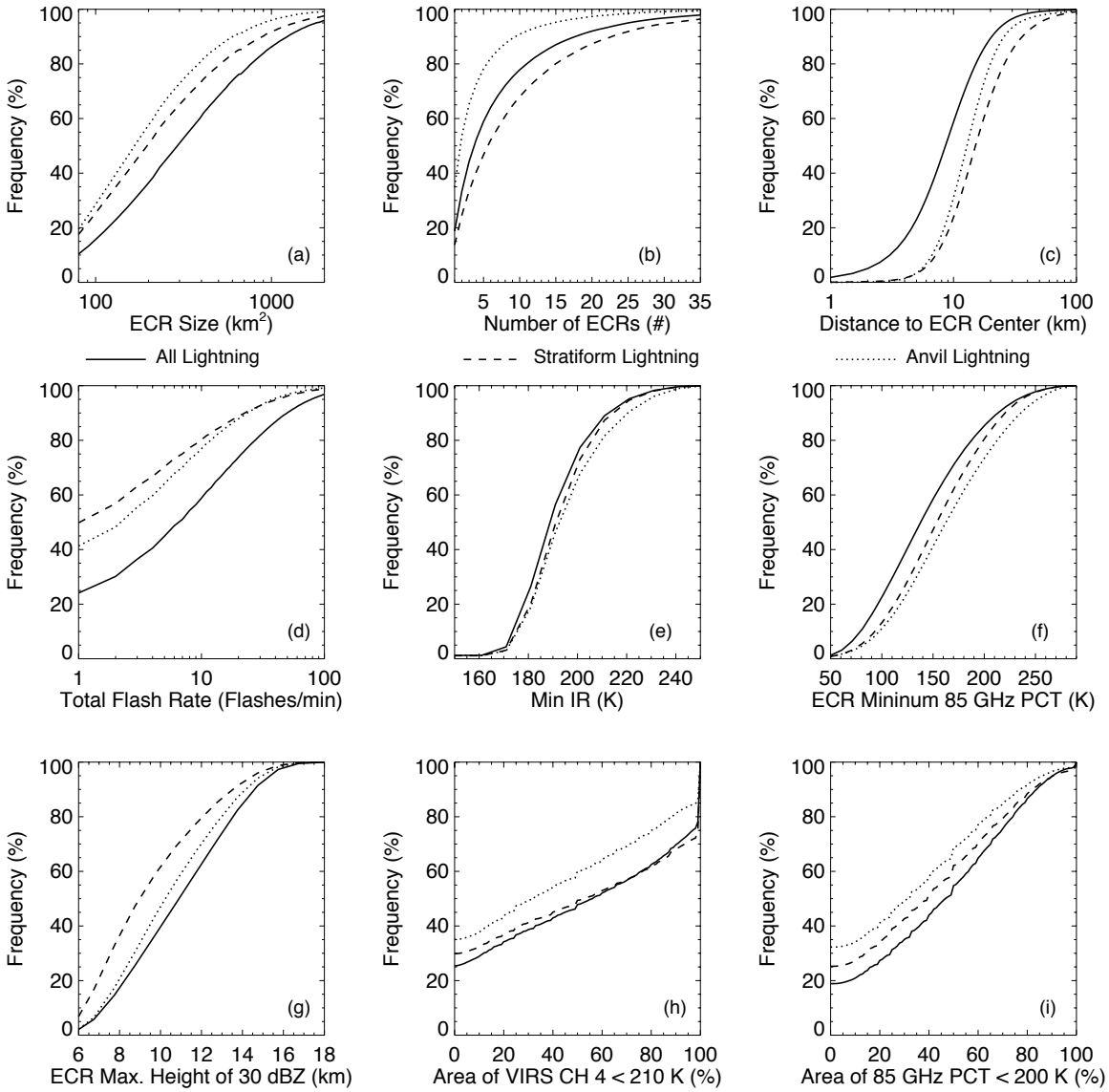

Figure 3.9 Cumulative Distribution Frequency of the convective properties of ECRs associated with lightning > 4 PR pixels in size. a.) ECR size; b) number of ECRs in the large raining region; c) distance from flash to ECR center; d) total flash rate inside the parent ECR; e) minimum VIRS infrared temperature T_{B11}; f) minimum 85 GHz PCT; g) 20 dBZ echo top; h) the area with VIRS T_{B11} < 210 K; and i) the area with 85 GHz PCT < 200K.

with relatively smaller sizes than average ECRs with lightning, with anvil flashes associated with the smallest ECRs on average (Figure 3.9a). Also, stratiform flashes tend to occur with ECRs that are part of multicell systems, while anvil flashes are more likely to occur in systems comprised of only a small number of ECRs (Figure 3.9b). Just under 15% of ECRs with stratiform flashes occur in single-cell systems, compared to 35% for anvil flashes, and, nearly 80% of anvil flashes occur in systems that contain less than 5 ECRs, while over half of those with stratiform flashes contain more than 5 ECRs. One explanation of this trend is that stratiform lightning likely occurs in the late stage of convective systems with multiple dissipating convective cores, but anvil lightning often occurs in earlier stages of convective systems. This is consistent with the earlier results of the diurnal cycles of anvil and stratiform lightning in Section 3.1.

As seen in Figure 3.9c, anvil flashes tend to be relatively far from ECR centers, though not as far away as stratiform flashes. Based on the definition of anvil flashes described earlier, both flashes in the convective anvil and those in the nonraining stratiform region would be considered anvil flashes, and each case would result in lightning flashes at least somewhat far from ECR centers.

One thing ECRs have in common with either stratiform or anvil flashes is that they tend to be coincident with relatively low flash rates within the associated ECR (Figure 3.9d). Between 25% and 30% of ECRs with anvil flashes or stratiform flashes, respectively, have no flashes inside the ECR at all, compared to just 15% for all ECRs associated with lightning. For stratiform flashes, this could be a sign that the storm systems are in a state of decay, resulting in both a reduction in size of ECRs and weaker convective intensities.

The distributions of the convective properties of ECRs associated with stratiform and anvil flashes vary with each different sensor. Looking at the VIRS infrared brightness temperature, ECRs with anvil flashes are just as likely to contain cold cloud tops as those that produce stratiform flashes (Figure 3.9e), but, at the same time, ECRs with anvil flashes do no have as large areas of cold cloud top temperatures as those with stratiform flashes (Figure 3.9h).

Similar patterns can be found from TMI polarization corrected temperatures at the 85 GHz and 37 GHz (not shown) frequencies. While VIRS infrared brightness temperature can be a proxy for storm height, PCTs in these bands are sensitive to column ice content. Because of this, the relatively warm PCTs observed in ECRs associated with anvil flashes suggest that these primarily convective regions contain less ice than other lightning storms, and that areas that do have an abundance of ice only make up a small percent of the ECR (Figure 3.9i). ECRs that are associated with stratiform flashes also have warmer than average TMI and VIRS brightness temperatures, which is consistent with what would be expected in a maturing system but still tend to have colder brightness temperature in infrared and microwave than those associated with anvil flashes.

PR-based convective proxies show a slightly different picture. While ECRs with anvil flashes or stratiform flashes are both relatively weaker than average as before, ECRs with anvil flashes tend to have higher echo tops for 40 dBZ (not shown), 30 dBZ, and 20 dBZ (not shown), as well as storm height determined by the minimum detectible echo, than those with stratiform flashes.

All of the above statistics are based on the ECRs with at least 80 km^2 in size, as required by the filter described in Section 2.3. One may wonder how including small

ECRs would affect these statistics. These ECRs were removed for a number of reasons, including the potential of stratiform flashes being associated with very small, weak, ECRs within the stratiform region instead of intense convective cells slightly farther away. Figure 3.10 shows the statistics of the properties in Figure 3.9 with these very small ECRs included. For many parameters, the two figures resemble each other closely (e.g., Figure 3.9b and c and Figure 3.10b and c) or the trends discussed in this section are amplified (e.g., Figure 3.9/3.10d,e,g, and h). However, due to the sheer numbers of these small ECRs, introducing bias towards smaller, weaker ECRs washes out the differences between stratiform and anvil flashes for ECR minimum 85 GHz PCT (Figure 3.9/3.10f and i). This is likely due to the large footprint size of the TMI, since ECRs smaller than 4 PR pixels are likely contained within 1 or 2 TMI pixels along with non-ECR PR pixels. Due to the potential for collocation errors and beam filling of the large TMI footprint, the 85 and 37 GHz PCT may not be representative of the true ECR properties. Moreover, since many of these small ECRs occur in the stratiform region, the ECR size trend is even reversed when these small ECRs are included (Figure 3.9/3.10 a). In summary, including these small ECRs does what one might expect: weights the statistics in favor of small, weak ECRs, particularly for stratiform flashes, but does not nullify the trends discussed earlier, but rather in many cases amplifies them.

Storms that are associated with stratiform flashes and those with anvil flashes are both relatively weak compared to the average thunderstorm; however, this does not mean that they tend to occur in the dissipation stage of convection. Since storms can be relatively weak in early and late stages of convection, it is worth investigating the frequency of stratiform and anvil flashed throughout the life cycles of convective

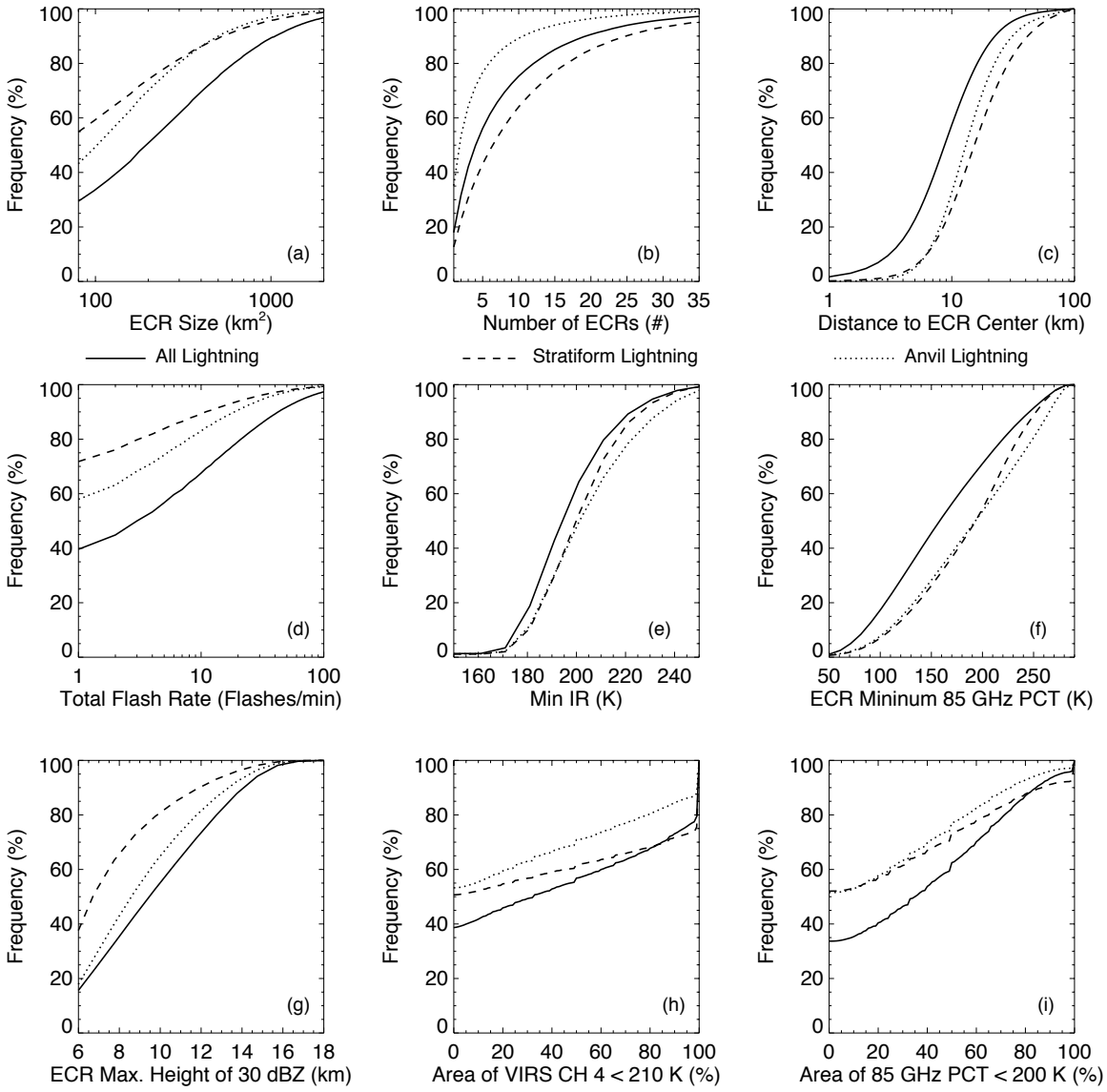

Figure 3.10 Same as Figure 3.9, except including the samples of ECRs with less than 4 pixels.

systems. However, since the TRMM satellite is unable to track individual storms throughout their life cycles, this is impossible with TRMM alone. For this reason, it is revisited in Chapter 5 using additional data from the TWP-ICE field campaign, particularly the ground-based CPOL radar and the LINET lightning detection network.

3.4 Relationships between ECR Convective Intensity and Flash Counts

The key motivation of introducing the concept of ECR is to assess the likelihood of lightning initiation in the stratiform and anvil regions based on the properties of nearby convection. Using TRMM data, it is possible to examine a number of properties and measures of convective intensity, instead of just ECR size, in search of an empirical relationship that explains lightning flash rates. Of course, not all lightning flashes occur inside ECRs since a significant number of lightning flashes are the result of in situ processes. Of the flashes that do occur inside ECRs, which account for 77% of all lightning in the sample, the correlation coefficient between ECR size and flash count is 0.66, which is not nearly as strong as seen in previous studies.

Relationships are even weaker when including all lightning flashes associated with ECRs rather than just those inside the ECR. Figure 3.11 examines the relationships for ECR size and flash count for each type of lightning. In this figure, the number density of these ECRs are contoured and the median (solid), 25th percentile, and 75th percentile (dashed) ECR sizes of each bin are overlain. In the case of all ECRs associated with lightning, there appears to be a general, positive trend between the area of 30 dBZ echoes at 6 km and flash count. Despite this linear drift in median, the correlation coefficient

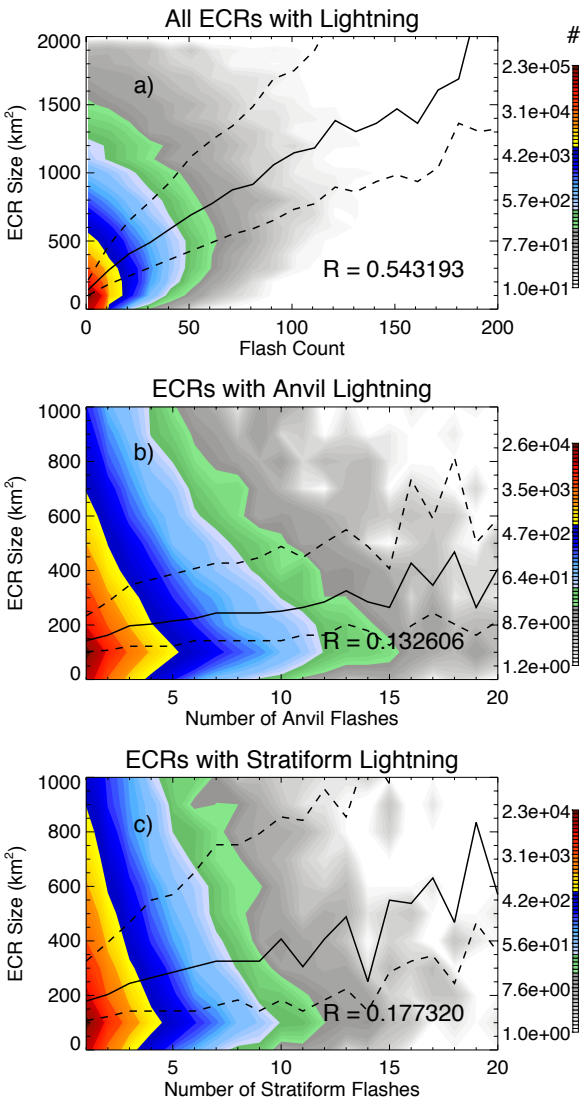

Figure 3.11 Two-dimensional histograms of ECRs categorized by their sizes and a) total flash counts, b) anvil flash counts, and c) stratiform flash counts. ECRs with the same of each type of flash count are grouped into bins, and the median, 25th percentile, and 75th percentile of each bin are overlain. Linear fit correlation coefficients are given. Linear fit correlation coefficients R are given for each set of parameters.

between flash count and ECR size is quite low. This may seem surprising, as one would expect there to be a strong correlation between flash counts and storm size based on the results of previous studies. However, on the other hand, the effect of including all flashes associated with ECRs on the correlation coefficient is only a drop of 0.1. At the same time, correlation coefficients for stratiform and anvil flash count are low. While deficiencies in the ECR definition and misassociations undoubtedly play a role in these low correlation coefficients, in situ charge generation, particularly for stratiform and anvil flashes, might also explain these low correlations.

Similar analyses for TMI-based convective proxies are shown in Figure 3.12. As in Figure 3.11, there is a better fit from all lightning to minimum 85 and 37 GHz PCTs of ECR than from stratiform and anvil flash counts. Since 37 and 85 GHz PCTs are sensitive to the total amount of ice in the column, as more ice is added, resulting in lower brightness temperatures, the range of possible lightning flash counts increases substantially. This brings up an important caveat in these TMI PCTs: the only information they give is related to the total column ice content, not the relative abundance of ice particles of different sizes. It is entirely possible that a storm with a thin layer of large ice particles will record the same 85 GHz or 37 GHz PCT as another with a thick layer of relatively smaller ice particles (Boccippio et al. 2005). For this reason, TMI-based proxies alone cannot accurately predict flash counts based on observed PCTs without taking into account the type of regime in which the ECR takes place. Stratiform and anvil flashes also show a clear decreasing trend in PCTs with increasing flash count. While the same caveats apply as for lightning in general, the dependence of stratiform flash count on the properties of ECRs and similarities between stratiform and anvil flash

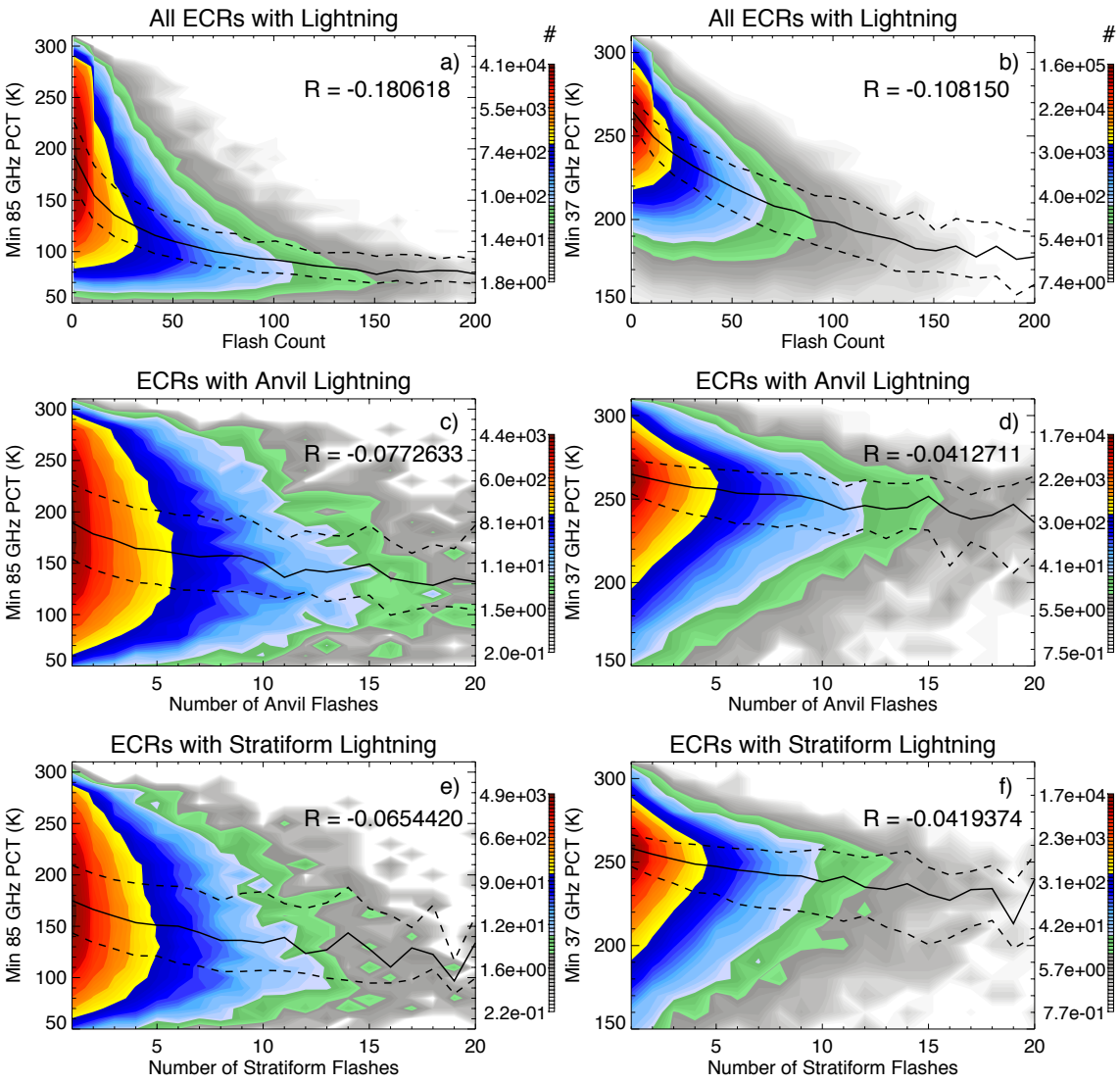

Figure 3.12 Two-dimensional histograms of ECRs categorized by their minimum 85 GHz PCTs and a) total flash counts, c) anvil flash counts, and e) stratiform flash counts, and ECR minimum 37 GHz PCTs and b) total flash counts, d) anvil flash counts, and f) stratiform flash counts. ECRs with the same of each type of flash count are grouped into bins, and the median, 25th percentile, and 75th percentile of each bin are overlain. Linear fit correlation coefficients are given for each grouping.

curves imply that at least some relationship exist between the abundance of stratiform flashes and the properties of nearby convection.

Relationships between PR-based convective proxies and flash production could potentially be used operationally with ground-based radars (Carey and Rutledge 2000; Petersen et al. 2005 and citations within). The correlation between 30 and 40 dBZ echo tops and flash counts are presented in Figure 3.13. Other reflectivity thresholds were also examined, including echo top and 20 dBZ. However, the relationship between lightning flash counts and these two relatively weak convective proxies are the weakest, and have the largest spread, and are therefore not shown. However, low correlation coefficients show that the current methodology is not sufficient to accurately predict stratiform and anvil flash counts using the intensity of nearby convection.

At the same time, correlation coefficients may be improved by abandoning the linear statistical model currently employed. Instead, a model based on a rational function might help explain these relationships, particularly one based on flash density (flashes per ECR lateral size) of the form of Equation 3.1.

$$FlashCount = f\left(\frac{LA_{area}}{LA_{strength}}\right) \tag{3.1}$$

Finding a rational function, F, that explains these data would be difficult, given the limitations of the current dataset. Additional information about each flash, such as the end point locations of each flash and flash size dimensions, as well as different ways of defining ECRs and various proxies for ECR convective intensity, would help in this type of analysis. However, this is beyond the scope of current research goals and therefore will

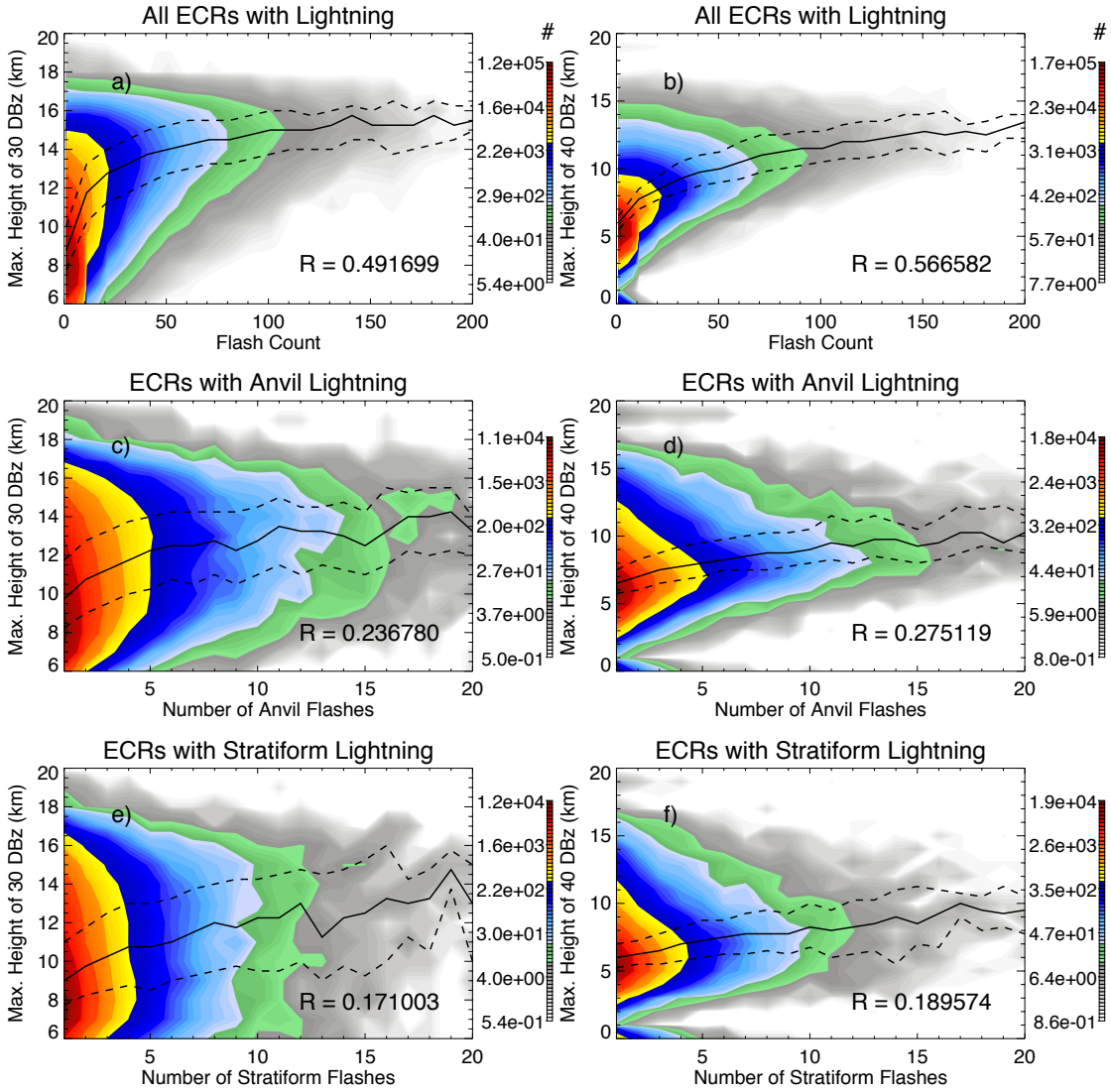

Figure 3.13 Two-dimensional histograms of ECRs categorized by their maximum 30 dBZ echo tops and a) total flash counts, c) anvil flash counts, and e) stratiform flash counts, and ECR maximum 30 dBZ echo tops and b) total flash counts, d) anvil flash counts, and f) stratiform flash counts. ECRs with the same of each type of flash count are grouped into bins, and the median, 25th percentile, and 75th percentile of each bin are overlain. Linear fit correlation coefficients are given for each grouping

be saved for the future.

3.5 Relationships between Convective Intensity of ECRs and Flash Distances

Distant lightning flashes have already been shown to be quite rare (Figure 3.10c), even for stratiform and anvil flashes. But they pose a higher threat to aviation because distant regions from active convective cores may be assumed to be relatively safe. For this reason, it is important to investigate what kinds of convection are associated with distant lightning. In order to examine the properties of ECRs associated with flashes at different distances, a similar analysis to that used in the previous section is employed, this time by constructing two-dimensional histograms of flashes based on flash distance to the center of the associated ECR and the convective intensity of that ECR. Figure 3.14 shows the distributions of distances of lightning flashes from ECR centers and two representative TMI-based and PR-based convective proxies: minimum 85 GHz PCT and maximum height of the 30 dBZ echo. The shape of these distributions is quite unique. Unlike flash count, which is a monotonic function of ECR strength, there is an inflection point in the relationship between flash distance and ECR strength at 30 km. For flashes closer than 30 km from ECR centers, distant flashes tend to require stronger convection, but after 30 km, the relations between the convective intensity of the ECR and the flashes are much weaker.

Figure 3.15 shows the relationships between flash distances and both ECR size and ECR minor radius, defined as the short axis of an ellipsoid fitted to the shape of the ECR. Most flashes are concentrated within 30 km of ECR centers, where the distance a

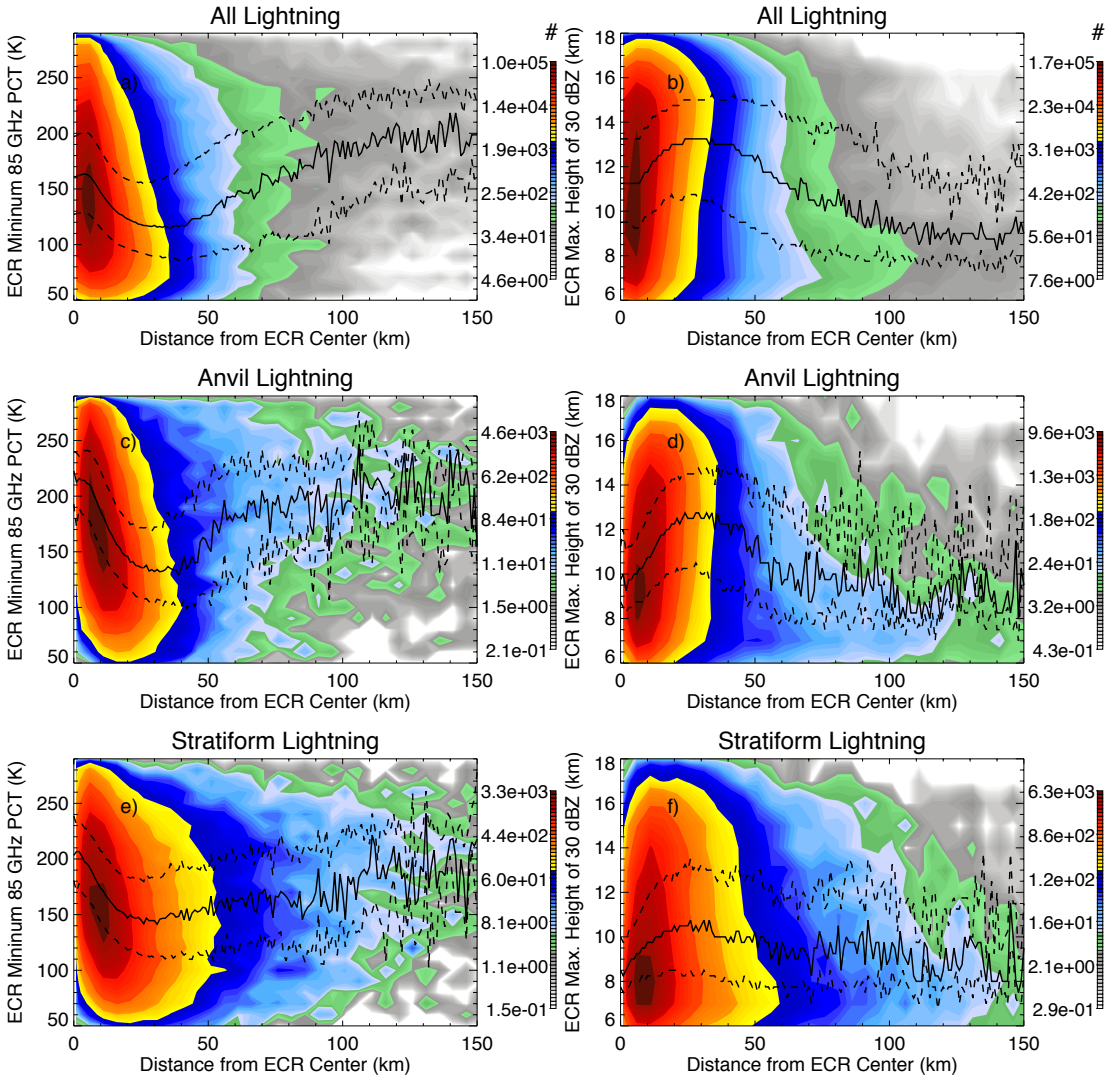

Figure 3.14 Two-dimensional histograms of flashes categorized by their nearest ECR minimum 85 GHz PCTs and flash distances to the center of ECRs for a) all flashes, c) anvil flashes, and e) stratiform flashes, and ECR maximum 30 dBZ echo tops and flash distances for b) all flashes, d) anvil flashes, and f) stratiform flashes. Flashes at similar distances from ECR centers are grouped into bins, and the median, 25th percentile, and 75th percentile of each bin are overlain.

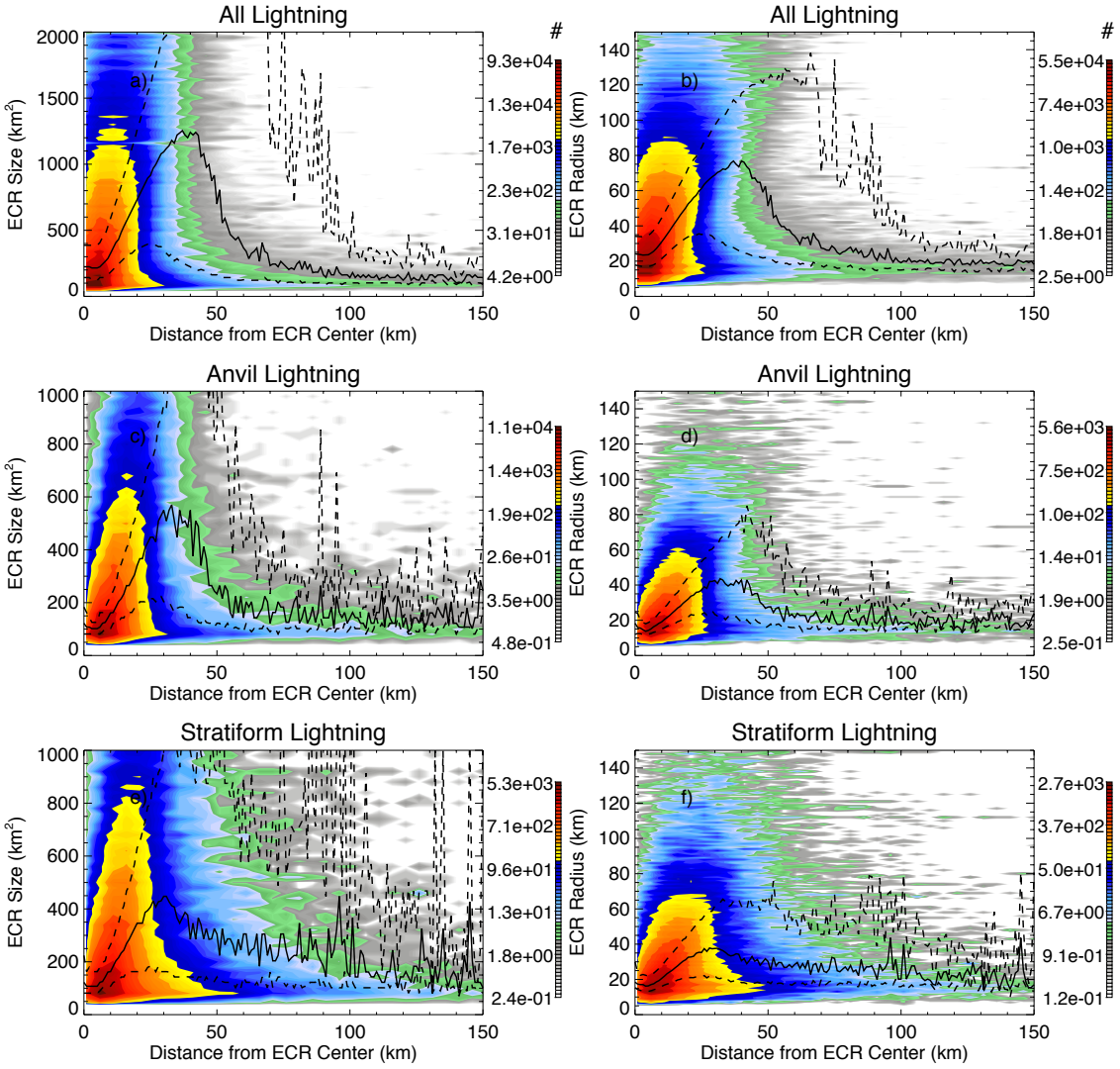

Figure 3.15 Two-dimensional histograms of flashes categorized by sizes of their nearest ECRs and flash distances to the center of the ECRs for a) all flashes, c) anvil flashes, and e) stratiform flashes and 2D histogram of flashes categorized by ECR minor radius and flash distances for b) all flashes, d) anvil flashes, and f) stratiform flashes. Flashes at similar distances from ECR centers are grouped into bins, and the median, 25th percentile, and 75th percentile of each bin are overlain.

flash occurs is largely dependent on the size of the ECR. The distributions of all three types of lightning exhibit this characteristic trend to varying degrees. However, beyond 30 km, much like the convective proxy statistics shown in Figure 3.14, the relationship between the ECR sizes and distances from flashes to the center of ECR diminishes.

Since TRMM can only see a snapshot of a particular storm at a single point in its lifetime, some details cannot be revealed. One possible explanation is that after a convective system starts to decay, a significant amount of charged particles aloft can be left behind in formerly-convective regions, though only small pockets still meet the ECR 6 km 30 dBZ definition. These ECRs with distant flashes tend to be relatively weak and small, and seem to dominate the sample beyond the 30 km inflection point in the total flash distance statistics. However, without more information about individual flashes it is impossible to gauge the validity of this scenario since the risk of bad associations by the nearest neighbor method is exceedingly high at large distances. Examining the storm properties associated with distant lightning flashes would also benefit from more information about lightning flash endpoints. Instead of just looking at the distance of the center of the lightning flash, information about the distance between the start and end locations to flash centers, and flash dimensions would make it possible to differentiate between large lightning flashes initiating in the convective line and propagating through the stratiform region, for instance, and distant stratiform flashes possibly resulting from in situ properties. For these reasons, further examination of this topic will be left as a subject for future research.

CHAPTER 4

TWP-ICE DATA AND METHODOLOGY

Perhaps the biggest limitation of using TRMM data in studying lightning is its inability to observe and track individual convective systems throughout the different stages of their lives. For this reason, the statistics of stratiform and anvil flashes, and how they relate to storm structure, are examined using data collected during the Tropical Warm Pool International Cloud Experiment (TWP-ICE, May et al. 2008) near Darwin, Australia.

4.1 Definitions of Stratiform Lightning, Anvil Lightning, and ECRs using TWP-ICE Data

The TWP-ICE was carried out near Darwin, Australia in January and February of 2006. The goal of this field campaign was to provide a comprehensive dataset for the study of factors that control tropical convection and the processes by which tropical convection affect the nature of cloud particles in convective anvils and tropical cirrus, and the surrounding environment in order to improve tropical convection parameterization in forecast and climate models. Observations were collected throughout the 150 km radius domain of the experiment centered on Darwin, Australia from 5 research aircraft, a research vessel, frequent soundings from 6 locations, an Atmospheric

Radiation Measurement (ARM) Program Atmospheric Cloud and Radiation Facility (ARCF), and Bureau of Meteorology (BOM) facilities (May et al. 2008).

Since this field campaign took place in the deep tropics, it is an ideal candidate for comparison with TRMM statistics over the tropics. The field campaign dataset includes observations from a research C-band polarimetric Doppler radar (CPOL, Keenan et al. 1998) and a Deutsche Zentrum für Luft- und Raumfahrt (DLR) lightning network (LINET). The LINET lightning network consists of multi-antenna electromagnetic flux detectors that operate in the LF to VLF range, specifically from ~1 kHz to upwards of 1 MHz, though frequencies in 200-400 kHz are discarded due to potential interference with radio signals. The locations at which lightning flashes occur are computed by examining the different arrival times of the electromagnetic pulses from lightning flashes at a number of sites in the network. These time-of-arrival calculations are performed at very high accuracies using GPS receivers with 300 ns accuracies. Locations of lightning flashes are given to accuracies better than 250m for both cloud-to-ground (CG) and intra-cloud (IC) flashes. CG and IC flashes can also be determined by examining deviations of arrival times at stations close to events as compared to those expected based on two-dimensional propagation paths (Betz et al. 2004).

Moreover, the detection efficiency is a function of range and differs between IC and CG flashes. For CG flashes, the detection efficiency is over 90%. The detection efficiency for IC flashes is significantly lower, however, because IC signals are much weaker in the VLF/LF waveband than CG signals. In fact, IC flashes often result in pulses below 2 kA, with vastly differing pulse shapes (Betz et al. 2008). Attempts to address these limitations by allowing for unique pulse shapes and small amplitudes can

lead to significant numbers of artifacts in the data. LINET data are collected continuously and collocated with the nearest CPOL 10-minute volume scan, such as the one shown in Figure 4.1. In this case, a large number of flashes are observed by LINET despite the CPOL domain showing no significant echoes whatsoever. These flashes are likely artifacts, particularly since the CPOL can detect much weaker echoes than TRMM, as low as 0 dBZ, in fact. Even on the most active days, it is common to see anywhere from a few flashes to the majority of detected flashes occurring in areas with no CPOL radar echo and that are far enough away from anything capable of causing lightning initiation that they must be erroneous flashes. In order to eliminate as many of these erroneous flashes as possible, any flash that occurs in areas with no significant radar echo (< 5 dBZ) is removed from the sample. This, of course, may remove some anvil flashes over regions with no CPOL reflectivity. Only flashes within 150 km of CPOL radar are included in the analysis in this study.

In this study, first COL radar volume scans are interpolated onto 1 km x 1 km grids with vertical resolution of 1 km by using REORDER software developed in NCAR. Since CPOL has a higher horizontal resolution than TRMM, the gridded CPOL radar data are degraded to a 4 km x 4 km resolution for comparison purposes. ECRs are then identified in CPOL data using the same definition of radar echoes greater than 30 dBZ at 6 km. The biggest disadvantage ground-based radars have over the TRMM PR is their inability to see the lowest parts of storms far from the radar due to the beam angle and the curvature of the earth. This makes it difficult to differentiate between different types of LINET lightning flashes using CPOL data. Anvil flashes observed by the TRMM LIS require the near surface rain rate to be known, but CPOL is not able to detect near surface

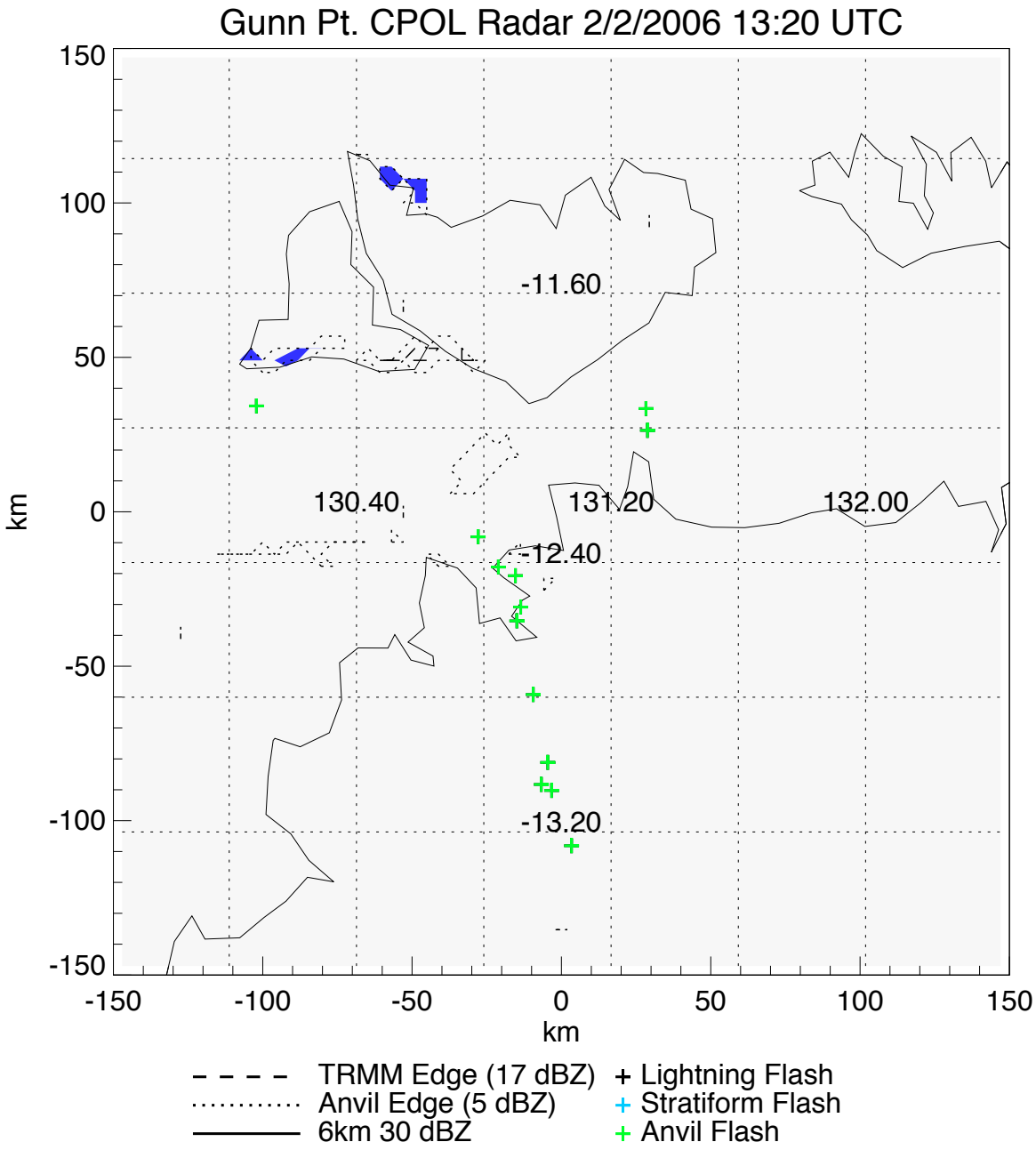

Figure 4.1 A clear-air case during TWP-ICE where the LINET reported a large number of erroneous flashes marked as plus signs. There is no radar echo close to these erroneous flashes.

echoes in the regions far away from the radar. However, at the same time, the CPOL radar has a much higher sensitivity (~0 dBZ depending on range, though 5 dBZ is used as a cutoff to reduce ground clutter), making it possible to better distinguish anvil flashes from artifacts. Because of these differences, a slightly different definition of anvil flash is used for the TWP-ICE dataset in order to address shortcomings in the data while keeping the observations somewhat comparable with TRMM LIS observations. In order for a flash to be considered an anvil flash in the TWP-ICE dataset, there must be at least 5 dBZ of CPOL reflectivity somewhere in the column in order to remove the artifacts, but no more than 17 dBZ in the lowest 3 km to be consistent with the sensitivity of TRMM PR.

Despite this filtering, there are still significant amounts of anvil flash artifacts in the data. This can be seen by looking at the Contoured Frequency by Altitude Diagram (CFAD, Yuter and Houze 1995) of CPOL radar reflectivity at the locations of anvil flashes presented in Figure 4.2. The distribution looks like what one would expect for anvil clouds with, in many cases, high radar echoes decreasing towards the surface. However, the majority of these flashes occurs in regions with echoes weaker than 17 dBZ, and would therefore not be observable by TRMM. There are also slight differences in the reflectivity profiles at the locations of anvil IC and CG flashes. For instance, anvil IC flashes are more likely to have higher reflectivity in the column. It is impossible to say how much of an impact artifacts have on these statistics. For this reason, the case study in the following section will examine anvil flashes and how they relate to storm structure throughout the lives of the storms.

Stratiform flashes are also subject to a slightly different definition due to the shape of the volume scan of the ground radar. Stratiform and convective precipitation

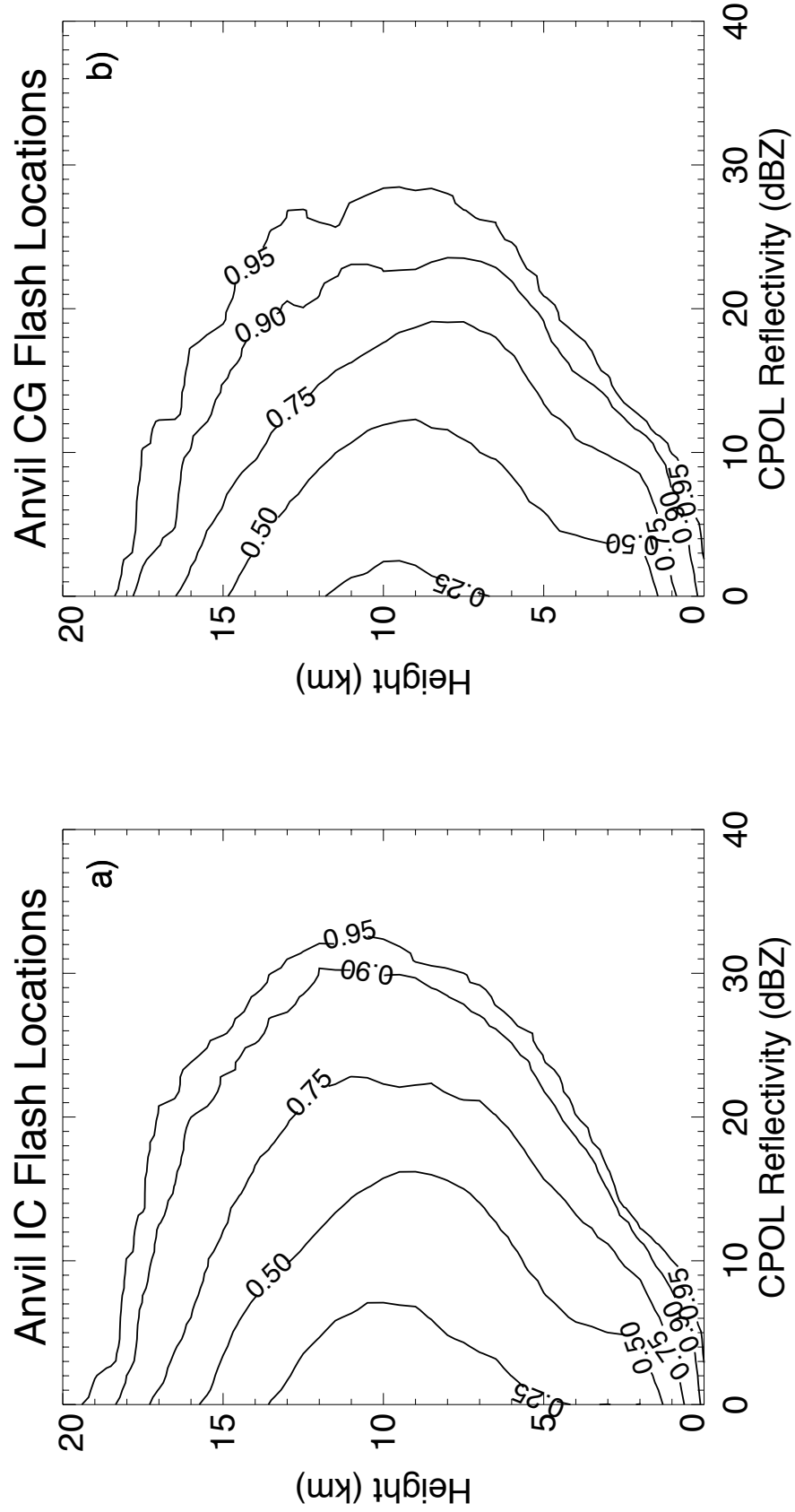

Figure 4.2 Contour Frequency by Altitude Diagram (CFAD) of CPOL radar reflectivity at the locations of a) IC anvil flashes and b) CG anvil flashes.

types are separated by the algorithm developed by Steiner et al. (1995), which was used as the basis for the 2A23 horizontal convective/stratiform separation method. Figure 4.3 shows a line of convection (color filled in yellow) in an otherwise predominately stratiform area (color filled in blue) over the southwestern domain of the radar. Each ECR that makes up the system is outlined in black contours, while the areal limits of the 17 dBZ echo region corresponding to the TRMM-visible range are represented by dashed contours, and the areal limits of the 5 dBZ echo region corresponding to the anvil region are represented by dotted contours. In this case, many of the observed flashes are over the regions designated by the Steiner algorithm as stratiform, including a few that occurred with 30 dBZ echoes at 6 km.

It is important to understand how much difference there is between the TRMM PR 2A23 and the Steiner et al. algorithm. ECRs from each dataset based on our 30 dBZ at 6 km definition are identified and the statistics of stratiform fraction are compared in Table 4.1. Note that only those ECRs observed by TRMM that occurred over the domain of the CPOL radar (129.8 E – 132.2 E and 13.6 S - 10.8 S) during the same season as TWP-ICE are included in the TRMM subset. With the TRMM 2A23, more than three-quarters of TRMM PR ECRs associated with lightning consist of less than 10% stratiform area, compared to just over half of CPOL ECRs with this same low stratiform fraction. About 15% of CPOL ECRs are even dominated (> 80%) by areas of stratiform rain according to Steiner algorithm.

Moreover, since the Steiner et al. algorithm primarily depends on horizontal radar reflectivity gradients, areas of weak convection often are considered stratiform, including relatively small and weak ECRs, as well as the rear flanks of the large convective regions

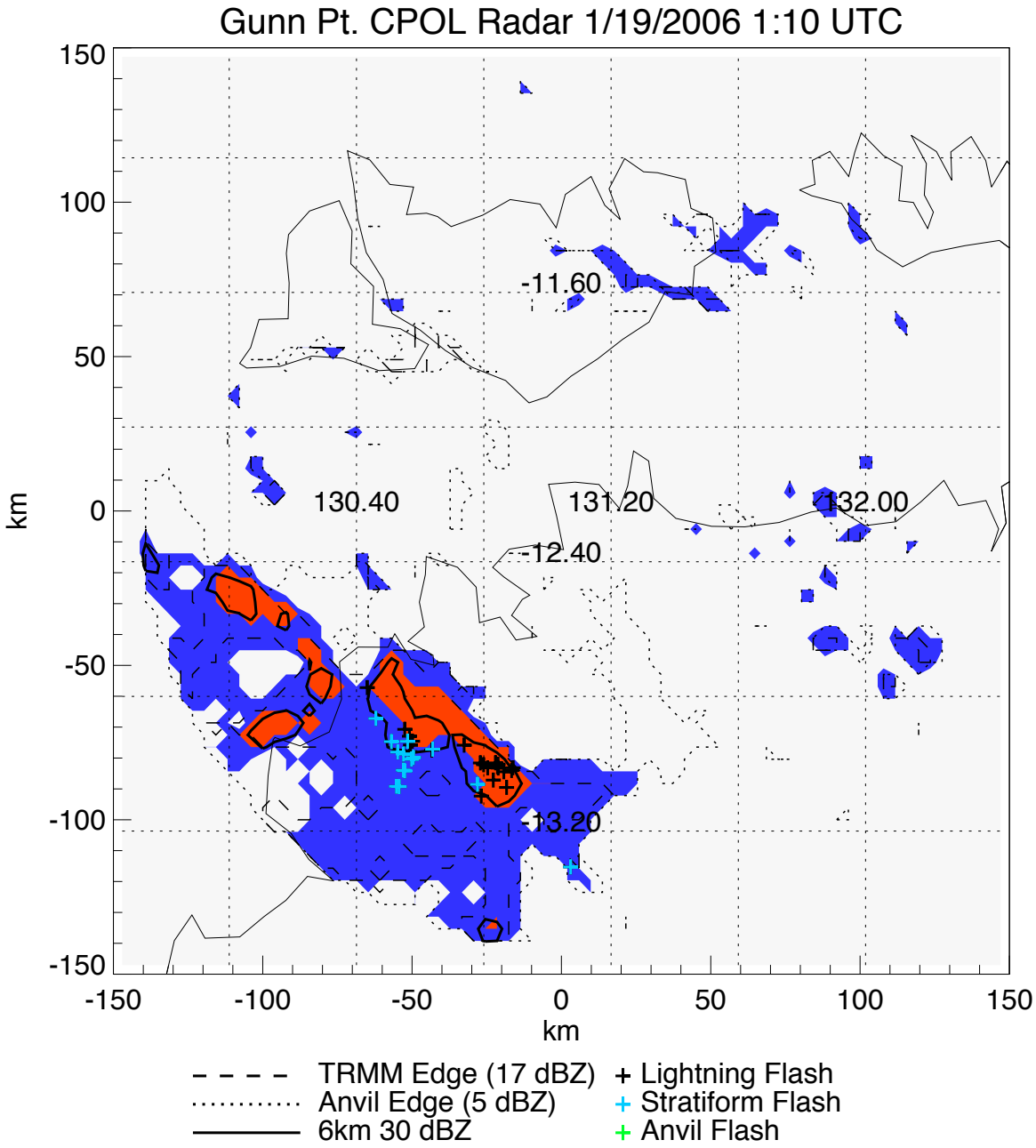

Figure 4.3 A leading-line-trailing-stratiform convective system observed by the CPOL radar and LINET during TWP-ICE. Areas shaded in blue are stratiform, and red areas are convective based on output from the Steiner algorithm. Blue region are the stratiform based on the output from Steiner Algorithm. Areas within solid contours meet our definition of ECR of >30 dBZ at 6 km, and the centers of these areas are designated by asterisks. Dotted contours represent 17 dBZ at 3 km. Lightning flashes are indicated by plus signs.

Table 4.1 Stratiform fractions of lightning-producing ECRs larger than 4 PR pixels observed during Jan and Feb in the TWP-ICE region (10.8°-13.6°S, 129.8°-132.2°E).

Stratiform Fraction	<5%	5-10%	10-20%	20-50%	50-80%	>80%
TRMM (1998-2010)	65.04%	12.19%	15.44%	5.69%	1.62%	0.00%
TWP-ICE	45.31%	12.96%	10.39%	10.39%	7.25%	14.67%

seen in Figure 4.1. This results in a large amount of stratiform flashes to be identified by the Steiner algorithm. Table 4.2 compares the statistics of each type of flash observed by TRMM over the CPOL domain (129.8 E – 132.2 E and 13.6 S - 10.8 S) in January and February from 1998 to 2010. Even though TWP-ICE lasted less than a month, the total number of observed flashes is much larger in this dataset than the total number of those observed in this region by the TRMM LIS since its launch due to its 80-second sampling time and relatively small number of overpasses. The TRMM LIS sample is quite small, consisting of only ~1000 flashes and ~50 stratiform and anvil flashes. Despite this small sample, stratiform and anvil flashes from TRMM each account for ~5% of the total, which is consistent with the global statistics discussed in Section 3.1. At the same time, anvil flashes observed during TWP-ICE accounted for nearly 7% of the total, and more than 20% of all observed lightning flashes are identified as stratiform flashes.

In order to reconcile some of the differences between the two stratiform separation schemes, an additional criterion is applied in order to deal with areas where the two algorithms conflict the most: areas of relatively weak convection that still meet our ECR definition. In order to accomplish this, a modified convective/stratiform separation scheme is used in which all areas with echoes greater than 30 dBZ at 6 km would be considered convective, regardless of what the Steiner et al. algorithm indicated. The statistics of stratiform flashes based on this modified scheme are shown in the last column of Table 4.2. After applying this criterion, the fraction of stratiform flashes in the sample dropped to 9.59%.

Due to the differences in the sensitivities and observing geometries of the TRMM PR and CPOL radars, as well as the LIS and LINET lightning detection systems,

Table 4.2 Sample size of flashes observed during January and February in the TWP-ICE region by the TRMM LIS, TWP-ICE LINET, and TWP-ICE LINET with a modified stratiform/convective algorithm forcing all flashes in areas with >30 dBZ at 6 km to be convective.

	TRMM		TWP-ICE		TWP-ICE (modified)	
	Count	%	Count	%	Count	%
All	1010		153674		153674	
Anvil	55	4.45	10710	6.97	10710	6.97
Stratiform	45	5.44	34303	22.32	14744	9.59

differences of the statistics from TRMM and TWP-ICE listed in Table 4.2 are not just understandable, but expected. The focus of this part of the study is to understand stratiform and anvil lightning through the life cycle of convection by using TWP-ICE data rather than build a regional climatology.

4.2 Comparison of TRMM and TWP-ICE Statistics

Similar analyses to those conducted in Chapter 3 are used to compare TRMM and TWP-ICE statistics. ECRs are defined from CPOL observations using the same definition of regions with 30 dBZ echoes exceeding 6 km. At the same time, lightning flashes from the LINET are categorized based on our modified definitions described in the previous section. Finally, each valid lightning flash (within 150 km of the CPOL radar) is associated with the nearest ECR using the nearest neighbor method. In order to reduce the number of bad associations, lightning flashes farther than 100 km away from the center of their associated ECR are removed from the sample. This does not noticeably affect the statistics for all lightning, since only ~1% are observed beyond 100 km from ECR centers, but it does help in eliminating LINET artifacts that happen to occur in areas of light precipitation that have never been near intense convection, which is somewhat common in the dataset. After removing both lightning flashes with less than 5 dBZ in the column and those that are greater than 100 km from ECR centers, the initial sample of LINET observations is reduced by 13%.

Using these data, it is possible to make a comparison between TWP-ICE observations and TRMM regional statistics over the TWP-ICE domain from 1998 to 2010. Figures 4.4 and 4.5 show the statistics of a number of properties at the center

locations of lightning flashes from TRMM and TWP-ICE observations, respectively. Similar to the global statistics shown in Section 3.2, TRMM observations over the Darwin region show that a large number of anvil flashes occur in regions with no detectible PR echo (Figure 4.4a and b). Both types of flashes tend to occur relatively far away from ECR centers (Figure 4.4f). Stratiform and anvil flashes occur in regions with relatively weak convective intensity proxies. However, there are some differences as well. Stratiform flashes in the TWP-ICE region, for instance, occur in thunderstorms that are significantly more intense than anvil flashes from a PR perspective as well as from a TMI perspective (Figure 4.4b, d and e).

Looking at the same radar-based convective properties computed using CPOL radar data, there appears to be some agreement between TRMM PR and TWP-ICE CPOL echo top height statistics, despite the different filtering and convective/stratiform separation technique used in the TWP-ICE dataset. The effects of the modifications made to the Steiner algorithm are clearly shown in Figure 4.5b. Due to this new definition, no stratiform flash has 30 dBZ echo top heights exceeding 6 km. The goal of this filtering is to remove misclassified stratiform flashes, but as seen in Figure 4.4b, as many as 1 in 4 stratiform flashes identified by the 2A23 algorithm have 30 dBZ echoes exceeding 6 km, and would be removed as well.

Another departure from the TRMM statistics lies in the distances that stratiform and anvil flashes occur from CPOL-observed ECR centers. Unlike Figure 4.4f, where there is little difference between the distance statistics for stratiform and anvil flashes in the TRMM dataset, anvil flashes observed during TWP-ICE tend to be significantly farther from ECR centers than stratiform flashes. This is possibly due to the significant

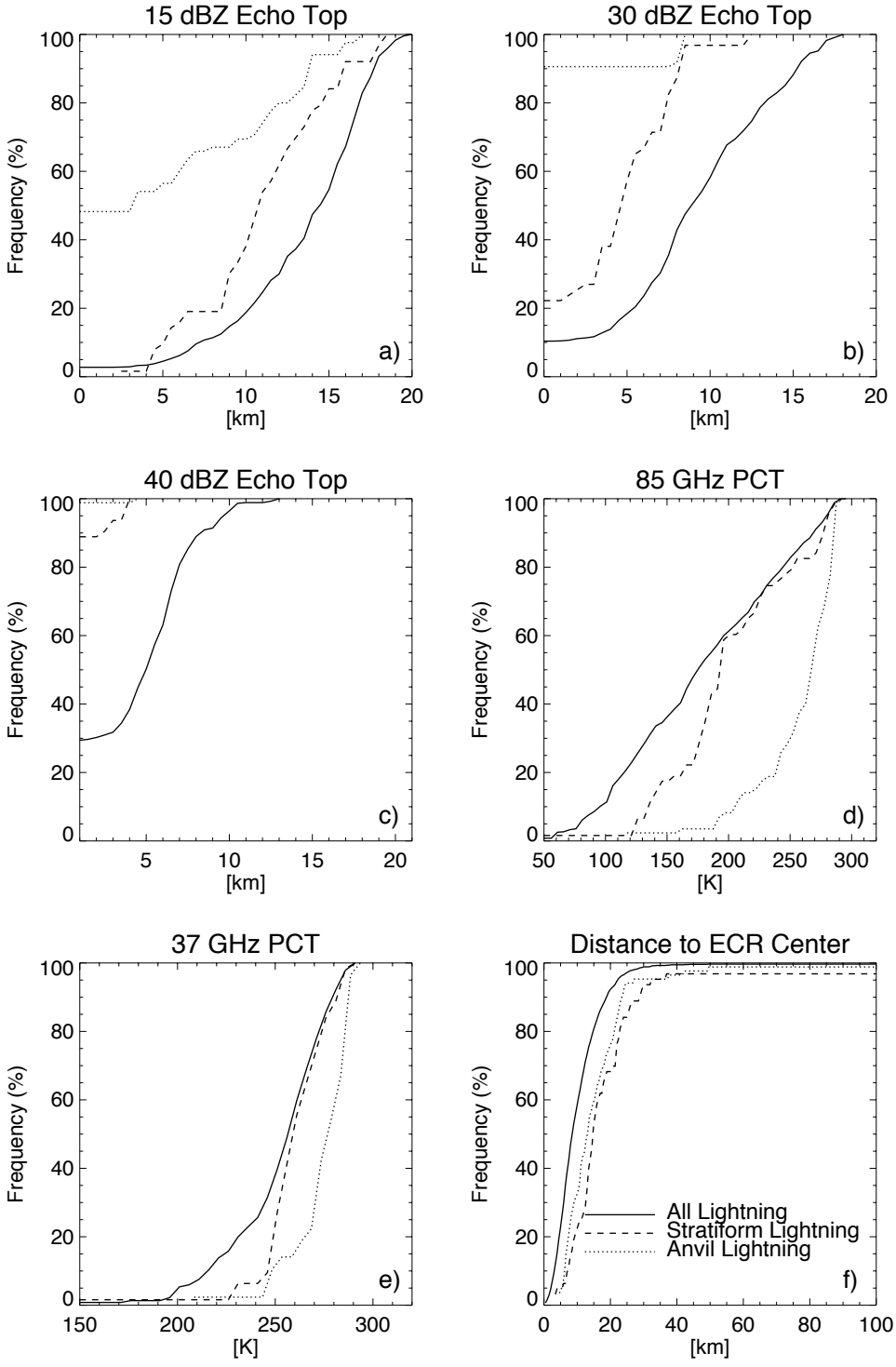

Figure 4.4 Cumulative distribution functions of TRMM-observed convective properties near the locations of lightning flashes separated by flash type including a) PR echo top; b) 30 dBZ echo top; c) 40 dBZ echo top; d) 85 GHz PCT; e) 37 GHz PCT; and f) distance from flash to ECR center. Here, TRMM observations are from 1998 to 2010 over 129.8 °E – 132.2 °E and 13.6 °S - 10.8 °S during December, January and February.

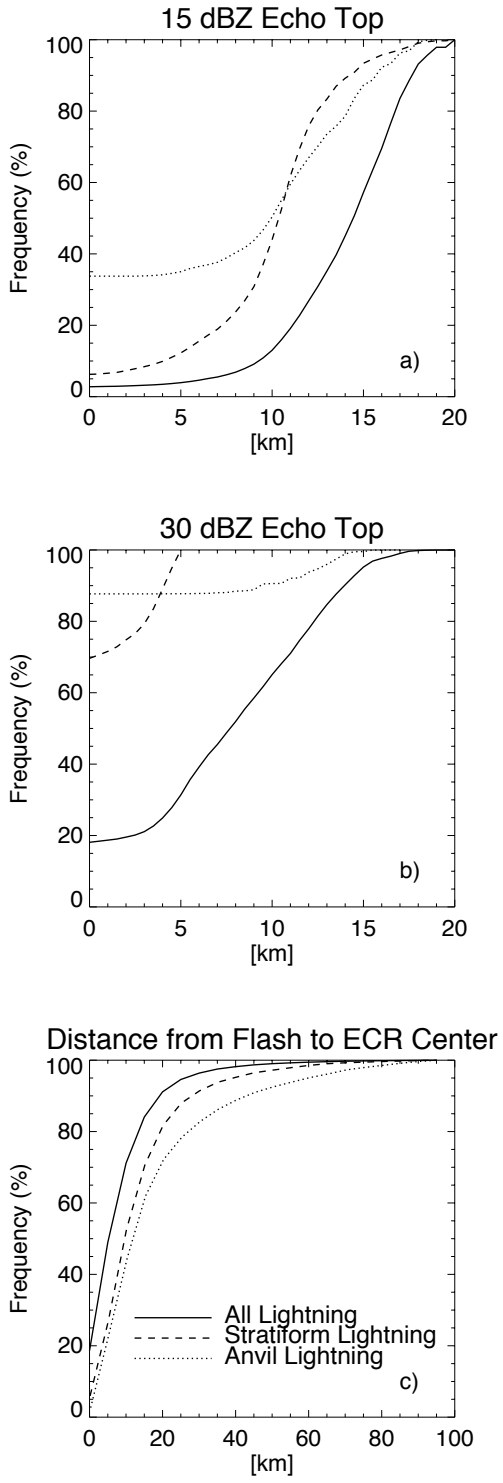

Figure 4.5 Cumulative distribution functions of CPOL-observed convective properties near the locations of lightning flashes during TWP-ICE separated by flash type including a) 15 dBZ echo top; b) 30 dBZ echo top; and c) distance from flash to ECR center.

amount of artifacts in LINET data.

The Cumulative Frequency at Altitude Diagrams (Yuter and Houze 1995) of radar reflectivity at the locations of all lightning and stratiform flashes for both CPOL and LINET observations during TWP-ICE (solid lines) and TRMM observations of the TWP-ICE region and season (dashed lines) are presented in Figure 4.6. Given the limits of TRMM, including the PR sensitivity and small sample size of TRMM observations, the reflectivity profiles resemble one another surprisingly well above 17 dBZ. There are some differences, however. The TRMM PR reflectivity, for instance, does not rapidly decrease to 0 below 2 km like the CPOL reflectivity profiles do due to the fact that the CPOL cannot resolve near surface reflectivity at range. Above 10 km, it the CPOL reflectivity profiles are stronger than the PR profiles. This is likely due to the coarse vertical resolution of CPOL with a large beam width at these altitudes.

The TRMM statistics of ECRs over TWP-ICE region and season are examined in Figure 4.7. As before, ECRs that are associated with stratiform or anvil flashes tend to be relatively small (Figure 4.7a) and weak (Figure 4.7b, d, e, f), and occur primarily in the early afternoon (Figure 4.7c). ECRs observed by CPOL during TWP-ICE with stratiform or anvil flashes also tend to be relatively small and weak as seen in Figure 4.8. There are some differences, however. While TRMM ECRs with anvil flashes tend to be small, for instance, TWP-ICE ECRs with anvil flashes are often relatively large (Figure 4.8a). Also, there also appear to be two distinct periods of the day where lightning is quite common (Figure 4.8c). Instead of just the one peak in the early afternoon seen in the TRMM statistics (Figure 4.7c), there is also a second peak present in the late morning, between 9 and 11am. This is likely because only a small number of lightning storms were

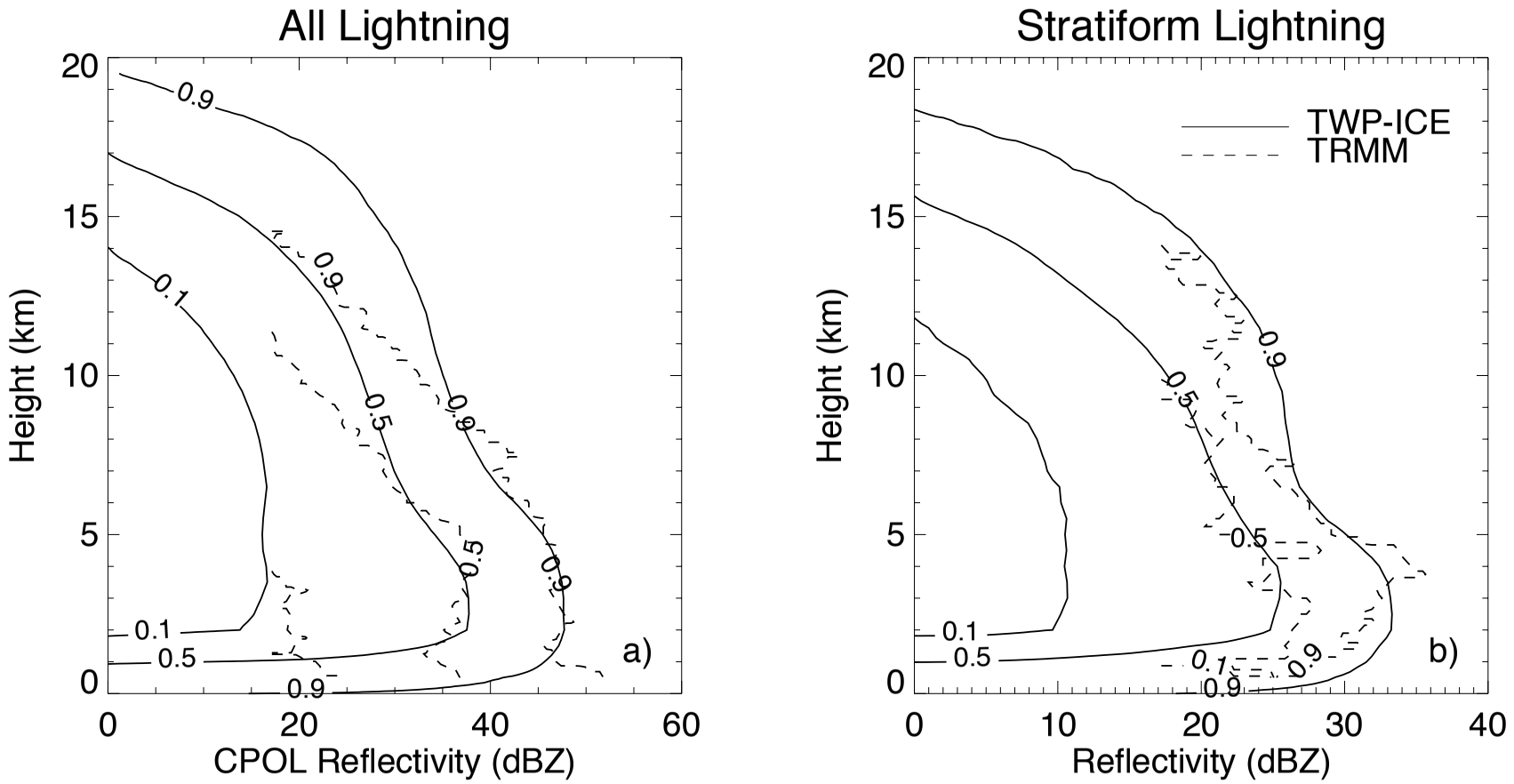

Figure 4.6 Contour Frequency by Altitude Diagram (CFAD) of CPOL radar reflectivity at the locations of a) all flashes and b) stratiform flashes for CPOL and LINET observations (solid lines) during TWP-ICE and TRMM observations (dashed lines) over the TWP-ICE region and season.

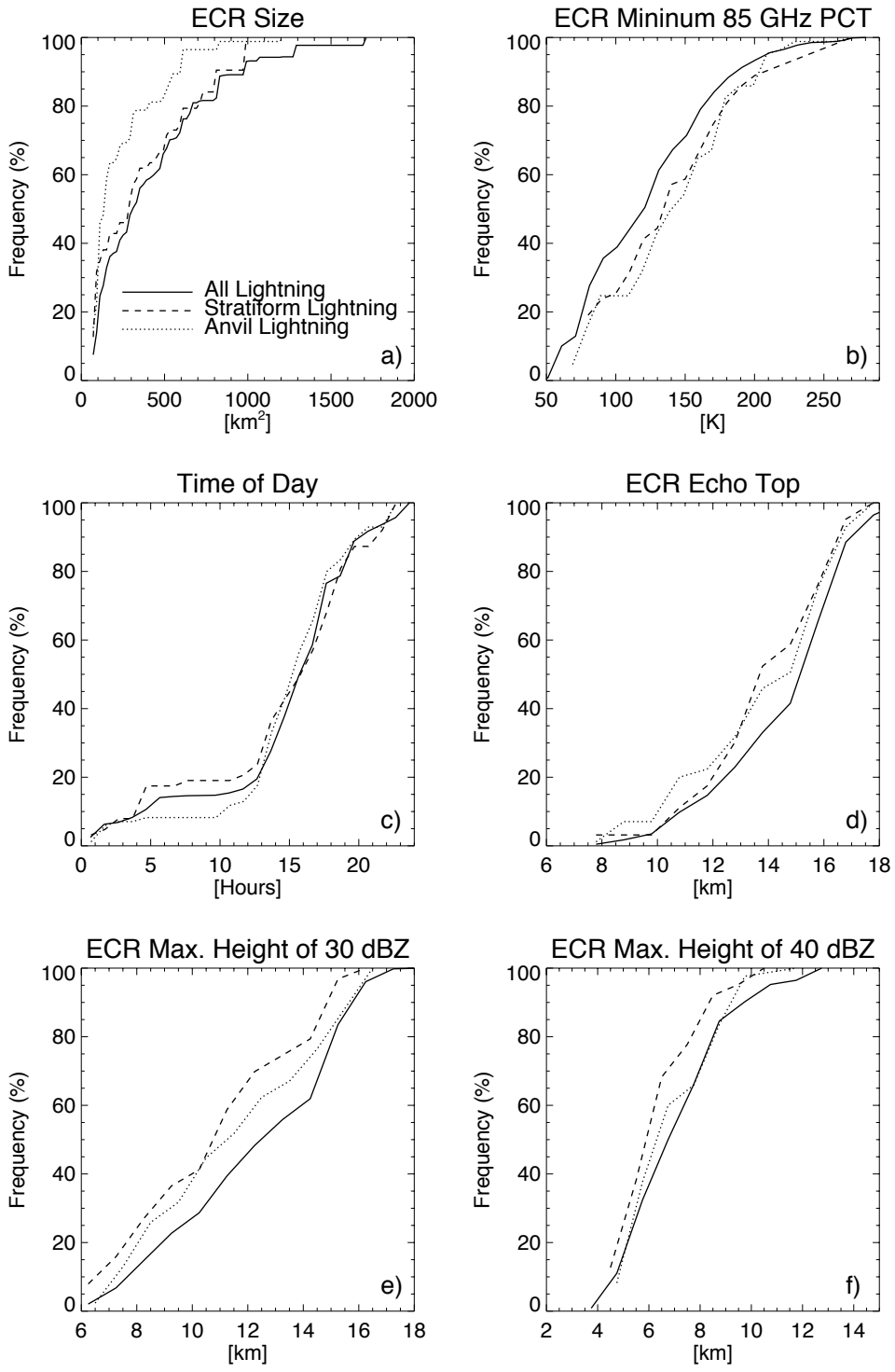

Figure 4.7 Cumulative distribution functions of the properties of TRMM PR-observed lightning-producing ECRs during December, January and February between 1998 and 2010 over 129.8 °E – 132.2 °E and 13.6 °S - 10.8 °S categorized by flash type and weighted by flash count of each type including a) ECR size; b) ECR minimum 85 GHz PCT; c) local time; d) ECR maximum echo top; e) ECR maximum 30 dBZ echo top; and f) ECR maximum 40 dBZ echo top.

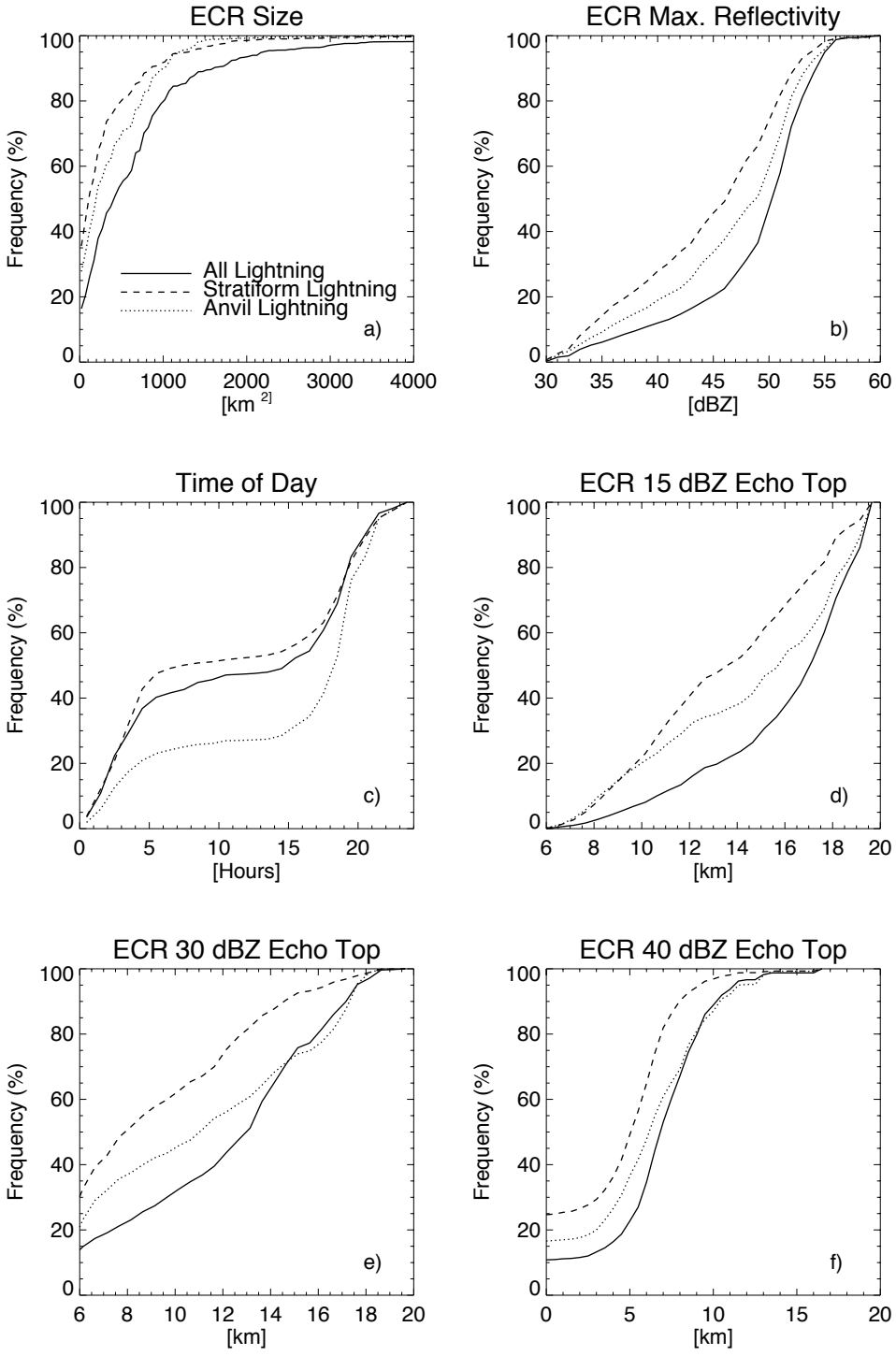

Figure 4.8 Cumulative distribution functions of the properties of CPOL-observed lightning-producing ECRs during TWP-ICE categorized by flash type and weighted by flash count of each type including a) ECR size; b) ECR maximum reflectivity; c) local time; d) ECR maximum 15 dBZ echo top; e) ECR maximum 30 dBZ echo top; and f) ECR maximum 40 dBZ echo top.

observed in TWP- ICE and some of them initiated an incredible number of lightning flashes – more than 1,000 in a 10-minute period, in some cases – introducing some bias into these statistics.

4.3 Tracking Convective Systems during TWP-ICE

To better understand the nature of stratiform and anvil flashes throughout the life cycle of convection, as well as to understand the differences in the statistics TRMM presented in the last section, it is important to investigate the properties of individual convective systems sampled during the TWP-ICE in addition to the properties of individual ECRs. Being able to track and analyze individual storms is one of the key advantages that TWP-ICE observations has over TRMM. To be able to describe the life cycles of all the convective systems, first, all of the ECRs within the convective systems are identified in each CPOL volume scan. Then, the life cycles of the ECRs as well as the convective systems are tracked manually between 1/19/2006 and 2/14/2006. During this time period, the region was under the influence of both land-based and oceanic systems.

There are many convective systems passing through the Darwin area during the TWP-ICE period; however, not all of them are suited for the study. In order for a case to be considered, a number of criteria must be met. First, the system must remain inside the CPOL radar domain and isolated from other convective systems for most of its life. These criteria reduce the risk of misassociations of lightning flashes to ECRs. Single-cell cases and cases where the original cells formed within the radar domain are preferred. Throughout the field campaign, 15 cases are identified and some of their properties can be found in Table 4.3. Daily flash counts for all lightning, stratiform lightning, and anvil

lightning are presented in Figure 4.9. All of the 15 cases are over land. No cases over the ocean are included because most of them had little lightning, or are in disorganized systems making it difficult to differentiate between ECRs in the system of interest and other nearby cells. However, these cases represent a variety of storms. Some of the systems last only an hour or two and produce a few flashes, while others last more than 7 hours and spawn thousands of lightning flashes. In one case, a 7-hour storm crosses virtually the entire radar domain, a distance of 250 km, while another case only manages to move 50km in the same amount of time. Most of the selected cases have 15 dBZ echoes taller than 18 km at some point in their lives, and all cases have 30 dBZ echoes exceeding 10km. All 15 cases are chosen during days with offshore flow. This is partly due to the fact that these periods have up to 3 orders of magnitude more lightning, but mostly due to the complex nature of oceanic convention making it difficult to track individual systems on days with onshore flow, as well as uncertainties in lightning flash associations induced by the extensive areas of stratiform rain and shallow convection prevalent in these systems. While these cases are interesting, it is difficult to get a "good," "solid" case out of this weather pattern given the limitations in the methodology and LINET artifacts. Three of these cases are selected for detailed discussion in Chapter 5. These three cases are chosen arbitrarily after examining the time series of each case based on their duration, size, intensity, and complexity. Cases that are excessively complex or that show evidence of significant contamination by misassociated flashes are not considered for the final 3.

Table 4.3 Overview of the properties of 15 convective systems examined during TWP-ICE. Bold columns represent selected cases to be discussed in Chapter 5.

#	Date	Start Time (UTC)	Traversed Distance (km)	Duration (hr)	Maxht 15 (km)	Maxht 30 (km)	Largest ECR (km^2)	Flash Count	Strat. Flash Count	Anvil Flash Count
1	**1/22**	**6:50**	**100.38**	**5.50**	**19.49**	**14.36**	**1119.2**	**570**	**62**	**15**
2	1/23	7:30	178.36	7.00	20.00	15.90	305.25	857	121	75
3	2/6	7:10	136.18	7.50	18.97	16.41	407.00	2120	434	368
4	2/6	7:30	92.29	3.83	18.46	14.36	477.70	1807	210	134
5	2/7	4:20	108.28	1.67	15.90	12.82	325.60	55	3	1
6	2/7	4:20	50.59	2.83	19.49	15.38	305.25	753	59	38
7	2/7	4:50	113.02	4.83	17.44	13.84	162.80	440	47	43
8	**2/7**	**6:20**	**85.67**	**3.00**	**20.00**	**15.38**	**529.10**	**1077**	**126**	**138**
9	**2/9**	**5:20**	**156.11**	**6.67**	**20.00**	**17.94**	**1302.4**	**18185**	**1494**	**1826**
10	2/10	4:50	96.47	3.33	18.97	15.38	712.25	2243	60	137
11	2/11	6:10	45.68	1.33	17.43	11.79	325.60	401	64	56
12	2/11	11:00	251.54	7.67	17.94	13.33	223.85	1145	64	642
13	2/12	12:20	48.65	7.00	20.00	17.95	264.55	9858	1509	531
14	2/13	9:10	199.56	5.50	18.97	17.95	468.05	715	102	43
15	2/14	4:50	66.70	2.17	15.90	10.77	81.40	124	27	19

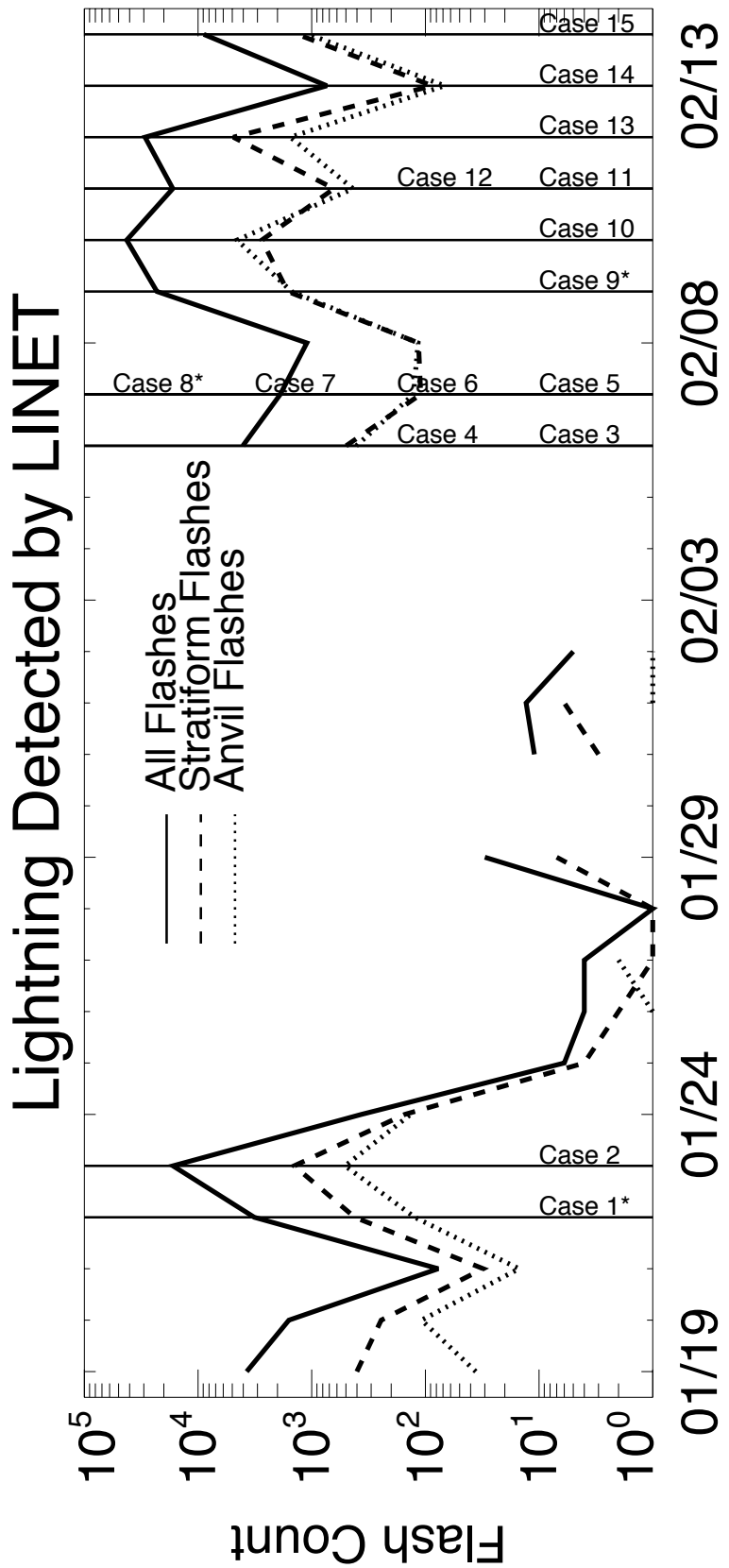

Figure 4.9 Daily flash counts, stratiform flash counts and anvil flash counts throughout the course of the TWP-ICE field campaign. Days with cases selected for examination are indicated by vertical lines. Case numbers on a particular day are shown to the right of the marker, and asterisks designate selected cases to be discussed in Chapter 5. Discontinuities indicate no flashes, due to the logarithmic y-axis.

CHAPTER 5

TWP-ICE CASE STUDY

5.1 Case 1: January 22nd, 2006

The first case selected for detailed analysis occurred on 1/22/2006. This particular case spawned 570 lightning flashes over the course of 5.5 hours, including 62 stratiform flashes and 15 anvil flashes, as it moved northwest across the CPOL domain. The life history of this storm is presented in Figure 5.1. The system started out as a single small convective cell with 15 dBZ echoes below 8 km. While no lightning was observed during the first hour of its life (6:50 – 7:50 UTC), it grew substantially, resulting in 15 dBZ echoes exceeding 18 km. The first lightning flashes were observed after 8:00 UTC.

The system continued to grow in size, becoming a multicell convective line, until it reached its maximum areal extent and flash rate at 9:20 UTC. Figure 5.2 shows the structure of the convective line at 9:20 UTC as well as a vertical cross section through the convective line. At this time, the system consisted of one large elongated ECR encompassing a number of convective cells. Most lightning flashes are concentrated in a cluster near the center of the system, and some anvil flashes are evident to their south. The vertical cross section bisects this anvil flash cluster, and the range-height structure of these flashes is given in Figure 5.2b superimposed on the CPOL vertical reflectivity. All of these anvil flashes are CG flashes (flash heights at 0 km), and occur in a region with a

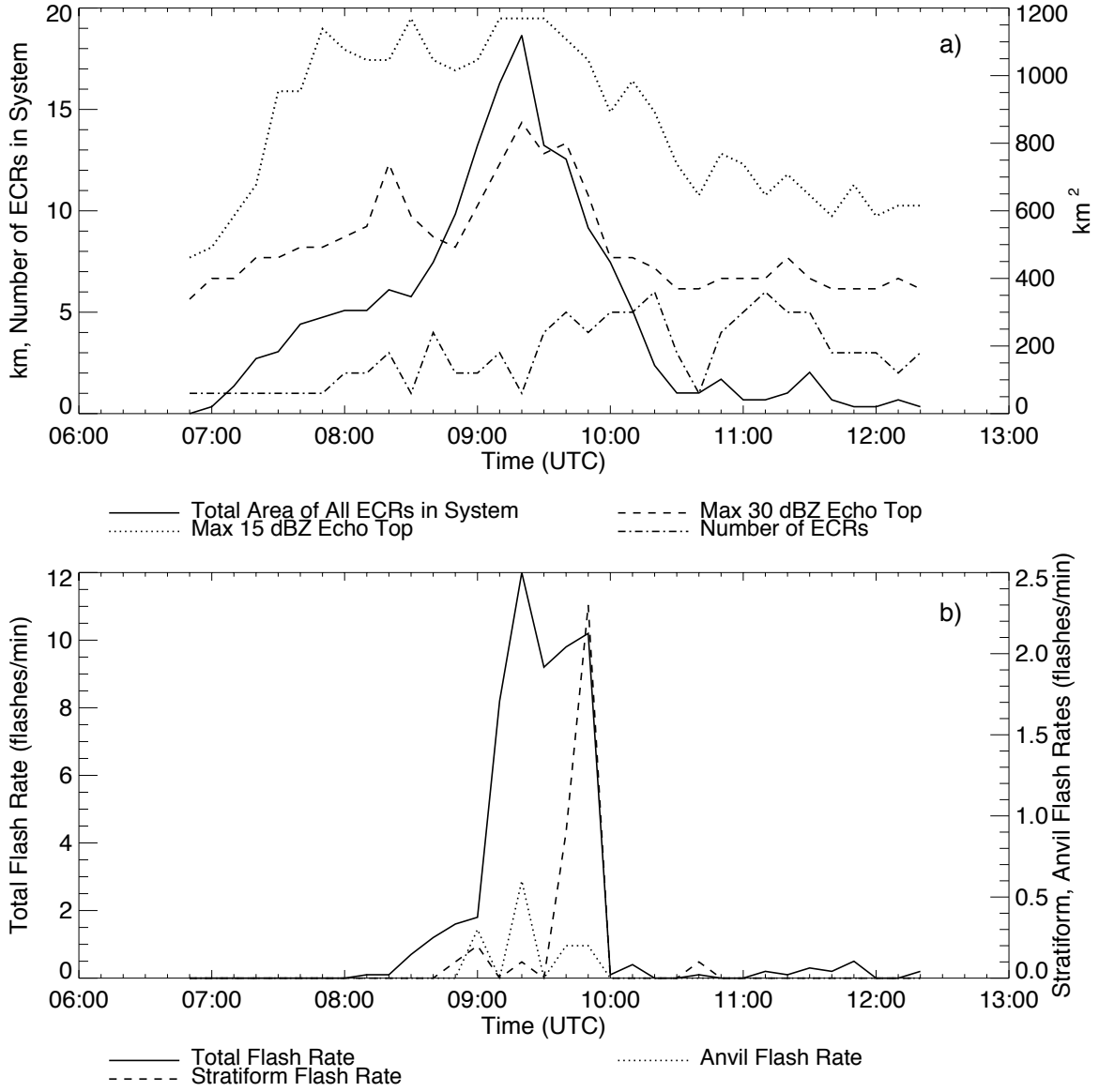

Figure 5.1 Time series of the properties of an isolated convective system observed on January 22nd, 2006 during TWP-ICE. a) Total areal extent of all ECRs within the system, system maximum 15 dBZ echo top height, system maximum 30 dBZ echo top height, and number of ECRs within the system, and b) Total flash rate, stratiform flash rate, and anvil flash rate.

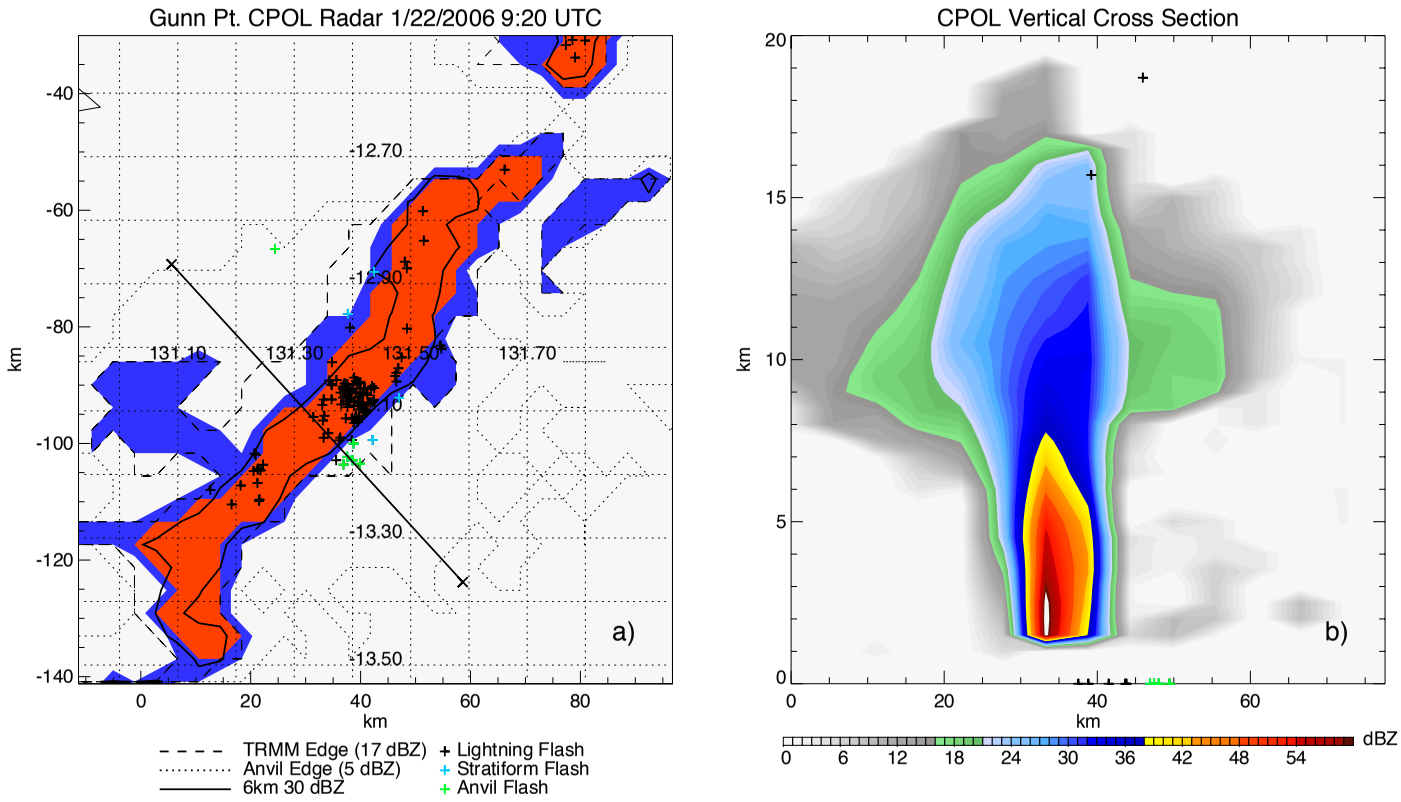

Figure 5.2 CPOL and LINET observations at 9:20 UTC on January 22nd, 2006. (a) Plan view of the structure of the convective system determined by CPOL. Axes show the distance relative to the CPOL radar. Areas shaded in blue are stratiform, and red areas are convective based on output from the Steiner algorithm. Solid contour shows regions with 30 dBZ at 6 km. Dashed contour shows reflectivity greater than 17 dBZ at any level (echoes the TRMM PR could detect). Dotted contour shows the region with 5 dBZ at any level. Lightning flashes are indicated by plus signs, with yellow corresponding to anvil flashes and indigo corresponding to stratiform flashes. (b) Vertical cross section of CPOL reflectivity along the solid line indicated in (a). The locations of nearby (within 10km) lightning flashes are shown in the same manner as (a). CG flashes are shown to be at z=0. Note that there is a large uncertainty in the height of flashes in LINET data.

pronounced anvil outflow structure. Weak echoes near the surface (< 15 dBZ) indicate that, while the Steiner algorithm does not classify this region as stratiform (Figure 5.2a), that a trailing stratiform region may be beginning to develop. Furthermore, all of these flashes occurred within 10 km of the convective core, and it is likely that these flashes originated in the convective line and struck a target outside the cell's boundaries.

Throughout the next half hour between 9:20 UTC to 9:50 UTC, the convective system begins to weaken considerably. Going back to Figure 5.1, not only does the total area of the system decrease, but also do the heights of the 15 and 30 dBZ echoes. Lightning remains fairly common, however, and a large number of stratiform flashes are observed as the system starts to decay. Figure 5.3 shows the storm structure at 9:40 UTC. Indeed, the stratiform region behind the southern flank of the convective system has grown since 9:20 UTC, and a number of stratiform flashes are evident in this region. Many of these stratiform flashes can be seen in the cross section in Figure 5.3b. Most of these flashes are CG flashes, however at least one of them is an IC flash.

The stratiform region determined by the Steiner algorithm is not extensive at this time, begging the question whether this region is stratiform at all, or merely a weaker part of the convective region. Forcing regions with 30 dBZ echoes at 6 km to be convective was a step in the right direction, but without a bright-band detection routine, there is still an elevated potential for misclassification. Of course, this question is not an issue for all stratiform flashes, in particular for those in more mature stratiform precipitation.

A large number of stratiform flashes are observed at 9:50 UTC, most of which on the northwest flank of the system. The storm structure at this time is shown in Figure 5.4, including a cross section through the region in which these stratiform flashes occur.

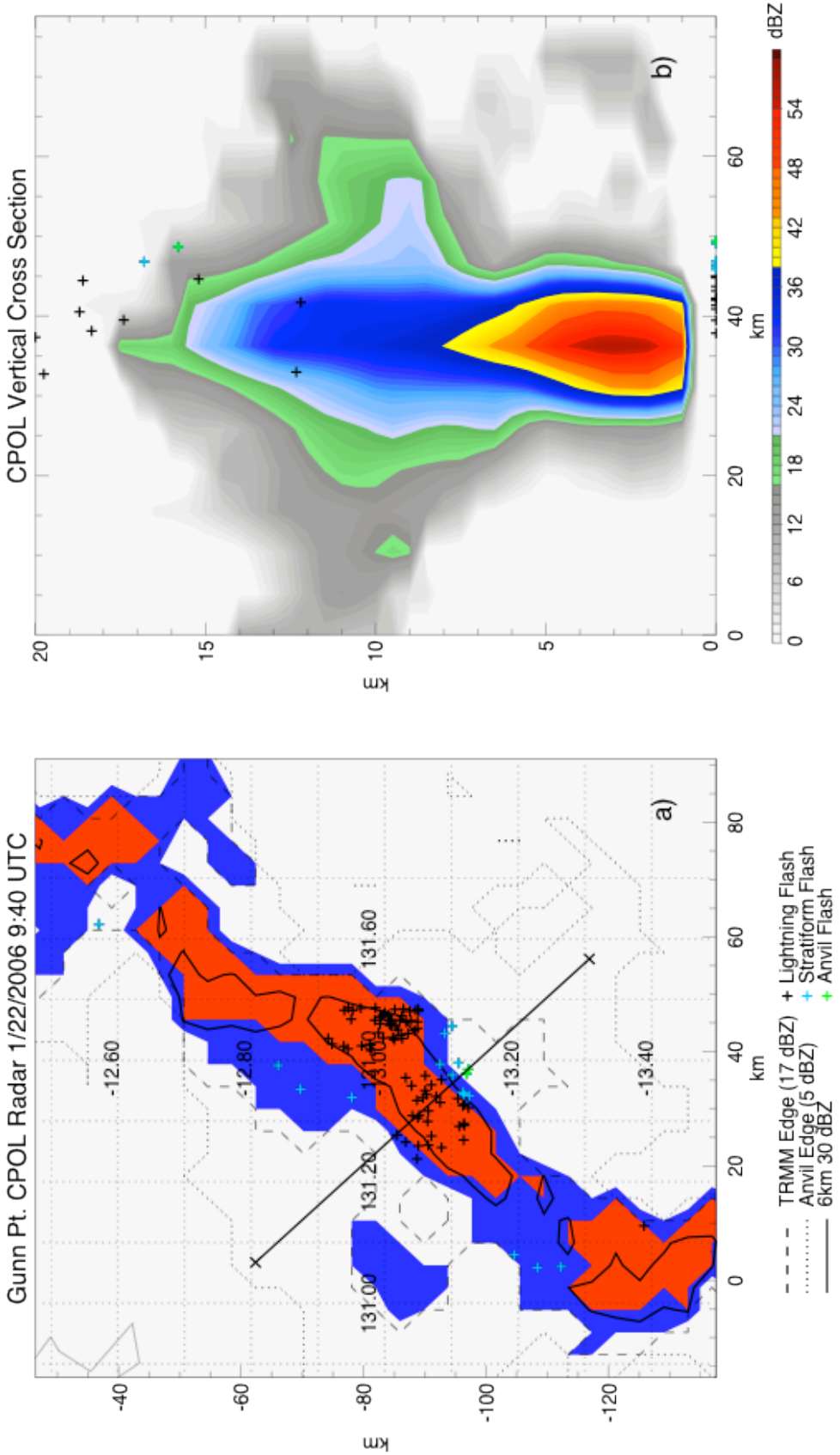

Figure 5.3 Same as Figure 5.2 except for CPOL and LINET observations at 9:40 UTC on January 22nd, 2006.

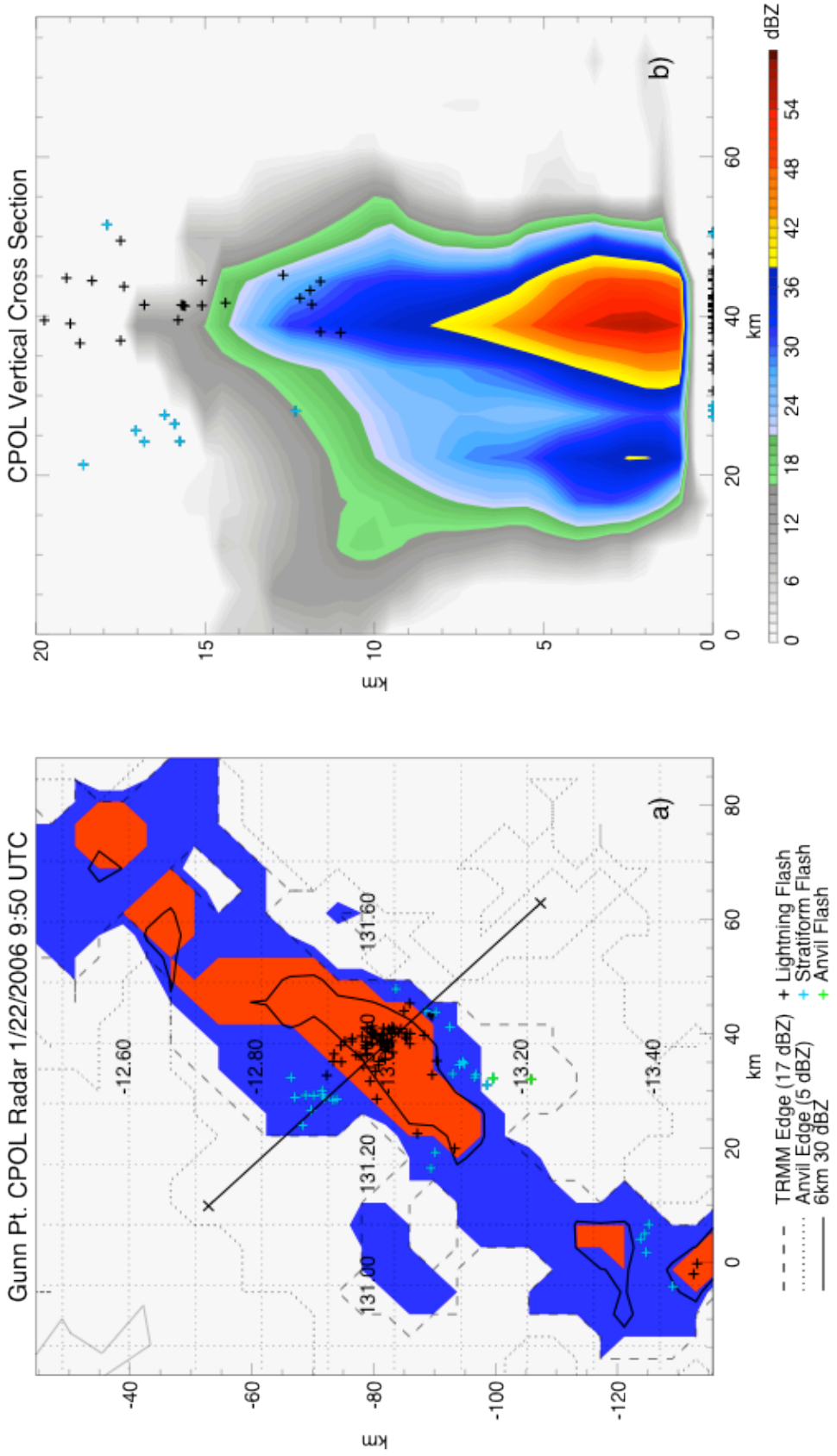

Figure 5.4 Same as Figure 5.2, except for CPOL and LINET observations at 9:50 UTC on Jan 22nd, 2006.

Unlike the previous group of stratiform flashes, more than half of these flashes are IC flashes between the main line of convection and the surrounding stratiform precipitation. In this case, it is likely that these stratiform flashes initiated within the convective core and propagated through the stratiform region.

After this, the system decayed rapidly, producing few lightning flashes. As the convective cells continued to decay, the storm system became dominated by stratiform rain, and eventually, the storm moved out of view of the radar.

5.2 Case 8: February 7th, 2006

The second case (#8 in the Table 4.3) occurred on February 7th, 2006. As seen in Table 4.3, this case had a short duration of only 3 hours. However, in that time, it traversed 85 km and spawned 1077 lightning flashes, including 126 stratiform flashes and 138 anvil flashes. The time series for this case is shown in Figure 5.5. Like the previous case, this system started out as a single shallow convective cell moving northwest across northern Australia. Between 7:30 and 8:00 UTC, however, the system strengthened and became a multicell convective system.

Both stratiform and anvil lightning flashes were observed during this time period, though anvil flashes were significantly more common. This can be seen in Figure 5.6. At 7:50 UTC, anvil flashes were occurring along the rear flank of a tall and thin convective core (Figure 5.6b) just to the southeast of a cluster of lightning within the convective region (Figure 5.6a). These flashes were mostly CG flashes; however, IC anvil flashes were also observed (Figure 5.6b), implying that the anvil may be charged and playing a role in the initiation of these flashes.

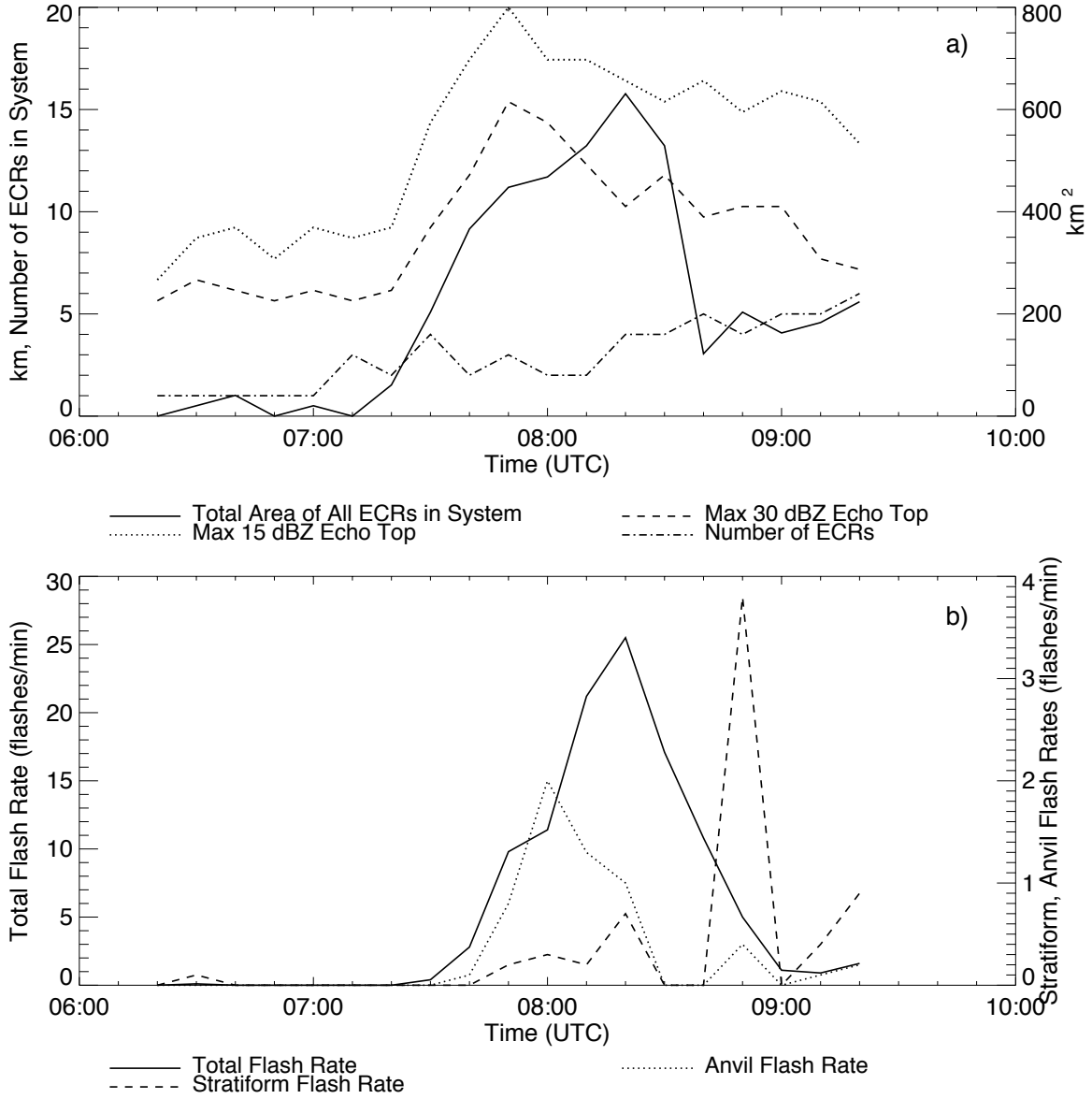

Figure 5.5 Time series of the properties of a short-lived convective system observed on February 7th, 2006 during TWP-ICE. a) Total areal extent of all ECRs within the system, system maximum 15 dBZ echo top height, system maximum 30 dBZ echo top height, and number of ECRs within the system, and b) total flash rate, stratiform flash rate, and anvil flash rate.

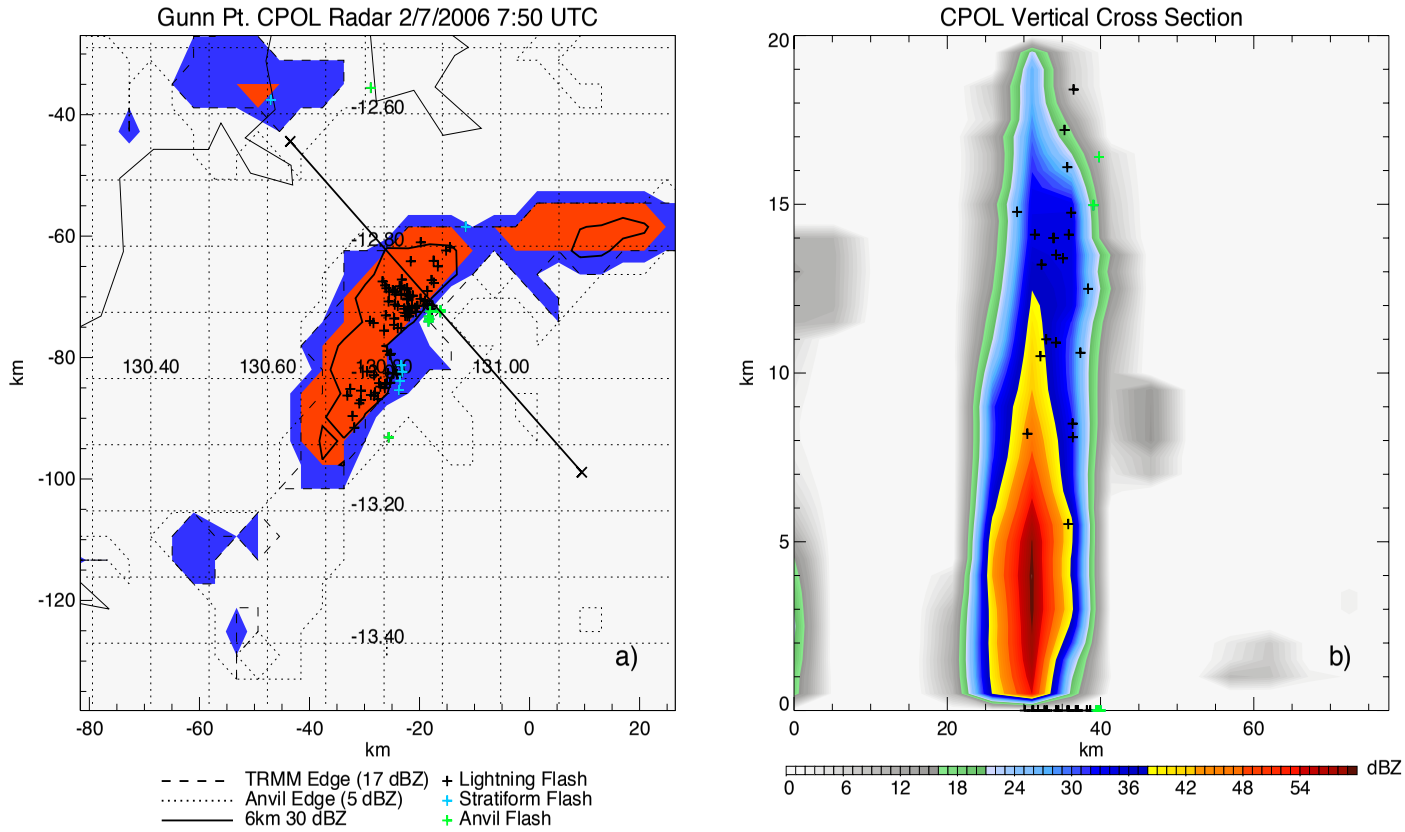

Figure 5.6 CPOL and LINET observations at 7:50 UTC on February 7th, 2006. (a) Plan view of the structure of the convective system determined by CPOL. Axes show the distance relative to the CPOL radar. Areas shaded in blue are stratiform, and red areas are convective based on output from the Steiner algorithm. Solid contour shows regions with 30 dBZ at 6 km. Dashed contour shows reflectivity greater than 17 dBZ at any level (echoes the TRMM PR could detect). Dotted contour shows the region with 5 dBZ at any level. Lightning flashes are indicated by plus signs, with yellow corresponding to anvil flashes and indigo corresponding to stratiform flashes. (b) Vertical cross section of CPOL reflectivity along the solid line indicated in (a). The locations of nearby (within 10km) lightning flashes are shown in the same manner as (a). CG flashes are shown to be at z=0. Note that there is a large uncertainty in the height of flashes in LINET data.

The stratiform flashes at this time step were observed further to the southwest, as seen in Figure 5.6a. CPOL and LINET observations with a different cross section through this cluster of stratiform flashes are shown in Figure 5.7. Compared to Figure 5.6b, the convective region close to these stratiform flashes is rather weak. This part of the storm probably is further into the mature and dissipation stage. There are a handful of stratiform flashes along this cross section, occurring mainly just behind the convective region, most of which are IC flashes.

More anvil flashes were observed 10 minutes later at 8:00 UTC. Storm structure and cross sections through two regions producing a large number of anvil flashes are shown in Figures 5.8 and 5.9. The northern cross section (Figure 5.8) cuts through the same cell as 10 minutes earlier in Figure 5.6. During the 10-minute time frame, the cluster of anvil flashes has expanded to include the entire rear flank of the convective region. The majority of anvil flashes along this cross section are IC flashes that occur in regions with PR-detectible reflectivity. Similarly, the anvil flashes along the southern cross section shown in Figure 5.9 are entirely IC flashes occurring behind the convective line.

By 8:20 UTC, the system had reached its maximum areal extent, but was already showing signs of weakening. As shown in Figure 5.10, the main convective region had already split into 3 different ECRs. The time series of the properties of the system in Figure 5.5 shows that the maximum 15 and 30 dBZ echo tops had already dropped significantly. The largest number of stratiform flashes in the time series so far was also observed between the two largest ECRs in Figure 5.10, and with a mix of IC and CG flashes.

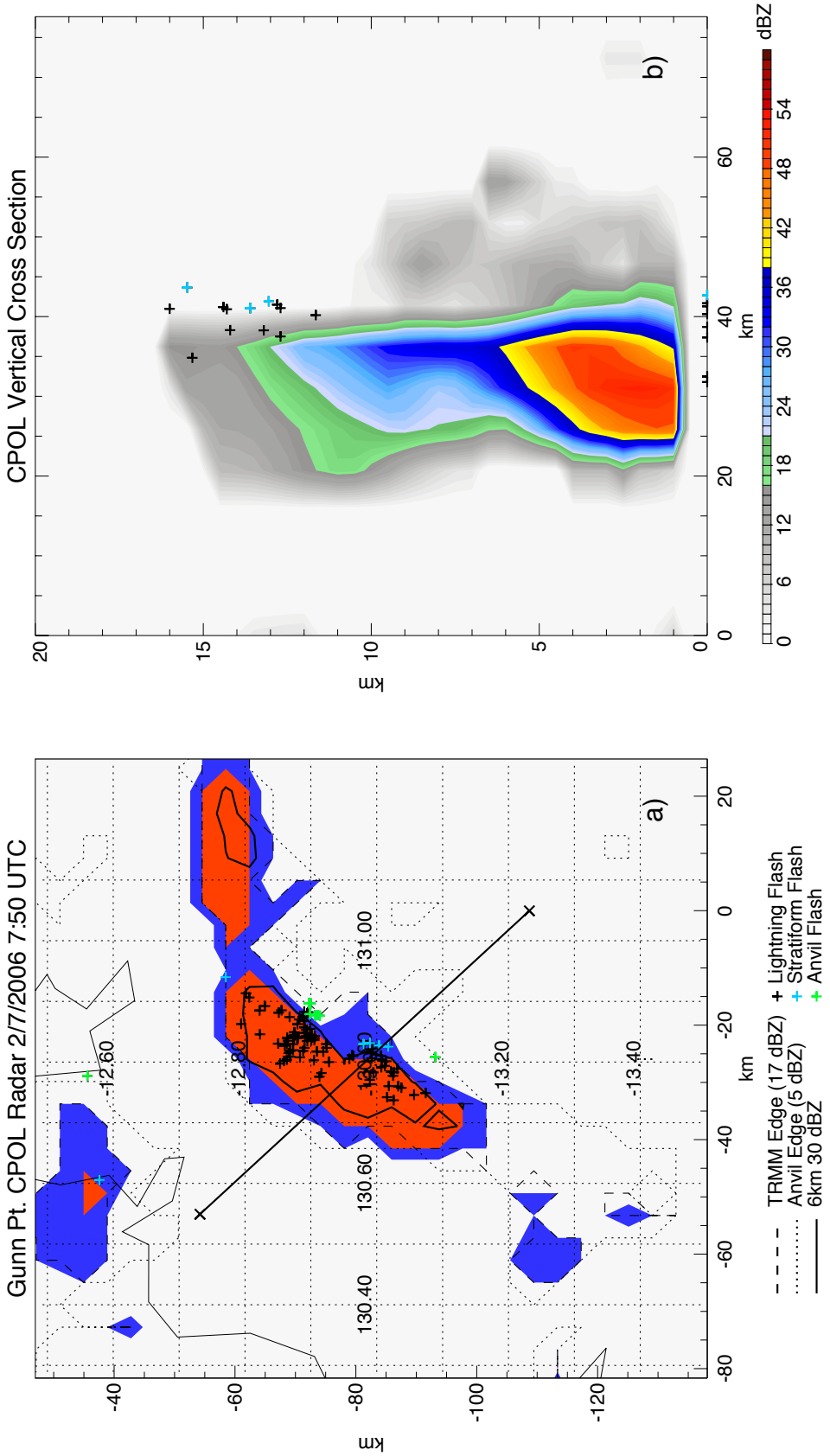

Figure 5.7 Same as Figure 5.6, except with a different cross section location.

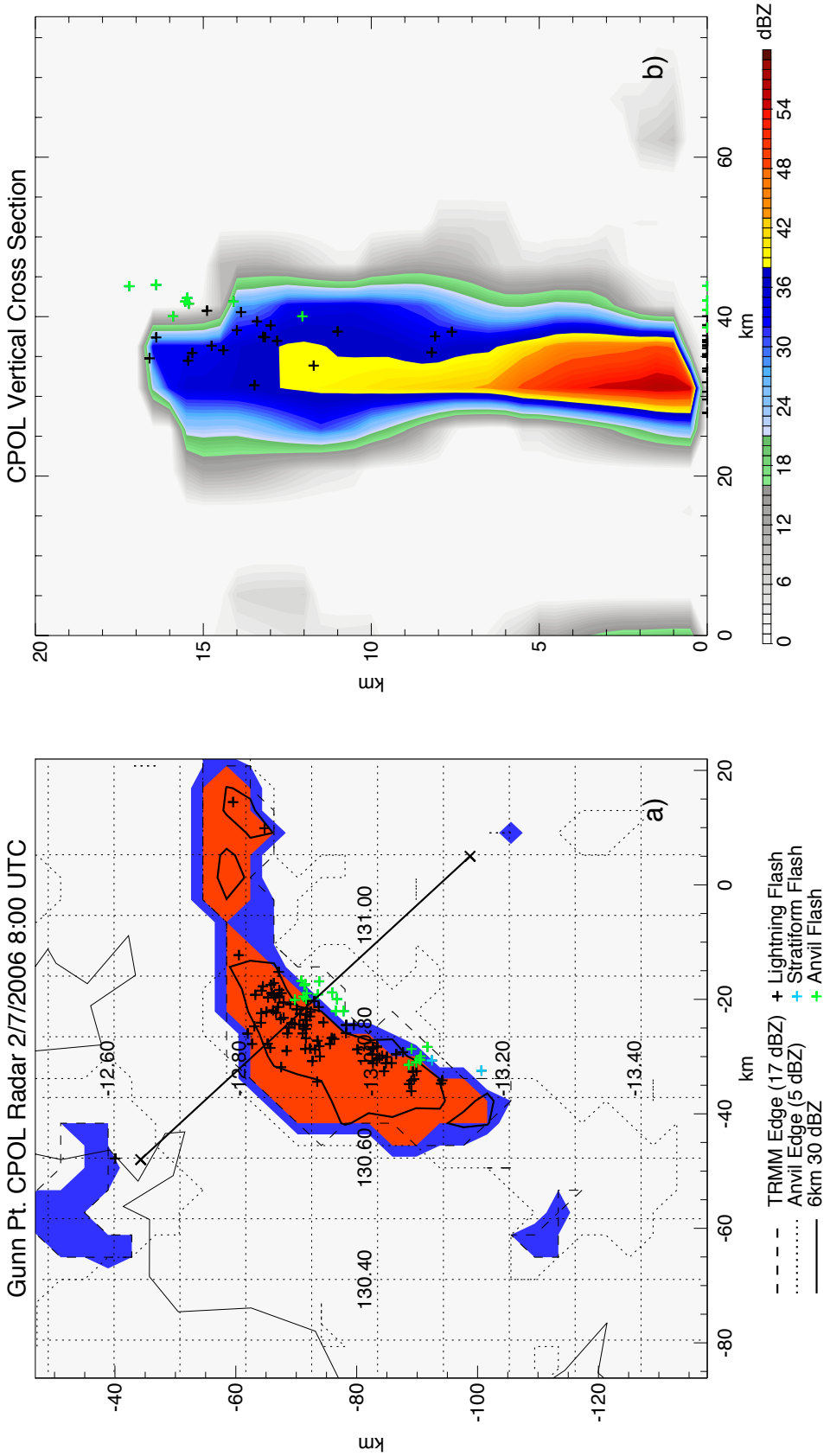

Figure 5.8 Same as Figure 5.6, except for CPOL and LINET observations at 8:00 UTC.

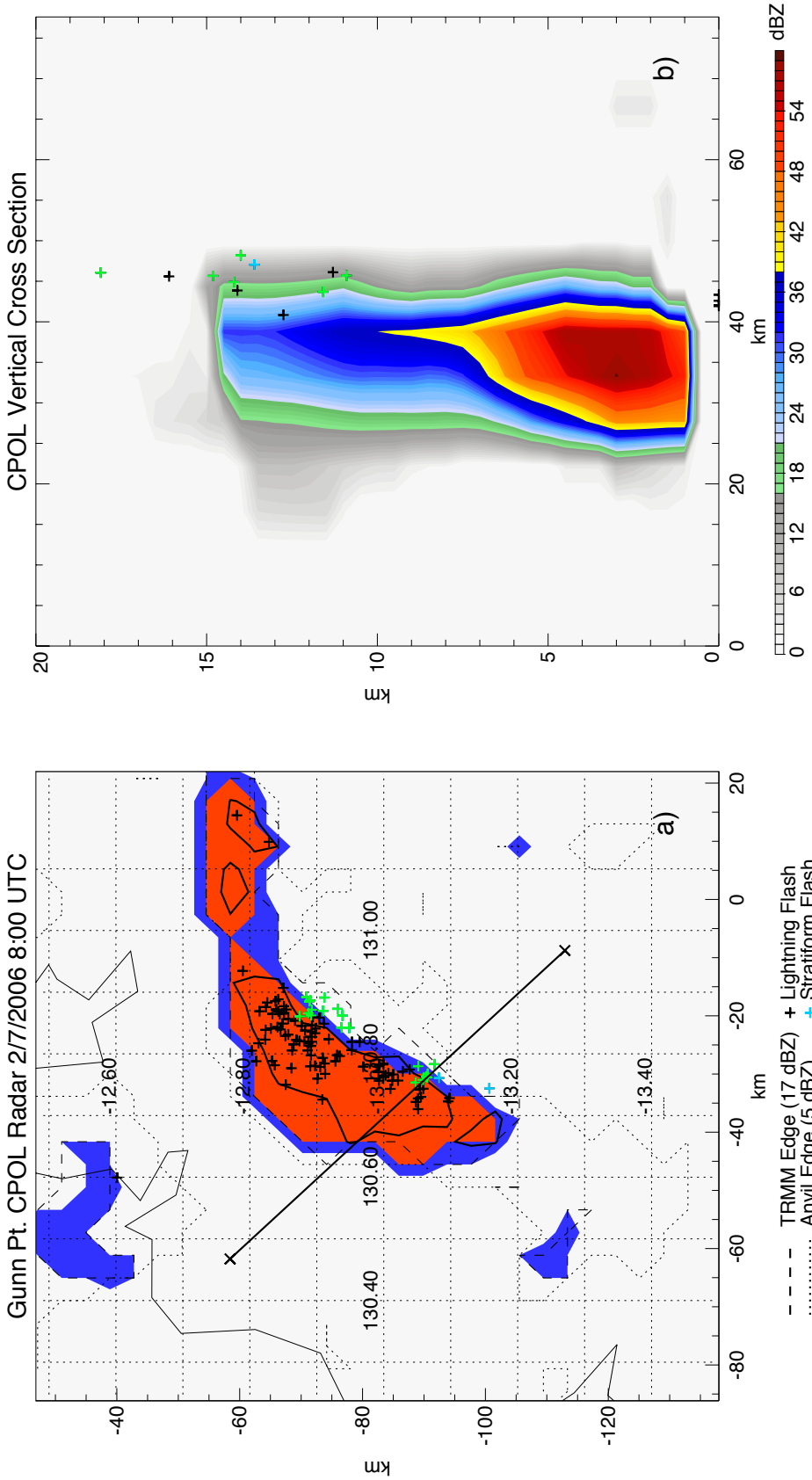

Figure 5.9 Same as Figure 5.6, except for CPOL and LINET observations at 8:00 UTC. Note this shows a different cross section from Figure 5.8.

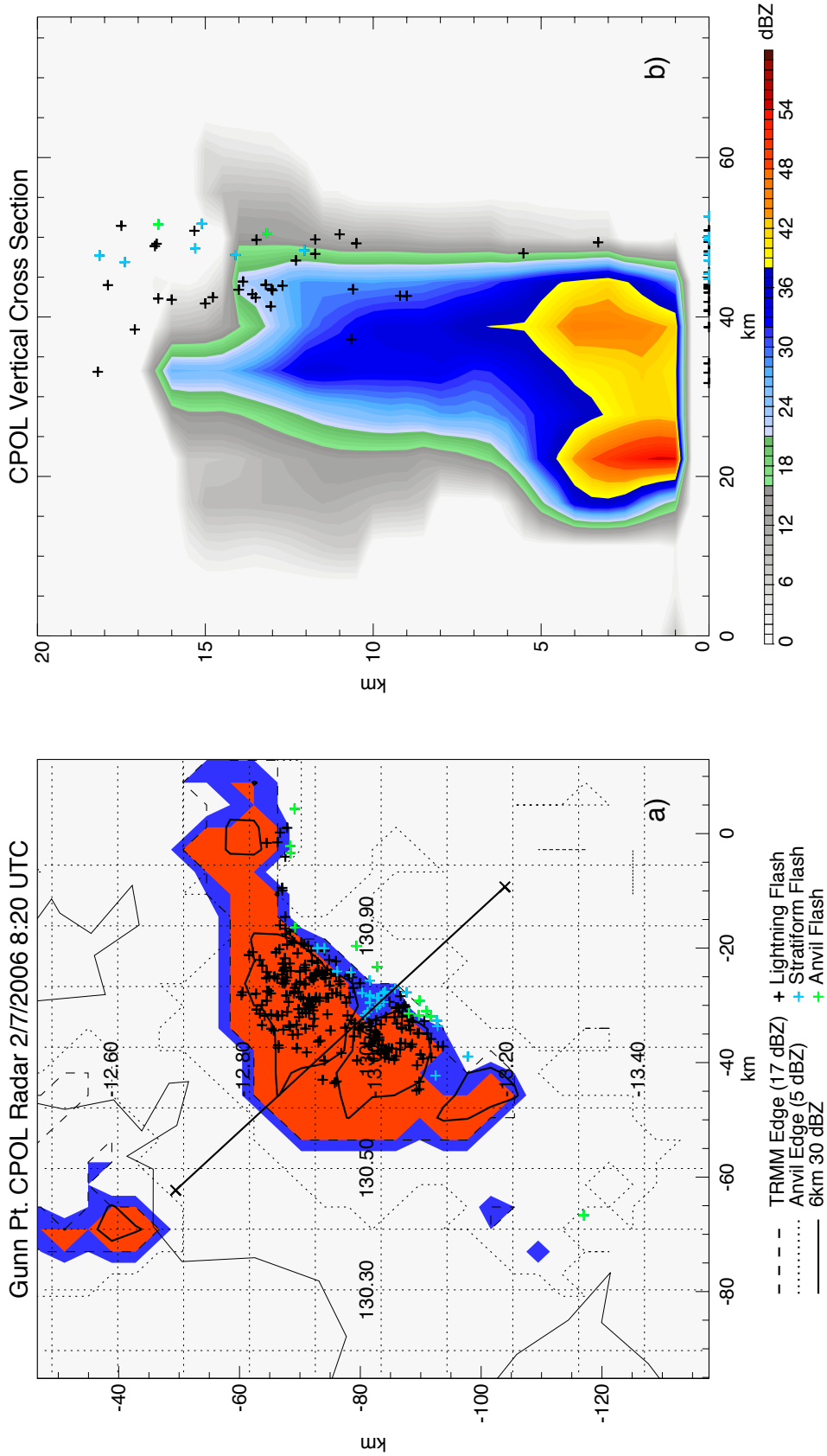

Figure 5.10 Same as Figure 5.6, except for CPOL and LINET observations at 8:20 UTC.

The system decayed rapidly, and just 20 minutes later at 8:40 UTC, the large ECRs of Figure 5.10 had turned into several small ECRs with an extensive region of stratiform precipitation shown in Figure 5.11. A large number of stratiform flashes were observed during this time period within a large area of stratiform precipitation, which is different from the smaller stratiform regions right along the convective line like in previous examples. Many of these flashes are likely the result of in situ processes as well as charge left behind by the rapidly decaying convective cells rather than the usual process of charge advection from the convective regions.

5.3 Case 9: February 9th, 2006

The third case (#9 of list on Table 4.3) chosen for discussion is the most active of all the cases examined. This convective system, unlike the others, started out as a disorganized line of convective cells that progressed 150 km to the southwest across the radar domain over the course of 6 hours and 40 minutes. During this time, the convective system spawned 18,185 lightning flashes, including 1,494 stratiform flashes and 1,826 anvil flashes. In fact, this case produced almost as much lightning as the total from all of the other cases in Table 4.3 combined, and likely is dominating in the TWP-ICE statistics mentioned in Chapter 4.

The time series of the storm properties is shown in Figure 5.12. The systems started moving into the CPOL range around 5:00 UTC. Then it gradually intensifies throughout the next hour. The first stratiform and anvil flashes associated with this system were observed at 6:40 UTC. The storm structure at this time step is shown in Figure 5.13. While still early in the convective system's time history, many of the

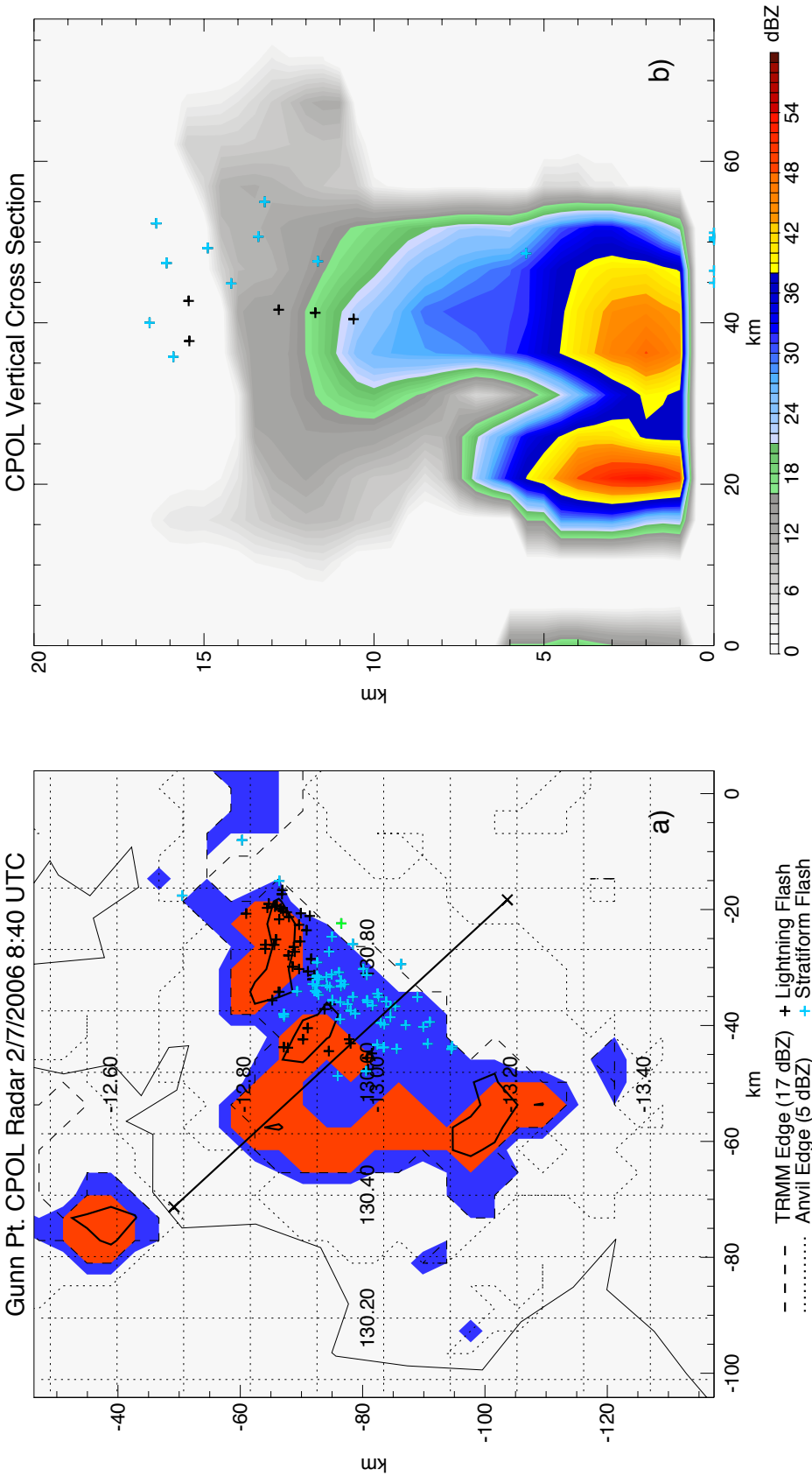

Figure 5.11 Same as Figure 5.6, except for CPOL and LINET observations at 8:40 UTC.

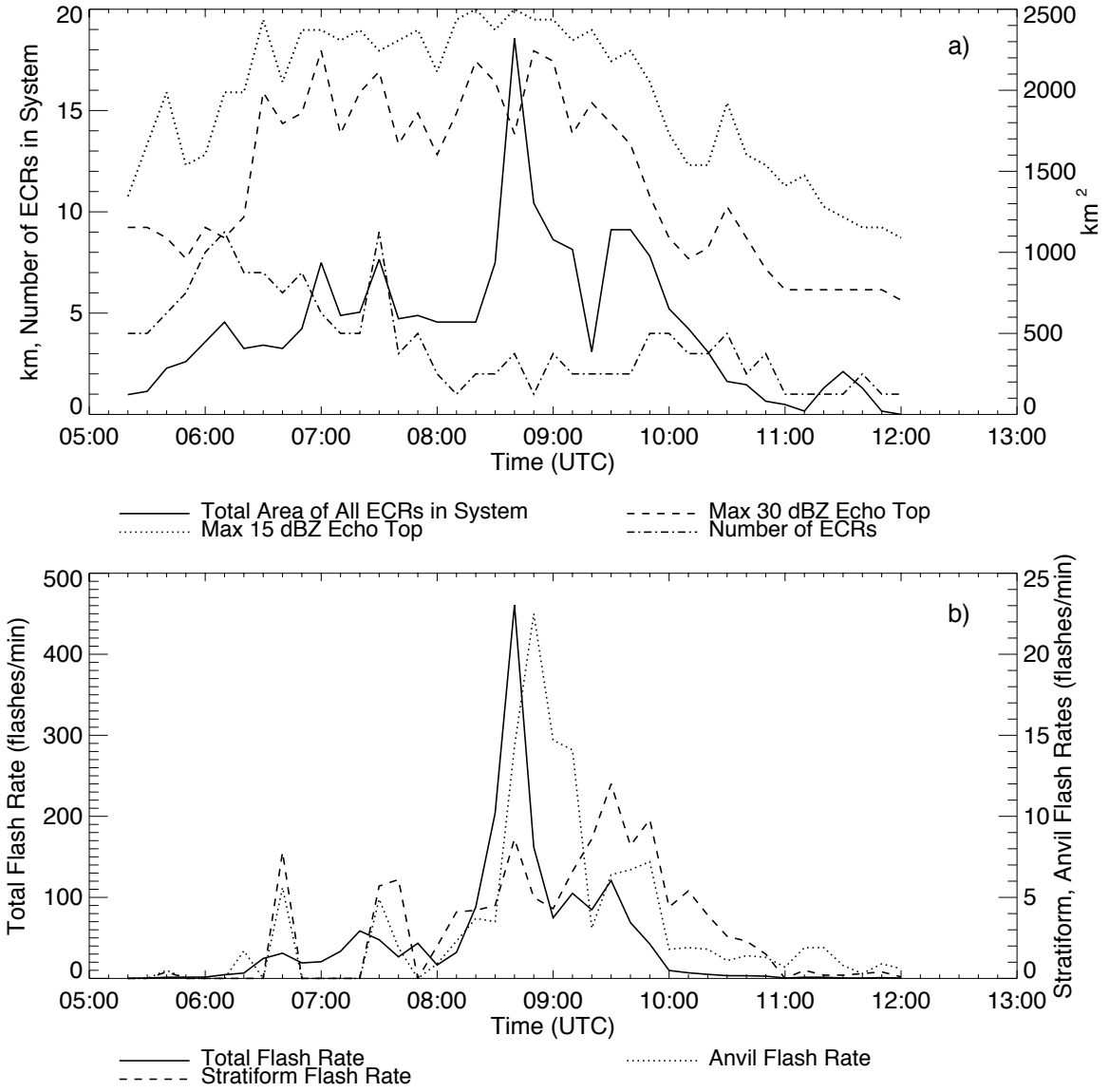

Figure 5.12 Time series of the properties of a multicell convective system observed on February 9th, 2006 during TWP-ICE. a) Total areal extent of all ECRs within the system, system maximum 15 dBZ echo top height, system maximum 30 dBZ echo top height, and number of ECRs within the system, and b) total flash rate, stratiform flash rate, and anvil flash rate.

individual ECRs in the line are already surrounded by extensive regions of stratiform precipitation. Stratiform and anvil flashes are behind each of the 4 main ECRs in the system, including a number of IC flashes shown in Figure 5.13b. There are also a number of anvil flashes at locations without 17 dBZ (outside of the dashed line) both directly behind the major cells in the system and between the two central ECRs, that would not be detected by TRMM.

The next peak in stratiform and anvil flashes occurs at 7:20 UTC. As seen in the storm structure presented in Figure 5.14, the northern cells have dissipated and the cells on the southern flank have weakened and are not producing lightning at this time. The central cells have become enveloped by a single extensive ECR. This ECR has a large number of lightning flashes and it is surrounded by a large region of stratiform precipitation. The stratiform and anvil flashes associated with this ECR occur primarily along the northern flank, where there is a large region of overhanging radar echo (Figure 5.14b).

Within 20 minutes, this area became entirely stratiform, and a large number of stratiform flashes were observed at 7:40 UTC (Figure 5.15). At the same time, a number of anvil flashes appeared in the north, where new convection had developed to the west of the maturing cells. The stratiform region continued to develop behind the largest ECR and, by 8:20 UTC (Figure 5.16), began to resemble the structure of a leading-line trailing stratiform mesoscale convective system with a mixture of both IC and CG stratiform flashes.

Over the next 20 minutes, the convective system grew rapidly, and reached its maximum flash rate. Then, at 8:50 UTC, a large number of anvil flashes were observed.

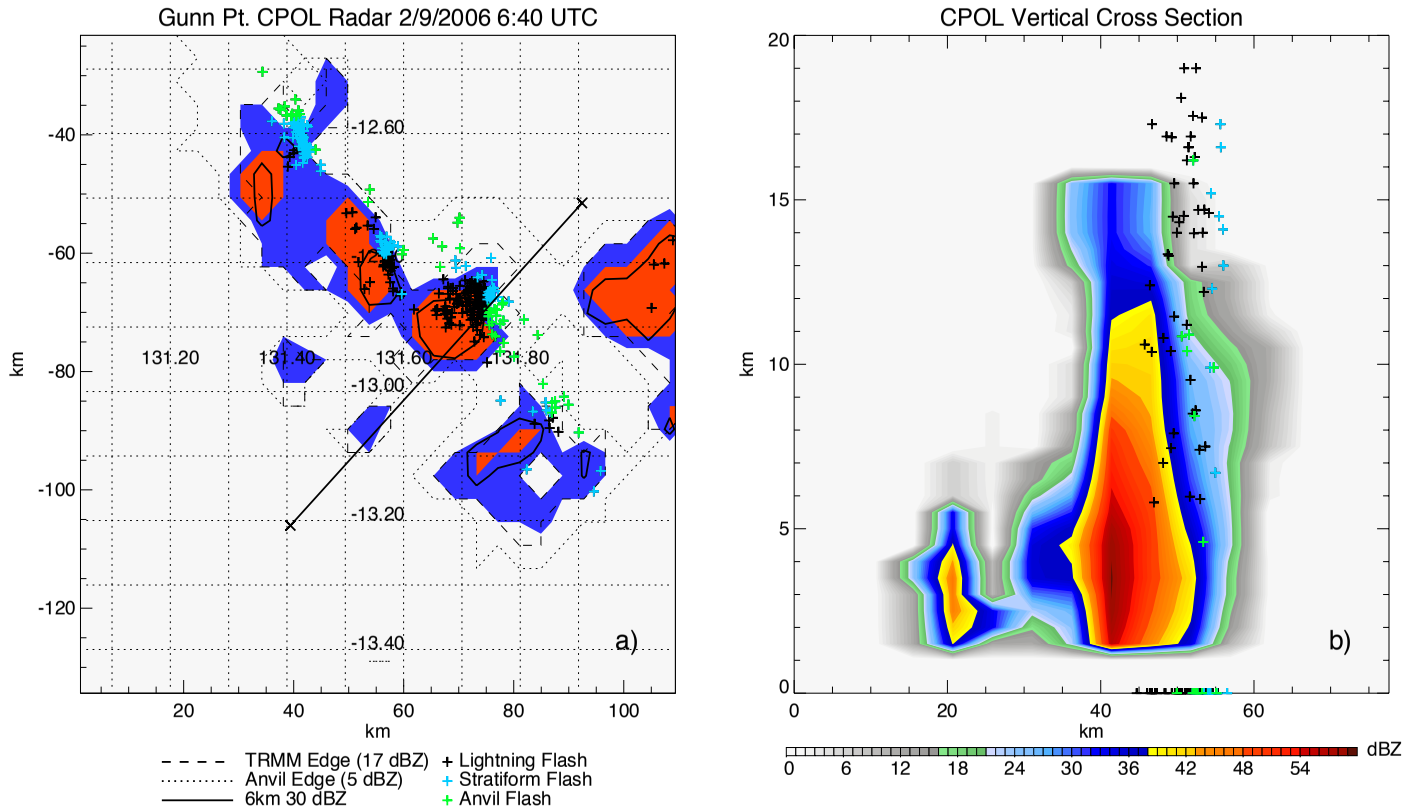

Figure 5.13 CPOL and LINET observations at 7:50 UTC on February 9th, 2006. (a) Plan view of the structure of the convective system determined by CPOL. Axes show the distance relative to the CPOL radar. Areas shaded in blue are stratiform, and red areas are convective based on output from the Steiner algorithm. Solid contour shows regions with 30 dBZ at 6 km. Dashed contour shows reflectivity greater than 17 dBZ at any level (echoes the TRMM PR could detect). Dotted contour shows the region with 5 dBZ at any level. Lightning flashes are indicated by plus signs, with yellow corresponding to anvil flashes and indigo corresponding to stratiform flashes. (b) Vertical cross section of CPOL reflectivity along the solid line indicated in (a). The locations of nearby (within 10km) lightning flashes are shown in the same manner as (a). CG flashes are shown to be at z=0. Note that there is a large uncertainty in the height of flashes in LINET data.

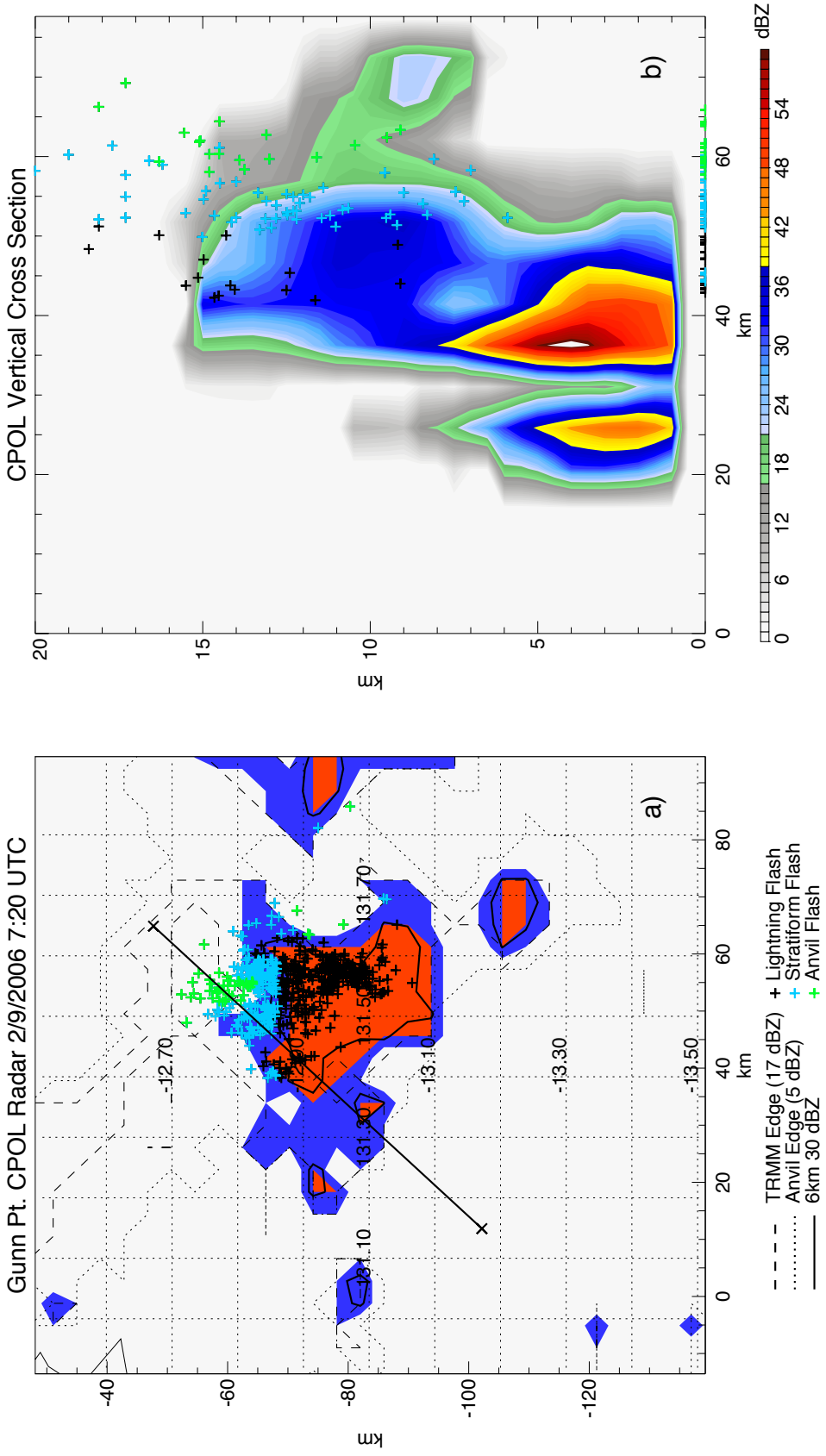

Figure 5.14 Same as Figure 5.13, except for CPOL and LINET observations at 7:20 UTC.

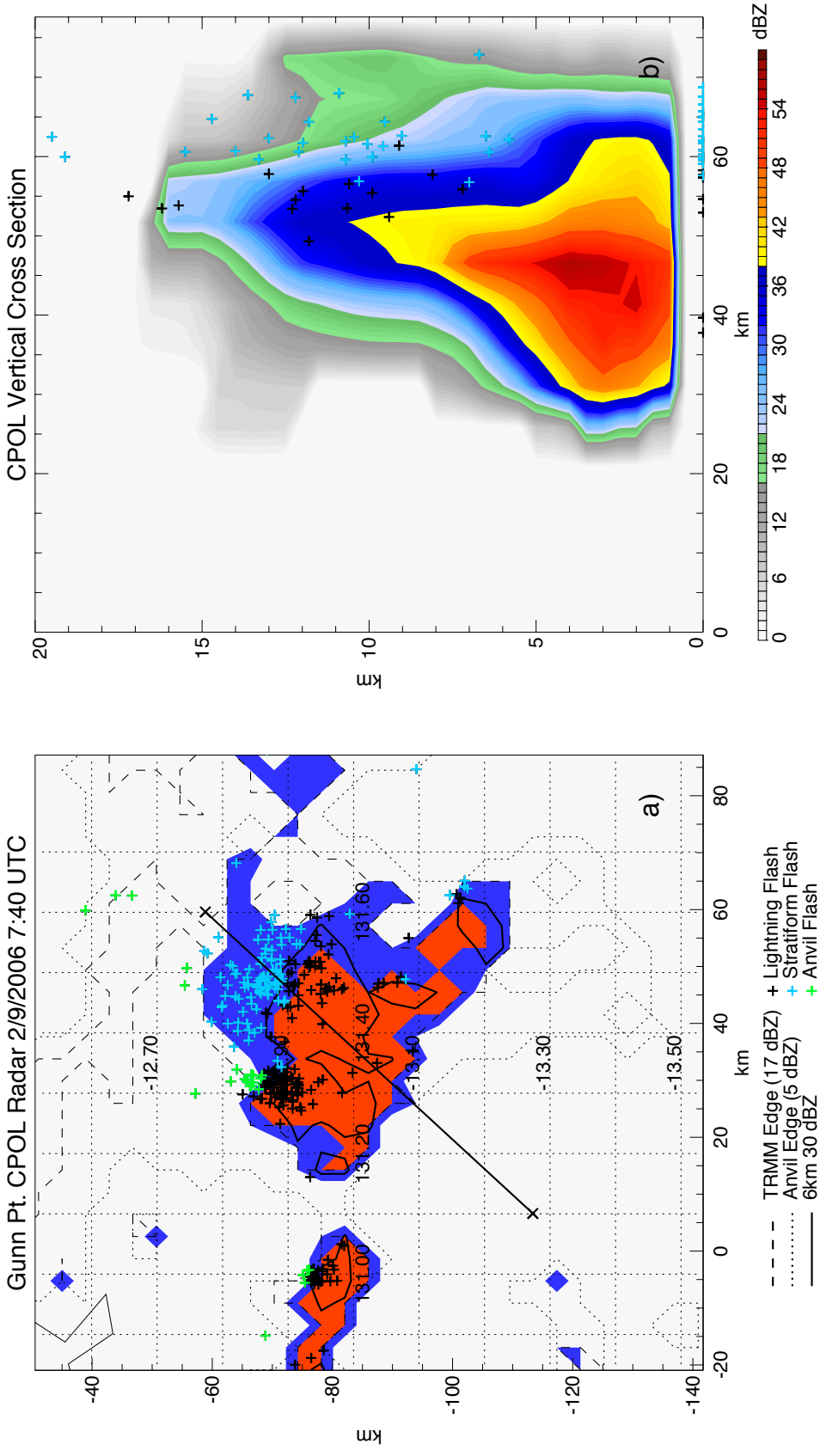

Figure 5.15 Same as Figure 5.13, except for CPOL and LINET observations at 7:40 UTC.

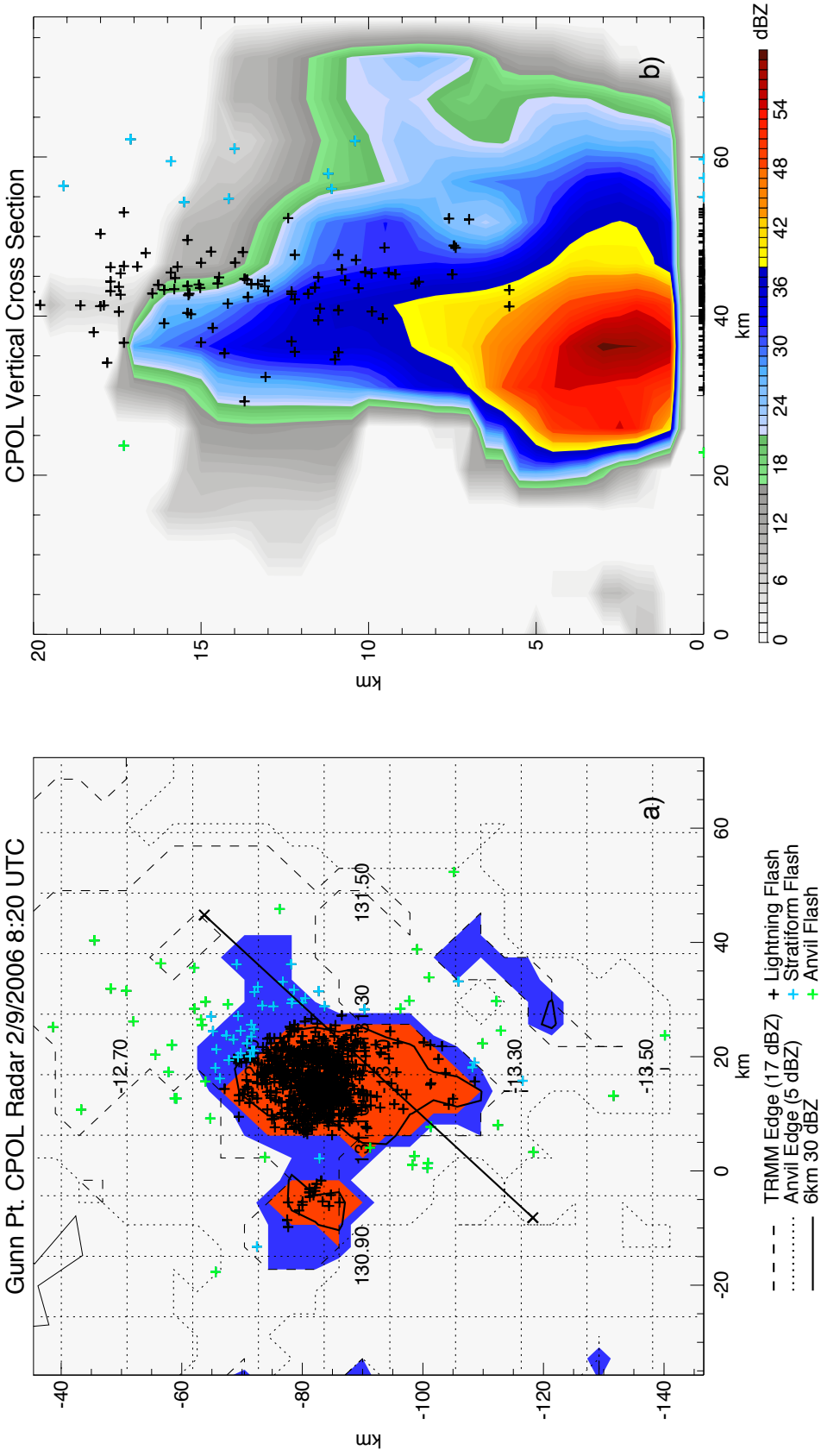

Figure 5.16 Same as Figure 5.13, except for CPOL and LINET observations at 8:20 UTC.

Figure 5.17 shows the convective structure of the system at this time. The major gains in storm area over this time period occurred in a region of new development to the south of the convective line. The overwhelming majority of anvil flashes occurred in this new convective region, though the older northern cells still were producing the most lightning overall. At this point, the new convective cells were tall and narrow (Figure 5.17b) with overhanging radar echoes to the rear. Substantial amounts of both IC and CG anvil flashes occurred along the cross section, and most anvil flashes occurred in regions with echoes below 17 dBZ.

The southern convective region continued to develop, and within 10 minutes, overtook the mature northern cells as the primary location of lightning flashes (Figure 5.18). Large amounts of anvil lightning occurred in the same region as the previous time step while the northern region began to fracture into multiple ECRs. By 9:10 UTC (Figure 5.19), a large portion of the northern region of the convective line had become stratiform, while echo top heights in even the southern convective region began to lower. Finally, by 9:30 UTC, stratiform lightning overtook anvil lightning as the predominate type of lightning behind the convective line, as seen in Figure 5.20. While most stratiform flashes still occur close to the convective line, distant stratiform flashes are particularly common at this stage of convective development, and can even occur at distances exceeding 30 km from the nearest ECR.

5.4 Case Study Summary

In general, these three cases have shown that, despite the differences in the systems' development, anvil flashes often occur in regions of new convection, while

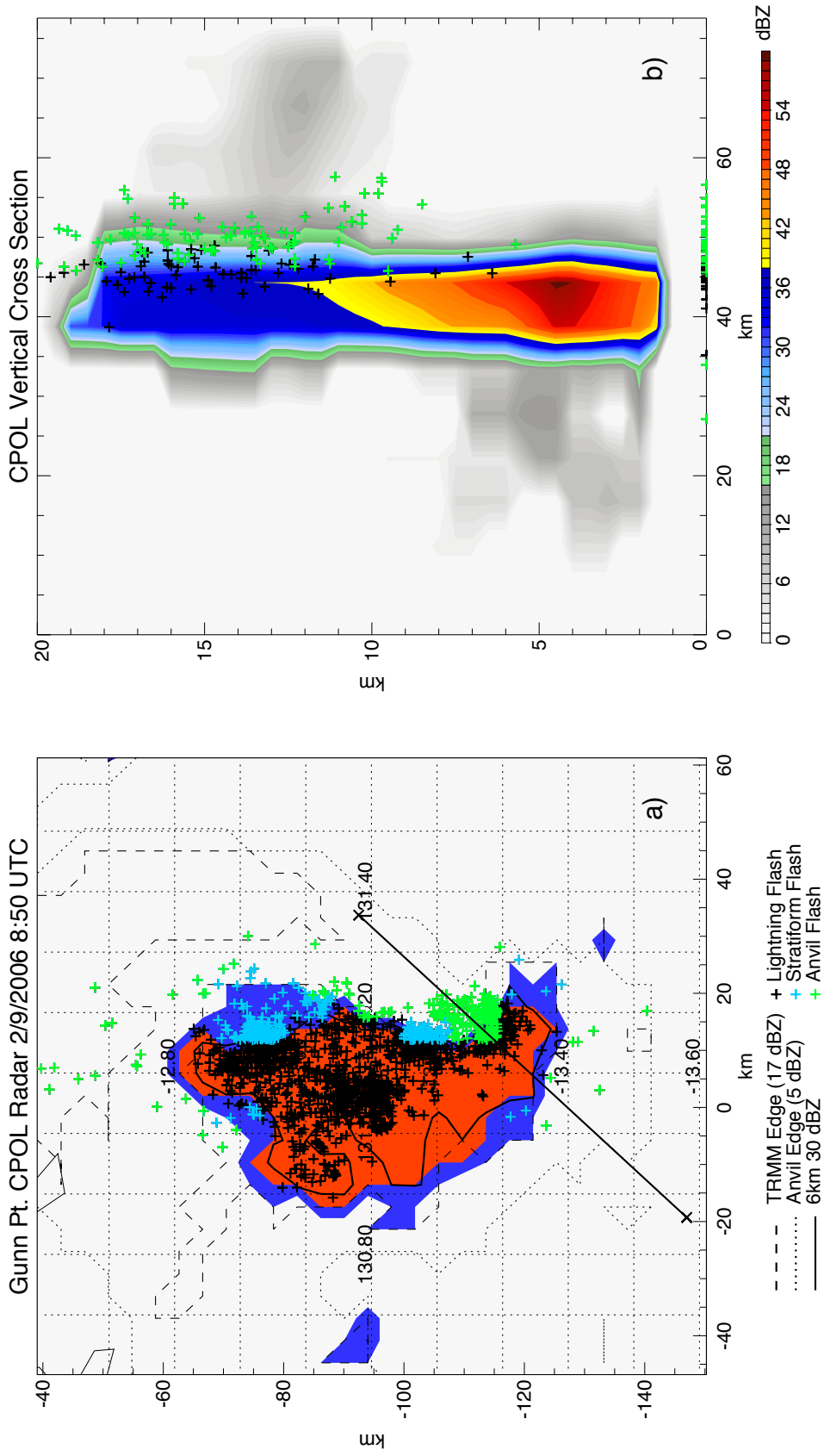

Figure 5.17 Same as Figure 5.13, except for CPOL and LINET observations at 8:50 UTC.

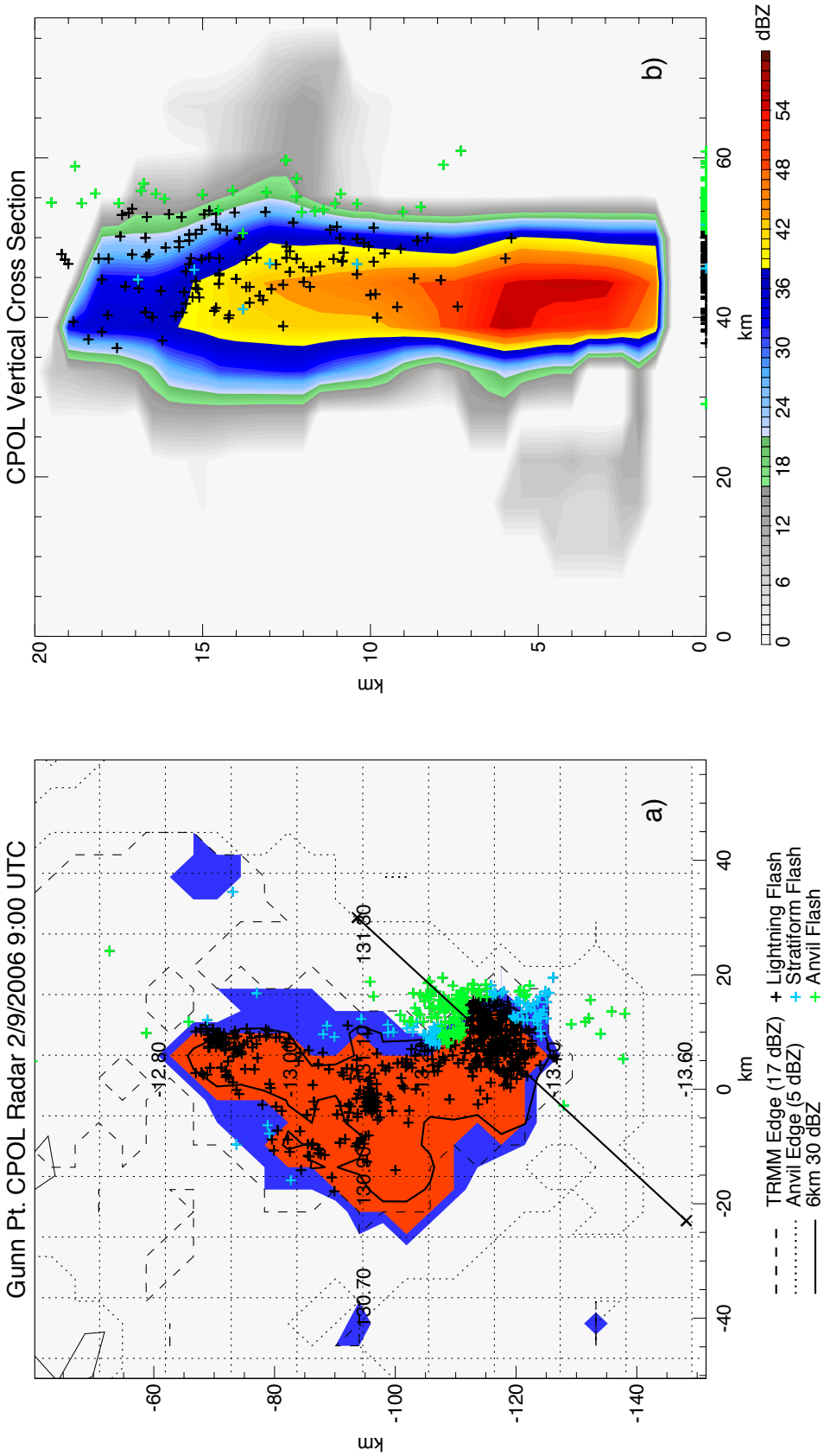

Figure 5.18 Same as Figure 5.13, except for CPOL and LINET observations at 9:00 UTC.

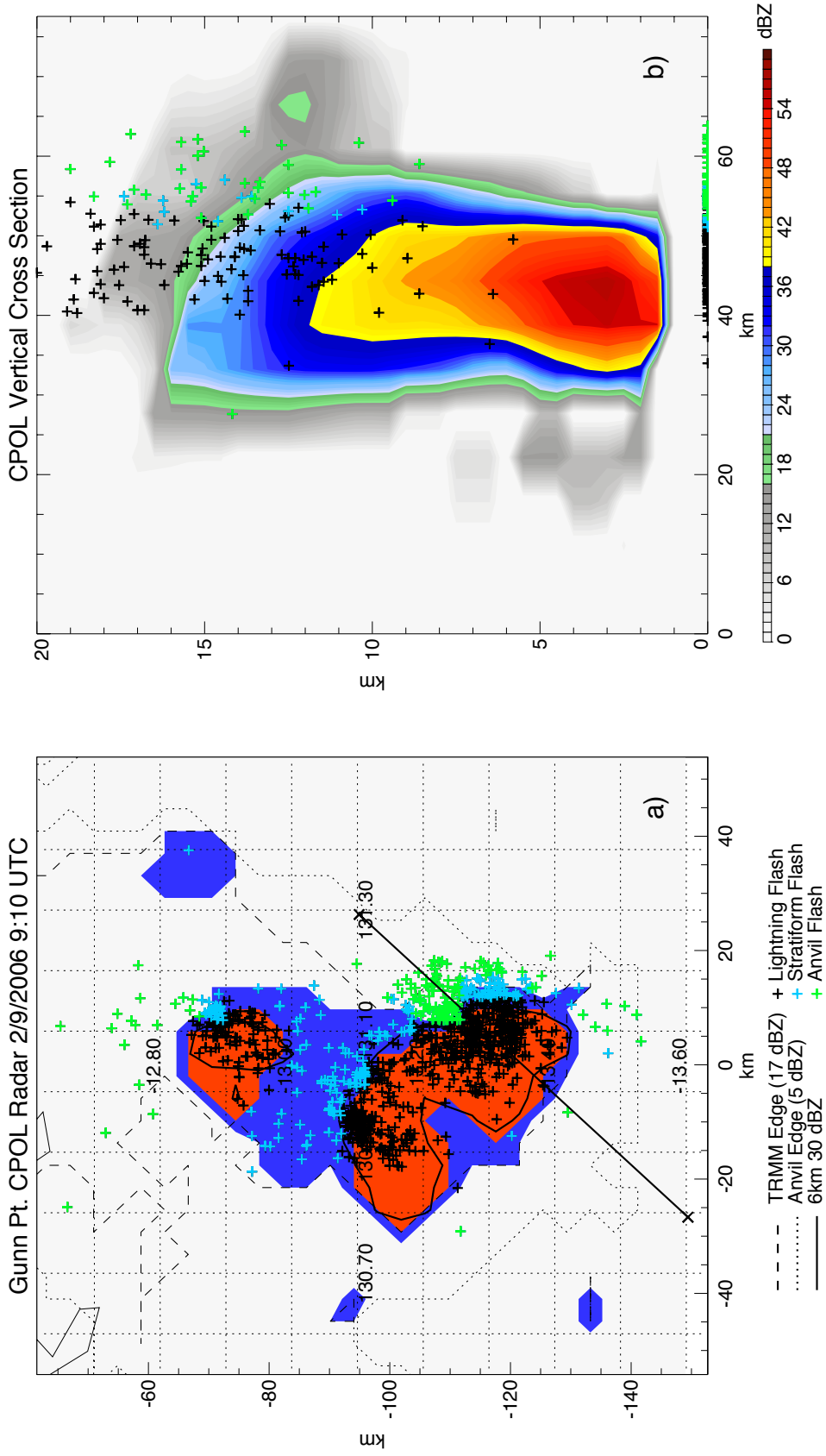

Figure 5.19 Same as Figure 5.13, except for CPOL and LINET observations at 9:10 UTC.

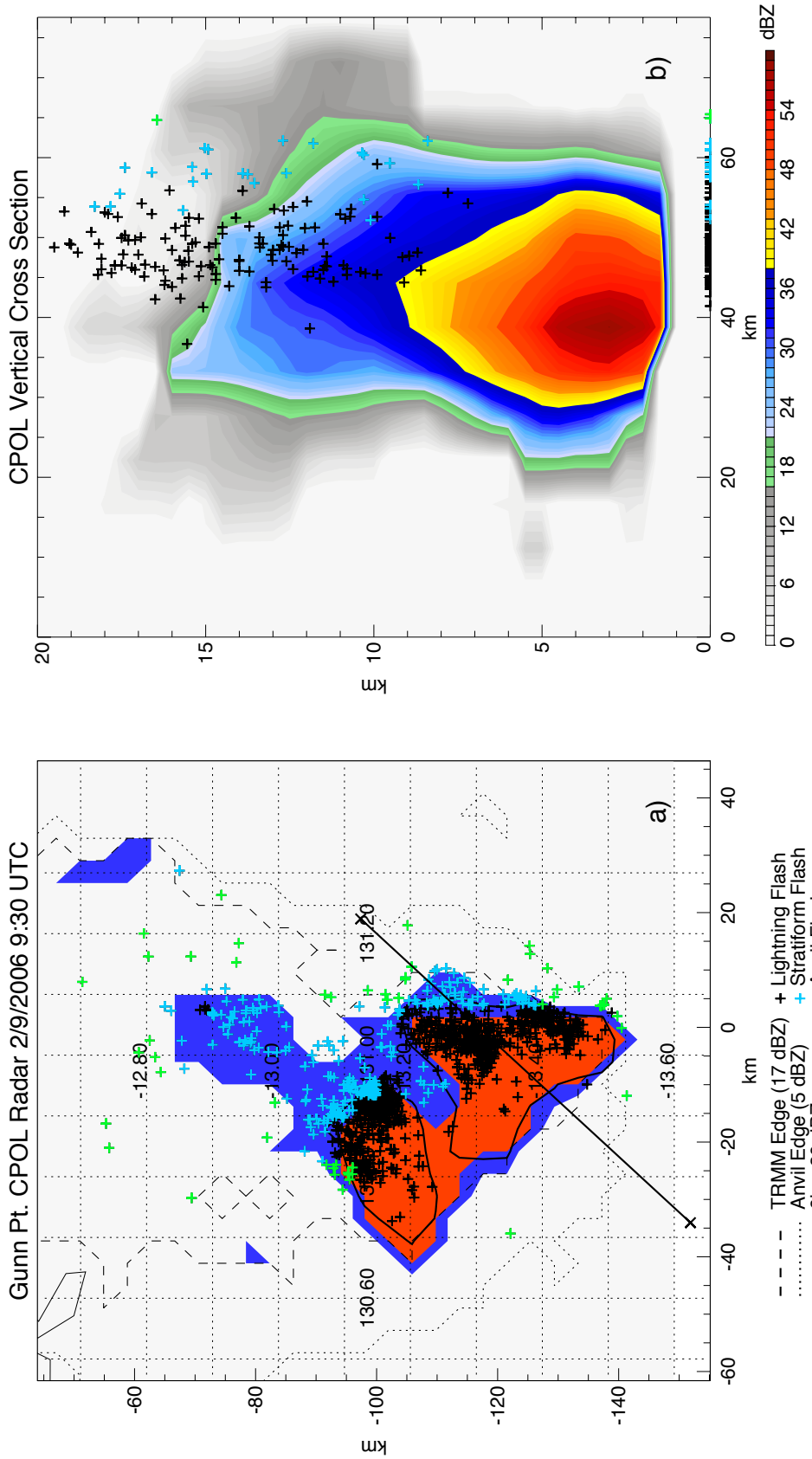

Figure 5.20 Same as Figure 5.13, except for CPOL and LINET observations at 9:30 UTC.

stratiform flashes often occur in mature systems that are either just starting to decay, or far along in the dissipation stage of convection. Moreover, distant stratiform flashes are found in both extensive stratiform regions (possibly the result of charge advection or in situ generation, or both), as well as formerly convective areas, particularly in the case of rapid decay discussed in Section 5.2.

The remaining 12 cases have also been examined, and they are, in general, consistent with the idea proposed earlier that a large amount of anvil flashes occur initially, relatively early in the lifetime of a convective system, while stratiform flashes tend to occur later, as the system is decaying and reaching the end of its life. This, of course, does not mean that all stratiform and anvil flashes occur in these situations, but it does provide some indication as to where and when these types of flashes may be common.

CHAPTER 6

SUMMARY

In this study, 12-year TRMM observations are used to examine storm systems that produce lightning flashes in stratiform and anvil regions. It is found that stratiform and anvil lightning flashes each account for roughly 5% of lightning flashes observed by the LIS globally. Stratiform flashes are found to make up a relatively larger percent of the total number of lightning flashes over the ocean, especially off the coast of major continents. In certain regions such as high terrain including the Andes and Himalayas, this relative abundance of stratiform flashes is likely due to deficiencies in the 2A23 rain type. Fortunately, despite being biased towards stratiform precipitation (and therefore stratiform flashes) the number of flashes in these regions is small compared to the total, and the bias in the global statistics from these issues is negligible. Anvil flashes also appear to be more common in mountainous and desert regions, particularly the Himalayas, Andes, Rocky Mountains, Sierra Madres, the Sahara, and western Saudi Arabia.

Seasonal variations of stratiform and anvil flashes have also been examined. In the subtropics, stratiform flashes tend to account for a higher percentage of lightning during the winter, and a lower fraction of lightning in the summer. However, some of these subtropical stratiform flashes in the winter may be misclassified due to inaccuracies

in the separation of stratiform and convective precipitation under these circumstances. The seasonal cycle for the anvil flash fraction in the subtropics appears to be six months out of phase of the stratiform fraction seasonal cycle, and anvil flashes account for a higher fraction of summertime flashes than lightning in the winter. In the tropics, however, there does not appear to be much seasonal oscillation in the fractions of stratiform and anvil lightning.

Stratiform flashes are also shown to be more common in the late afternoon and overnight over land compared to other types of flashes. In contrast, anvil flashes over land are more common in the early afternoon and less common throughout the evening and morning hours. These diurnal cycles of lightning generation generally agree with accepted models of the diurnal cycles of convection and MCSs. On the other hand, there is little difference between different types of lightning over the ocean, and the peak of oceanic lightning production occurs nearly 12 hours out of phase with that of land-based lightning. Due to the limited sample size over ocean, differences in the diurnal cycles of stratiform and anvil lightning may not be able to be shown.

Anvil flashes are shown to occur often near the edges of storm systems, with over half of all observed anvil flashes occurring in regions with no detectible PR echoes whatsoever, corresponding to reflectivities throughout the column of less than 17 dBZ. A number of systematic reasons are given for this statistic, including the fact that flashes are defined as the center of illumination, and are not necessarily representative of the conditions of the point at which the flash originated in the case of horizontally extensive flashes, the sensitivity of the PR, among others.

To investigate the types of the thunderstorm likely to have flashes in stratiform

and anvil region, regions likely to contain significant amounts of charged particles potentially leading to lightning initiation are identified from PR data. This is accomplished by using a systematic definition based on moderate echoes in the mixed-phase region. These signatures are an indication of the presence of graupel, which is a key component of the noninductive charging mechanism. Each flash is then associated with its nearest charging region in order to investigate the properties of nearby convection when these flashes do occur. While stratiform and anvil flashes are rare from an occurrence standpoint, 15% of ECRs with lightning are associated with at least one stratiform or anvil flash. This means that large numbers of these flashes in a given storm are rare, but a sizable fraction of storms produce stratiform or anvil flashes regularly, just in smaller numbers than other types of flashes.

Both stratiform and anvil flashes are shown to be associated with relatively weak ECRs compared to those with flashes in the convective region. However, the relative strength of ECRs associated with the two types of lightning tends to be slightly different depending on which convective proxy is used. TMI-based and VIRS-based convective proxies show that ECRs that produce anvil flashes are weaker than those that produce stratiform flashes, while the opposite is true for PR-based convective proxies.

The relationships between these convective proxies and number of flashes of each type are also explored. While the area of 30 dBZ at 6 km seems to have some correlation with the total flash count, relationships between this parameter and the number of stratiform or anvil flashes is very weak. Weak relationships are also found between the ECR minimum 85 and 37 PCTs, and maximum 20, 30, and 40 dBZ echo tops for stratiform and anvil flash counts. This indicates that identifying the threat of lightning in

these regions is extremely challenging, particularly when looking only at the properties of nearby convection. Of course, in situ processes are likely to play a role in many flashes, particularly stratiform flashes, and therefore many of these flashes may be more accurately explained by examining the storm properties at their endpoints.

Relationships are also sought between each of these convective proxies and the distances flashes occur from the centers of the nearest ECR center. A rather unique set of statistics has been discovered, which seem to point to two different scenarios that result in distant lightning. The first is the case of large ECRs, which can contain complex precipitation and charge structures. In this case, the distances flashes occur away from ECR centers depends principally on ECR size, and since most ECRs are small, these flashes dominate the population of flashes on the near side of the 30 km inflection point of the statistics. This results in a general increase in size and strength with flash distance in this region, since ECR size is a proxy for convective intensity. Beyond 30 km, there is no clear relationship found between ECRs and distant flashes. Since TRMM can only see a snapshot of a particular storm at a single point in its lifetime, some details cannot be revealed. The speculation is that after a convective system starts to decay, a significant amount of charged particles aloft can be left behind in formerly convective regions, though only small pockets still meet the ECR definition. These ECRs with distant flashes tend to be relatively weak and small, and seem to dominate the sample beyond the 30 km inflection point in the total flash distance statistics.

These TRMM statistics are compared with ground-based radar and lightning data taken during the TWP-ICE field campaign. Despite key differences in the amount and quality of the data, the differing lightning detection efficiencies between LINET and LIS,

domain limitations, and even the way stratiform and convective precipitation areas are identified, the statistics match reasonably well between the two datasets.

The key advantage to using TWP-ICE data for comparison is the added possibility of tracking individual storm systems throughout their life history. In doing so, a number of hypotheses are confirmed as plausible. These include the ability of new convection of producing high echo tops despite remaining relatively small in area, the tendency of anvil flashes to often occur relatively early and stratiform flashes to occur relatively late in the storms life, the possibility of CG flashes occurring outside the convective core that are often considered anvil flashes according to the proposed definitions, and that distant flashes, particularly distant stratiform flashes, tend to occur as the storm system matures and begins to dissipate.

Though this study has produces some interesting and potentially useful results, much more needs to be done in order to understand lightning flashes in the stratiform and anvil regions of storms. Much more can be accomplished by refining the methods and using different datasets. First, by examining the endpoints of individual lightning flashes observed by LIS, it will be possible to understand the storm structure at the beginning and ending locations of large lightning flashes. Moreover, such information will also be able to indicate whether a particular flash was initiated in the stratiform or anvil regions, or whether it originated in the convective line and propagated outward.

It would also be beneficial to perform a regional climatology of stratiform and anvil flashes using LIS, particularly in coastal regions for stratiform flashes and desert regions for anvil flashes, in order to examine the characteristics of convection that produce these flashes under some very unique weather regimes. Also it would be

interesting to examine if there are differences in the properties of flashes, such as area and brightness, under different weather regimes. Along these lines, it would also be beneficial to refine the ECR definition based on a constant temperature using reanalysis data.

Examining better lightning observations from other ground-based lightning detection network would also further refine these results, particularly a VHF network like the Northern Alabama LMA. The convective systems observed during the MC3E field campaign have also been extensively probed with many ground-based and airborne instruments, making them good candidates as well. Combining these observations with the lightning observations from ground-based networks would give a better description of the initiation of lightning during the life cycles of the thunderstorms.

REFERENCES

Awaka, J., T. Iguchi, and K. Okamoto, 1998: Rain type classification algorithm. *Measuring Precipitation from Space*, **3,** 213-224.

Brooks, C. E. P., 1925: The distribution of thunderstorms over the globe. *Geophys. Memo,* **3,** No. 24, 147-164. Air Ministry, Meteorological Office, London.

Battan, L. J., 1964: Some observations of vertical velocities and precipitation sizes in a thunderstorm. *J. Appl. Meteor.*, **3,** 415-420.

Betz, H. D., K. Schmidt, P. Oettinger, and M. Wirz, 2004: Lightning detection with 3-D discrimination of intracloud and cloud-to-ground discharges. *Geophys. Res. Lett.*, **31,** L11108, doi:10.1029/2004GL019821.

Bluestein, H. B., and D. R. MacGorman, 1998: Evolution of cloud-to-ground lightning characteristics and storm structure in the Spearman, Texas, tornadic supercells of 31 May 1990. *Mon. Wea. Rev.,* **126**, 1451-1467.

Boccippio, D. J., W. Koshak, R. Blakeslee, K Driscoll, D. Mach, D. Buechler, W. Boeck, H. J. Christian, and S. J. Goodman, 2000: The Optical Transient Detector (OTD): Instrument characteristics and cross-sensor validation. *J. Atmos. Oceanic Tech.*, **17,** 441-458.

------, ------, and ------, 2002: Performance assessment of the Optical Transient Detector and Lightning Imaging Sensor. Part I: Predicted diurnal variability. *J. Atmos. Oceanic Tech.*, **19,** 1318-1332.

------, W. A. Petersen, and D. J. Cecil, 2005: The tropical convective spectrum. Part I: Archetypal vertical structures. *J. Climate,* **18,** 2744-2769.

Carey, L. D., and S. A. Rutledge, 2000: The relationship between precipitation and lightning in tropical island convection: a C-band polarimetric study. *Mon. Wea. Rev.*, **128**, 2687-2710.

------, M. J. Murphy, T. L. McCormick, and N. W. S. Demetriades, 2005: Lightning location relative to storm structure in a leading-line, trailing-stratiform mesoscale convective system. *J. Geophys. Res.,* **110,** D03105.

Cecil, D. J., S. J. Goodman, D. J. Boccippio, E. J. Zipser, and S. W. Nesbitt, 2005: Three years of TRMM precipitation features. Part I: Radar, radiometric, and lightning characteristics. *Mon. Wea. Rev.*, **133**, 543–566.

Christian, H. J., and S. J. Goodman, 1987: Optical observations of lightning from a high-altitude airplane. *J. Atmos. Oceanic Tech.*, **4,** 701-711.

------, and coauthors, 1994: Algorithm Theoretical Basis Document (ATBD) for the Lightning Imaging Sensor (LIS). NASA, 53 pp.

------, R. J. Blakeslee, D. J. Boccippio, W. L. Boeck, D. E. Buechler, K. T. Driscoll, S. J. Goodman, J. M. Hall, W. J. Koshak, D. M. Mach, and M. F. Stewart, 2003: Global frequency and distribution of lightning as observed from space by the Optical Transient Detector. *J. Geophys. Res.* **108**, 4005-4020.

Davis, M. H., M. Brook, H. Christian, B. G. Heikes, R. E. Orville, C. G. Park, R. G. Roble, and B. Vonnegut, 1983: Some scientific objectives of a satellite-borne lightning mapper. *Bull. Amer. Meteor. Soc.*, **64,** 114-119.

Deierling, W., and W. A. Peterson, 2008: Total lightning activity as an indicator of updraft characteristics. *J. Geophys. Res.,* **113,** doi: 10.1029/2007JD009598.

------, ------, J. Latham, S. Ellis, and H. J. Christian, 2008: The relationship between lightning activity and ice fluxes in thunderstorms. *J. Geophys. Res.,* **113,** doi: 10.1029/2007JD009700.

Dotzek, N., R. M. Rabin, L. D. Carey, D. R. MacGorman, T. L. McCormick, N. W. Demetriades, M. J. Murphy, and R. L. Holle, 2005: Lightning activity related to satellite and radar observations of a mesoscale convective system over Texas on 7-8 April 2002. *Atmos. Res.* **76**, 127-166.

Dye, J. E., M. G. Bateman, H. J. Christian, E. Defer, C. A. Grainger, W. D. Hall, E. P. Krider, S. A. Lewis, D. M. Match, F. J. Merceret, J. C. Willett, and P.T. Willis, 2007: Electric fields, cloud microphysics, and reflectivity in anvils of Florida thunderstorms. *J. Geophys. Res.*, **112,** D11215.

Ely, B. L., R. E. Orville, D. C. Lawrence, and C. L. Hodapp, 2008: Evolution of the total lightning structure in a leading-line, trailing-stratiform mesoscale convective system over Houston, Texas. *J. Gephys. Res*., **113,** doi:10.1029/2007JD008445.

Fu, Y., and G. Liu, 2007: Possible misidentification of rain type by TRMM PR over Tibetan plateau. *J. Appl. Meteor. Climat*., **46**, 667-672.

Hendon, H., and K. Woodberry, 1993: The diurnal cycle of tropical convection. *J. Geophy. Res*., **98**, 16623-16637.

Iguchi, T., T. Kozu., R. Meneghini, J. Awaka, and K. Okamoto, 2000: Rain-profiling algorithm for the TRMM precipitation radar. *J. Appl. Meteor.*, **39,** 2038-2052.

Jayaratne, E. R., C. P. R. Saunders, and J. Hallet, 1983: Laboratory studies of the charging of soft hail during ice crystal interactions. *Quart. J. Roy. Meteor. Soc.,* **109,** 609–630.

Keenan, T., K. Glasson, and F. Cummings, 1992: The BMRC/NCAR C-band polarimetric (C-POL) radar system. *J. Atmos. Oceanic Technol.*, **15**, 871-886.

Keighton, S. J., H. B. Bluestein, and D. R. MacGorman, 1991: The evolution of a severe mesoscale convective system: cloud-to-ground lightning location and storm structure. *Mon. Wea. Rev.,* **119**, 1533-1556.

Kuhlman, K. M., D. R. MacGorman, M. I. Biggerstaff, and P. R. Kreibiel, 2009: Lightning initiation in the anvils of two supercell storms. *Geophys. Res. Lett.*, **36**, L07802.

Kummerow, C., W. Barnes, T. Kozu, J. Shiue, and J. Simpson, 1998: The Tropical Rainfall Measuring Mission (TRMM) sensor package. *J. Atmos. Oceanic Technol.*, **15**, 809–817.

Lang, T. J., S. A. Rutledge, and K. C. Wiens, 2004: Origins of positive cloud-to-ground lightning in the stratiform region of a mesoscale convective system. *Geophys. Res. Lett.*, **31,** doi: 10.1029/2004GL019823.

------, and ------, 2008: Kinematic, microphysical, and electrical aspects of an asymmetric bow echo mesoscale convective system observed during STEPS. *J. Geophys. Res*., **113,** doi: 10.1029/2006JD007709.

------, W. A. Lyons, S. A. Rutledge, J. D. Meyer, D. R. Macgorman, and S. A. Cummer, 2010: Transient luminous events above two mesoscale convective systems: Storm structure and evolution. *J. Geophys. Res.,* **115**, doi: 10.1029/2009JA014500.

Larsen, H. R., and E. J. Stansbury, 1974: Association of lightning flashes with precipitation cores extending to height 7 km. *J. Atmos. Terr. Phys*., **36,** 1547-1553.

Lay, E. H., R. H Holzworth, C. J. Rodger, J. N. Thomas, O. Pinto Jr., and R. L. Dowden, 2004: WWLL global lightning detection system: Regional validation study in Brazil. *Geophys. Res. Lett.*, **31,** doi: 10.1029/2003GL018882.

Lewis, E. A., R. B. Harvey, and J. E. Rasmussen, 1960: Hyperbolic direction finding with sferics of transatlantic origin. *J. Geophys. Res.,* **65,** 1879-1905.

Liu, C., E. J. Zipser, D. J. Cecil, S. W. Nesbitt, and S. Sherwood, 2008: A cloud and precipitation feature database from 9 years of TRMM observations. *J. Appl. Meteor. Climate*, **47**, 2712-2728. DOI:10.1175/2008JAMC1890.

------, and ------, 2008: Diurnal cycles of precipitation, clouds, and lightning in the tropics from 9 years of TRMM observations. *Geophys. Res. Lett.*, **35**, doi: 10.1029/2007GL032437.

Lund, N. R., D. R. MacGorman, T. J. Schuur, M. I. Biggerstaff, and W. D. Rust, 2009: Relationships between lightning location and polarimetric radar signatures in a small mesoscale convective system. *Mon. Wea. Rev.,* **137**, 4151-4170.

MacClement, W. D., and R. C. Murty, 1978: VHF direction finder studies of lightning. *J. Appl. Meteor.,* **17,** 786-795.

Marshall, J. S., and S. Radhakant, 1978: Radar precipitation maps as lightning indicators. *J. Appl. Meteorol.*, **17,** 206-212.

Marshall, T. C., W. D. Rust, W. P. Winn, and K. E. Gilbert, 1989: Electrical structure in two thunderstorm anvil clouds. *J. Geophys. Res.*, **94,** 2171-2181.

------, and ------, 1993: Two types of vertical electrical structures in stratiform precipitation regions of mesoscale convective systems. *Bull. Amer. Meteor. Soc.*, **74,** 2159-2170.

------, M. Stolzenburg, P. R. Krehbiel, N. R. Lund, and C. R. Maggio, 2009. Electrical evolution during the decay stage of New Mexico thunderstorms, *J. Geophys. Res.*, **114**, D02209, doi: 10.1029/2008JD010637.

May, P. T., J. H. Mather, G. Vaughan, C. Jakob, G. M. McFarquhar, B. K. Bower, and G. G. Mace, 2008: The Tropical Warm Pool International Cloud Experiment. *Bull. Amer. Meteor. Soc.*, **89,** 629-645.

Mazur, V., and W. D. Rust, 1983: Lightning propagation and flash density in squall lines as determines with radar. *J. Geophys. Res.,* **88**, 1495-1502.

McCormick, T.L., 2003: Three-dimensional radar and total lightning characteristics of a mesoscale convective system. M.S. thesis, Dept. of Marine, Earth, and Atmospheric Sciences, North Carolina State University, 354 pp.

Murty, R. C., and W. D. MacClement, 1973: VHF direction finder for lightning location. *J. Appl. Meteor.,* **12,** 1401-1045.

Nesbitt, S. W., and E. J. Zipser, 2003: The diurnal cycle of rainfall and convective intensity according to three years of TRMM measurements. *J. Climate,* **16**, 1456-1475.

Oetzel, G. N., and E. T. Pierce, 1969: VHF Technique for Locating Lightning. *Radio Sci.,* **4,** 199-201.

Orville, R. E., and D. W. Spencer, 1979: Global lightning flash frequency. *Mon. Wea. Rev.,* **107,** 934-943.

------, and R. W. Henderson, 1986: Global distribution of midnight lightning: September 1977 to August 1978. *Mon. Wea. Rev.,* **114,** 2640-2653.

------, 2008: Development of the National Lightning Detection Network. *Bull. Amer. Meteor. Soc.*, **89,** 182-190.

Petersen, W. A., H. J. Christian, and S. A. Rutledge, 2005: TRMM observations of the global relationship between ice water content and lightning. *Geophys. Res. Lett.*, **32,** L14819, doi: 10.1029/2005GL023236.

Rutledge, S. A., and D. R. MacGorman, 1988: Cloud-to-ground lightning activity in the 10-11 June 1985 mesoscale convective system observed during the Oklahoma-Kansas PRESTORM project. *Mon. Wea. Rev.*, **116**, 1393–1408.

Saunders, C. P. R., W. D. Keith, and R. P. Mitzeva, 1991: The effect of liquid water content on thunderstorm charging. *J. Geophys. Res.,* **96,** 11,007–11,017.

Schuur, T. J., and S. A. Rutledge, 2000: Electrification of stratiform regions in mesoscale convective systems. Part II: Two-dimensional numerical model simulations of a symmetric MCS. *J. Atmos. Sci.*, **57,** 1983-2006.

Shackford, C. R., 1960: Radar indications of a precipitation-lightning relationship in New England thunderstorms. *J. Meteor.,* **17,** 15-19.

Spencer, R. W., H. G. Goodman, and R. E. Hood, 1989: Precipitation retrieval over land and ocean with the SSM/I: Identification and characteristics of the scattering signal. *J. Atmos. Oceanic Tech.*, **6,** 254-273.

Steiner, M., R. A. Houze, and S. E. Yuter, 1995: Climatological characterization of three-dimensional storm structure from operational radar and rain gauge data. *J. Appl. Meteor.* **34**, 1978-2007.

Stolzenburg, M., T.C. Marshall, W. D. Rust, and B.F. Smull, 1994: Horizontal distribution of electrical and meteorological conditions across the stratiform region of a mesoscale convective system. *Mon. Wea. Rev.*, **122,** 1777–1797.

------, ------, and P. R. Krehbiel, 2010: Duration and extent of large electric fields in a thunderstorm anvil cloud after the last lightning. *J. Geophys. Res.*, **115**, D19202, doi:10.1029/2010JD014057.

Takahashi, T., 1978: Riming electrification as a charge generation mechanism in thunderstorms. *J. Atmos. Sci.,* **35,** 1536–1548.

Takayabu, Y. N., 2006: Rain-yield per flash calculated from TRMM PR and LIS data and its relationship to the contribution of tall convective rain. *Geophys. Res. Lett.*, **33**, L18705, doi:10.1029/2006GL027531.

Thomas, R. J., P. R. Krehbiel, W. Rison, S. J. Hunyady, W. P. Winn, T. Hamlin, and J. Harlin, 2004: Accuracy of the Lightning Mapping Array. *J. Geophys. Res.,* **109,** doi: 10.1029/2004JD004549.

Toracinta, E. R., D. J. Cecil, E. J. Zipser, and S. W. Nesbitt, 2002: Radar, passive microwave, and lightning characteristics of precipitating systems in the tropics. *Mon. Wea. Rev.*, **130**, 802–824.

Vaughan, O. H. Jr., 1990: Mesoscale lightning experiment (MLE): a view of lightning as seen from space during the STS-26 mission. NASA Technical Memorandum (NASA TM-103513), 70 pp.

Vonnegut, B., O. H. Vaughan Jr., M. Brook, and P. K. Krehbiel, 1985: Mesoscale observations of lightning from space shuttle. *Bull. Amer. Meteor. Soc.*, **66**, 20-29.

------, ------, and ------, 1989: Nocturnal photographs taken from a U-2 airplane looking down on tops of clouds illuminated by lightning. *Bull. Amer. Meteor. Soc.*, **70**, 1263-1271.

Williams, E. R., M. E. Weber, and R. E. Orville, 1989: The relationship between lightning type and convective state of thunderclouds. *J. Geophys. Res.,* **94,** 13,213-13,220.

Xu, W., E. Zipser, C. Liu, and H. Jiang, 2010: On the relationships between lightning frequency and thundercloud parameters of regional precipitation systems. *J. Geophys. Res.*, **115,** doi:10.1029/2009JD013385.

Yamamoto, M. K., A. Higuchi, and K. Nakamura, 2006: Vertical and horizontal structure of winter precipitation systems over the western Pacific around Japan using TRMM data. *J. Geophys. Res.*, **111**, D13108, doi: 10.1029/2005JD006412.

Yuter, S. E., and R. A. Houze Jr., 1995: Three-dimensional kinematic and microphysical evolution of Florida cumulonimbus. Part II: Frequency distribution of vertical velocity, reflectivity, and differential reflectivity. *Mon. Wea. Rev.,* **123,** 1941-1963.

Zipser, E. J., D. J. Cecil, C. Liu, S. W. Nesbitt, and D. P. Yorty, 2006: Where are the

most intense thunderstorms on earth? *Bull. Amer. Meteor. Soc.*, **87**, 1057-1071.